University of Tennessee, Knoxville
TRACE: Tennessee Research and Creative Exchange

Masters Theses | Graduate School

5-1999

# The Development and Application of a Digitized Image Database for the Estimation of Age Based on Bone Histology

John Edward Mailen
*University of Tennessee, Knoxville*

Follow this and additional works at: https://trace.tennessee.edu/utk_gradthes

Part of the Anthropology Commons

## Recommended Citation

Mailen, John Edward, "The Development and Application of a Digitized Image Database for the Estimation of Age Based on Bone Histology. " Master's Thesis, University of Tennessee, 1999.
https://trace.tennessee.edu/utk_gradthes/4143

This Thesis is brought to you for free and open access by the Graduate School at TRACE: Tennessee Research and Creative Exchange. It has been accepted for inclusion in Masters Theses by an authorized administrator of TRACE: Tennessee Research and Creative Exchange. For more information, please contact trace@utk.edu.

To the Graduate Council:

I am submitting herewith a thesis written by John Edward Mailen entitled "The Development and Application of a Digitized Image Database for the Estimation of Age Based on Bone Histology." I have examined the final electronic copy of this thesis for form and content and recommend that it be accepted in partial fulfillment of the requirements for the degree of Master of Arts, with a major in Anthropology.

William M. Bass, Major Professor

We have read this thesis and recommend its acceptance:

Murray K. Marks, Lyle W. Konigsberg

Accepted for the Council:
Carolyn R. Hodges

Vice Provost and Dean of the Graduate School

(Original signatures are on file with official student records.)

To the Graduate Council:

I am submitting herewith a thesis written by John Edward Mailen entitled "The Development and Application of a Digitized Image Database for the Estimation of Age Based on Bone Histology." I have examined the final copy of this thesis for form and content and recommend that it be accepted in partial fulfillment of the requirements for the degree of Master of Arts, with a major in Anthropology.

William M. Bass, Major Professor

We have read this dissertation
and recommend its acceptance:

Accepted for the Council:

Associate Vice Chancellor and
Dean of The Graduate School

# The Development and Application of a Digitized Image Database for the Estimation of Age Based on Bone Histology

A Thesis
Presented for the
Master of Arts
Degree
The University of Tennessee, Knoxville

John Edward Mailen
May 1999

# DEDICATION

This thesis is dedicated to my parents

Dr. James C. Mailen

And

Mrs. Jean H. Mailen

who have always been supportive and invaluable in their support,

and in memory of my father.

# ACKNOWLEDGMENTS

I appreciate and am grateful for the opportunities and experiences at the University of Tennessee Knoxville, which have been memorable and rewarding. The programs offered at the University of Tennessee, along with the excellence of the faculty, and the graduate students whom I met, are outstanding. I am grateful for my Masters committee for their invaluable assistance, advice, and encouragement of Dr. William M. Bass, Dr. Lyle W. Konigsberg, and Dr. Murray W. Marks, during my graduate program. Through their suggestions and answers to my questions the process has come to completion.

Additionally, I would like to thank Dr. Sam D. Stout at the University of Missouri in Columbia, Missouri, for his assistance in procuring additional histological sample data. I would like to thank Dr. William M. Bass and the Department of Anthropology at the University of Tennessee for making available the histological cross-sections from the Anthropology Forensic Center, where the majority of the data was collected.

Further, I would like to express the greatest debt of gratitude to my mother, who gave invaluable financial assistance in acquiring research equipment. Without her encouragement, the research would have taken longer to complete. Finally, I would like to express my appreciation to the many relatives and friends who listened and gave encouragement.

# ABSTRACT

In this study, digital image analysis was incorporated into existing regression formulas for age estimation. Previous studies in forensic anthropology have utilized only the manual counting of Basic Structural Units (BSUs) within the bone matrix for age estimation. The integration of an image database with the accepted regression formulas (Kerley 1965 and Kerley and Ubelaker 1978) allows for data to be reexamined without having to be sampled from the original slides. Thus, the data will have a more dynamic nature, where it could be investigated by other researchers from the original readings. In addition, the data can help train future observers and be capable of more efficient communication to other researchers electronically.

The sample consisted of thirty (30) femoral thin-section slides from the histological collection in University of Tennessee Forensic Center, which is part of the Department of Anthropology at the University of Tennessee Knoxville. The slides were chosen based on their clarity for image analysis. Of the thirty slides, nineteen had known ages, which were indicated in the Forensic Center records. The data was collected according to the prescribed methodology (Kerley 1965 and Kerley and Ubelaker 1978) and the regression equations were generated.

The resulting age estimates for eighteen (18) of nineteen (19) slides with known ages were within the standard error of the regression equations. In fourteen (14) of nineteen (19) slides with known ages, the age estimate was within six years of the known age. In Case #30 (O82-2), the estimated age was more than ten years from the actual age of 6 to 7 years. As a result, it is believed that the eleven (11) unknown slides will have accurate estimated ages, as long as the slides did not come from young subjects.

# TABLE OF CONTENTS


1. **INTRODUCTION** ..... 1
Rationale ..... 1
Statement of the Problem ..... 2
Objectives of the Research ..... 2
Advantages of the Proposed Research ..... 3

2. **REVIEW OF THE LITERATURE** ..... 4
Review of Calcified Tissue ..... 4
Review of Bone Histology ..... 5
Review of the Histological Literature for Age Estimation ..... 14
Review of Digital Image Technology: Development and Applications ..... 18
The Development of Digital Image Analysis ..... 23
Digital Analysis Procedures and Techniques ..... 25
Conclusions ..... 27

3. **METHODS** ..... 29
Equipment for the Research ..... 29
Digital Image Microscopy and Global Image Lab™ v3.0 ..... 30
Adobe Photoshop™ v3.0 ..... 31
Other Equipmennt ..... 32
Selection of the Sample ..... 35
Procedure for Additional Samples ..... 35
Description of the Method ..... 36
Technical Note 1: Procedure to Combine Images ..... 37
Technical Note 2: Procedure for Acquiring the Images ..... 41
Field of View (FOV) ..... 43
Technical Note 3: FOV Mask Procedure ..... 43
Procedure to Eliminate Extraneous Variables ..... 45
Technical Solutions for Data Image Processing ..... 49
Technical Note 4: Repairing the Corruption of Program Files ..... 49
Usage of Filters and Morphological Transformations ..... 51
Basic Structural Identification Definitions ..... 55
Counting Procedure ..... 57
Calibrating the Counting Procedure ..... 58
Time and Image Requirements for Data Collection ..... 62
Data Collection Procedure ..... 63
The Formulas for the Data Collection ..... 63
Regression Formulas ..... 63
Procedure for Determining the Age Estimation Midpoint ..... 64
Data Record Sheet ..... 69
Procedure to Print the Images ..... 69

4. **RESULTS** ..... 71

5. **DISCUSSION** ..... 74

6. **CONCLUSION** ..... 77

**BIBLIOGRAPHY** ..... 79

**APPENDIX** ..... 83

**VITA** ..... 160

# LIST OF TABLES


| TABLE | | PAGE |
|---|---|---|
| 1. | The Current Applications for Digital Image Analysis | 22 |
| 2. | Case #2: (ID 72-3) | 67 |
| 3. | Case #9 (ID 80-3) | 67 |
| 4. | Case #10 (ID 80-6) | 67 |
| 5. | Summary of Age Estimations | 72 |
| A-1. | 30 Selected Forensic Slides from the UTK Forensic Histology Collection | 84 |
| A-2. | Data Submitted by Dr. S. D. Stout | 85 |
| A-3. | Data Collection Sheets (Case #1 to #3) | 87 |
| A-3. | Data Collection Sheets (Case #4 to #6) | 94 |
| A-3. | Data Collection Sheets (Case #7 to #9) | 101 |
| A-3. | Data Collection Sheets (Case #10 to #12) | 108 |
| A-3. | Data Collection Sheets (Case #13 to #15) | 115 |
| A-3. | Data Collection Sheets (Case #16 to #18) | 122 |
| A-3. | Data Collection Sheets (Case #19 to #21) | 129 |
| A-3. | Data Collection Sheets (Case #22 to #24) | 136 |
| A-3. | Data Collection Sheets (Case #25 to #27) | 143 |
| A-3. | Data Collection Sheets (Case #28 to #30) | 150 |
| A-4. | Histological Collection Overview | 157 |
| A-5. | Histological Collection Age Distribution | 157 |
| A-6. | Histological Thin-Sections Descriptions | 157 |
| A-7. | Femur Sections from Histological Collection | 158 |
| A-8. | Fibula Sections from Histological Collection | 158 |
| A-9 | Tibia Sections from Histological Collection | 159 |
| A-10. | Burn Case Sections from Histological Collection | 159 |

A-11. Records of Sections from Histological Collection without Slides ..... 159

A-12. Sections without Records Found from the Histological Collection ..... 159

# LIST OF FIGURES

FIGURE PAGE


1. Left tibia with major features identified ..... 6
2. Three major types of bone identified ..... 7
3. The cross-section of a long bone shaft illustrating the composition ..... 9
4. A cross-section of long bone shaft illustrating the positions of other structural features ..... 9
5. Three types of bone cells are Osteoblasts (A), Osteocytes (B), and Osteoclasts (C), while the diagonal lines represent bone ..... 11
6. Growth series of the left human tibia exhibiting the morphological changes from Birth to 18 years of age ..... 12
7. Diagram illustrating the remodeling process of a long bone ..... 13
8. Microscopic Field of View locations represented by circles (Kerley) and Squares (Ahliqvist and Damsten) ..... 14
9. Digital Image Systems existing during the 1960s ..... 19
10. Digital Image Systems existing during the Late 1970s ..... 19
11. Digital Image Systems existing during the Early 1980s ..... 19
12. Digital Image Systems existing during the Late 1980s ..... 20
13. Digital Image Systems existing during the 1990s ..... 20
14. Diagram illustrating research equipment setup ..... 29
15. A femoral histological section displayed with identified BSUs ..... 56
16. A sample of the data checklist used when combining images ..... 63
17. Age Range Chart for Femoral Osteons ..... 65
18. Age Range Chart for Femoral Fragments ..... 65
19. Age Range Chart for Femoral Lamellar ..... 66
20. Age Range Chart for Femoral non-Haversian ..... 66

21. A blank record sheet illustrating its organizational format ..... 69

22. Plotted Age Estimates from 30 Slides ..... 73

# LIST OF PLATES

PLATE PAGE


1. The first image is opened in the combination sequence ..... 38
2. The canvas area is enlarged with the first image present ..... 38
3. The second image is opened in the combination sequence ..... 38
4. Overlaying the first and second images in the operation ..... 39
5. The first and second images are aligned properly ..... 39
6. The FOV mask is opened ..... 39
7. The FOV mask is positioned ..... 40
8. The brightness is altered ..... 40
9. An image displayed without modification at 100x ..... 42
10. The image from Plate 9 with illumination adjusted ..... 42
11. An image of the micrometer slide used with calibration marks ..... 44
12. An image displaying the extended ruler measurement to 1.62 mm ..... 44
13. FOV circle aligned with the extended ruler to create the FOV mask ..... 44
14. FOV circle displayed without the calibration marks ..... 46
15. The FOV mask displayed ..... 46
16. Two combined images displayed with the FOV mask ..... 46
17. Positive view of an image displayed ..... 48
18. Negative view of image from Plate 17 displayed ..... 48
19. An image displayed with marked structures for identification ..... 54
20. An initial image is displayed prior to modification ..... 59
21. The initial image displayed after the pixelation operation ..... 59
22. The initial image from Plate 21 displayed after sharpen edges operation ..... 59
23. An image displayed ..... 61
24. Image displayed after marking ..... 61

A-1. Case #1: 22781 FOV ..... 88
A-2. Case #1: 22781 FOV Marked ..... 89
A-3. Case #2: 72-3 FOV ..... 90
A-4. Case #2: 72-3 FOV Marked ..... 91
A-5. Case #3: 73-1 FOV ..... 92
A-6. Case #3: 73-1 FOV Marked ..... 93
A-7. Case #4: 74-2 FOV ..... 95
A-8. Case #4: 74-2 FOV Marked ..... 96
A-9. Case #5: 74-5 FOV ..... 97
A-10. Case #5: 74-5 FOV Marked ..... 98
A-11. Case #6: 79-13 FOV ..... 99
A-12. Case #6: 79-13 FOV Marked ..... 100
A-13. Case #7: 80-12 FOV ..... 102
A-14. Case #7: 80-12 FOV Marked ..... 103
A-15. Case #8: 80-15 FOV ..... 104
A-16. Case #8: 80-15 FOV Marked ..... 105
A-17. Case #9: 80-3 FOV ..... 106
A-18. Case #9: 80-3 FOV Marked ..... 107
A-19. Case #10: 80-6 FOV ..... 109
A-20. Case #10: 80-6 FOV Marked ..... 110
A-21. Case #11: 81-110 FOV ..... 111
A-22. Case #11: 81-110 FOV Marked ..... 112
A-23. Case #12: 81-13 FOV ..... 113
A-24. Case #12: 81-13 FOV Marked ..... 114
A-25. Case #13: 81-2005 FOV ..... 116
A-26. Case #13: 81-2005 FOV Marked ..... 117
A-27: Case #14: 81-9 FOV ..... 118
A-28. Case #14: 81-9 FOV Marked ..... 119

A-29. Case #15: 82-16 FOV ..... 120
A-30. Case #15: 82-16 FOV Marked ..... 121
A-31. Case #16: 82-1 FOV ..... 123
A-32. Case #16: 82-1 FOV Marked ..... 124
A-33. Case #17: 83-10 FOV ..... 125
A-34. Case #17: 83-10 FOV Marked ..... 126
A-35. Case #18: 83-215 FOV ..... 127
A-36. Case #18: 83-215 FOV Marked ..... 128
A-37. Case #19: 83-25 FOV ..... 130
A-38. Case #19: 83-25 FOV Marked ..... 131
A-39. Case #20: 83-9 FOV ..... 132
A-40. Case #20: 83-9 FOV Marked ..... 133
A-41. Case #21: 84-14 FOV ..... 134
A-42. Case #21: 84-14 FOV Marked ..... 135
A-43. Case #22: 85-1 FOV ..... 137
A-44. Case #22: 85-1 FOV Marked ..... 138
A-45. Case #23: 85-24 FOV ..... 139
A-46. Case #23: 85-24 FOV Marked ..... 140
A-47. Case #24: 85-7 FOV ..... 141
A-48. Case #24: 85-7 FOV Marked ..... 142
A-49. Case #25: F83-215 FOV ..... 144
A-50. Case #25: F82-215 FOV Marked ..... 145
A-51. Case #26: F83-539 FOV ..... 146
A-52. Case#26: F83-539 FOV Marked ..... 147
A-53. Case #27: FA-12 FOV ..... 148
A-54. Case #27: FA-12 FOV Marked ..... 149
A-55. Case #28: O80-120 FOV ..... 151
A-56. Case #28: O80-120 FOV Marked ..... 152

A-57. Case #29: O81-9 FOV ..... 153

A-58. Case #29: O81-9 FOV Marked ..... 154

A-59. Case #30: O82-2 FOV ..... 155

A-60. Case #30: O80-2 FOV Marked ..... 156

# LIST OF ABBREVIATIONS

| | |
|---|---|
| GLI | Global Image Lab software |
| DT3851 | Fidelity 200, the frame grabber card, which used the Global Image Lab software |
| PSD | Standard file extension for graphic images created under Adobe Photoshop |
| TIFF | Standard file extension for graphic images created under Global Image Lab. |
| TIGA | Texas Instruments Graphics Adapter, a software driver used by Global Image Lab |
| FOV | Field of View |
| Mask | Digital Image Object, which only permits certain areas to be displayed |
| B.S.U. | Basic Structural Units within the bone matrix |

# CHAPTER I

# INTRODUCTION

## Rationale

Forensic anthropology has developed many diverse methodologies in determining characteristics and features from the decomposed or skeletonized remains of unknown individuals. In "Essentials of Forensic Anthropology" T.Dale Stewart (1979) defined forensic anthropology as "that branch of physical anthropology which, for forensic purposes, deals with the identification of more or less skeletonized remains known to be, or suspected of being human." These methods and procedures have helped to shed light on criminal cases which might have otherwise remained unsolved. In criminal cases law enforcement when seeking the assistance of forensic anthropologists seeks answers to questions which will lead to a successful resolution of the investigation. The questions are concerned with the identification of the material. Is it bone and is the bone, animal or human? How old is the bone (i.e., modern or archaeological)? If the bone is human, how many individuals are present? Forensic anthropologists can make determinations as to the age, sex, race or ethnicity, stature, and manner of death.

The majority of techniques used to determine the identity of the individual focus on gross morphology and/or anthropomorphic measurements. Underlying the application of these techniques is the stage of the skeletal life of the individual, which can be either developmental or degenerative. Developmental processes are generally easier to observer when estimating the age of an individual than degenerative. The developmental stages mainly focus upon dental development, dental eruption patterns, epiphyseal union patterns, and diaphyseal length measurements. The degenerative stages mainly focus upon the pubic symphyseal patterns, the auricular area of the illium, ectocranial suture, and sternal ends of the ribs (Ubelaker 1978 and Krogman 1986). These methods assist in the determination of age estimation, but they focus on gross skeletal morphology. If the skeletal material is highly fragmented and/or burned, then microscopic analysis of the material is one of the few methods for age estimation.

Microscopic analysis of bone based upon histological counts began in the 1960s. In 1961 Kerley wrote his dissertation upon the usage of histological analysis of the human femur, tibia, and fibula for the estimation of age. The initial procedure was manual counting and classifying the types and frequencies of osteons, fragmentary osteons, lamellar, and non-Haversian tissue. As a result, the process was tedious and laborious to implement. The estimation of the percentage of the lamellar bone requiring the most effort within the methodology. However, over the years as computer technology has advanced and decreased in cost, the procedure has been subsequently expanded upon by other research but has remained manual. Only recent technology has allowed for the possibility for a computerized methodology to be created.

## Statement of the Problem

A paper presented by Dr. William C. Rodriguez III at the 1994 American Academy of Forensic Sciences symposium indicated a methodology for rapidly differentiating human and animal bone. Afterwards the realization that microscopic age estimation was still manual and noncomputerized indicated a potential area of research. The application of digital image technology within microscopic age estimation was believed possible. However, the differentiating the secondary osteons, fragmentary osteons, non-Haversian canals, and the lamellar bone within the FOV would be the task. The main benefit would be a faster calculation of the percentage of lamellar bone. If the technology could be applied to bone histology, then the age estimation would become more efficient. Another point of interest was determining solutions to the difficulties to use computerized images to study histological samples. The purpose of this research will focus upon testing the feasibility of such a system. It will determine the best regression formula for age estimation from the literature against a known sample (e.g., Kerley 1965, Ahlqvist and Damsten 1969, or Ericksen 1991), automate a portion of the counting procedure and examine the advantages of an image database.

## Objectives of the Research

The objectives include the creation of an digitized image database of femoral histological thin-section samples, demonstrate that training tool can be created from an image database, define technical

procedures for dealing with common problems, and attempt to apply the age estimation regression formula (Kerley 1965 and Kerley and Ubelaker 1978).

## Advantages of the Proposed Research

1. A sample image during data collection can be viewed on the computer monitor until the highest quality image can be obtained.
2. The live video can be captured as images, without having to use a darkroom or other developing facilities.
3. The samples will be from femoral bone histological thin-section slides with known ages. The calculated ages generated by the regression formulas can be compared to the slides for determining the accuracy of methodology.
4. A image can be manipulated through different filters and morphological enhancers with software packages to improve the overall image.
5. Images can be marked and features identified digitally so that other researchers can verify the features identified.
6. Identified images can help instruct other observers in the recognition of features within the bone histological cross-sections, which would reduce potential interobserver error.
7. Data can be exchanged digitally via storage media, the Internet, etc.
8. Perfect copies can be reproduced from the original image with no degradation in quality.
9. Properly highlighted images can be submitted to software analysis programs for increased efficiency in data collection and analysis.

# CHAPTER II

# REVIEW OF THE LITERATURE

## Review of Calcified Tissue

Human bone histology was been described by various researchers since the 17th century. The first descriptions were made by Clopton Havers in 1691. Havers provided accurate descriptions and drawings of the basic structures, which are found within the long bone. These structures included osteons, Sharpey's Fibers, lamellar bone, and Volkmann's Canals. Non-Haversian canals are named after Havers. In addition, he observed the zonal effects of osteons, lamellar bone, and osteocytes (Havers 1691). The first description of the process of reabsorption was observed microscopically by von Ebner in 1675 (LaCroix 1971).

Amprino and Bairati (1936) observed thin-sections under polarized and nonpolarized light and described the progressive change in the number of osteons from childhood through adulthood. Their observations indicated an increase in the number of osteons, while the cortical thickness decreased at the midshaft of the femur.

Through the research of Enlow and Brown (1956; 1957; and 1958) presented in three papers, they described the bone structure from early fish through primates. These studies indicated that structural differences could be discernable between different species at the microscopic level. A notable distinction is the presence of plexiform bone which is found in nonhuman bone, primarily within artiodactyls. Kerley concluded that Enlow and Brown (1958) indicated that it would allow the microscopic age estimation between different species (Kerley 1961).

Jowsey (1960) examined cross-sections of the human femur describing developmental and degenerative changes which were observed in the number of osteons, the thickness of the cortex, and the number of canals. In general, the number of osteons steadily increased through adulthood, where a increased frequency of incomplete calcification of osteons occurred. In addition, older individuals were found to have an increased frequency of canals within the cross-section, along with a decrease in the

thickness of the cortex. Descriptions of the effects of aging on Haversian systems were examined and defined the interactions of osteoblasts and osteoclasts in their interactions within the processes of bone growth and reabsorption.

Support of Enlow and Brown's (1958) belief that the differences between groups of species could be established by observing differences in arrangement of the BSUs was presented at the 1994 American Academy of Forensic Sciences meeting. At the conference Dr. William C. Rodriguez III presented a paper entitled "Rapid Screening Procedure for Histological Differentiation Between Human and Non-Human Fragmentary Skeletal Remains." He described a simple procedure to follow after thin-sectioning and a two-step sanding procedure. The method focused on determining the presence and ratio of plexiform bone. His results indicated that non-human bone is composed approximately 50% of plexiform bone while plexiform bone composed approximately 8% in the bone histology of human infants. Plexiform bone is the primary composition of artiodactyls, which are represented by cows, pigs, deer, sheep, and goats. Thus, Dr. Rodriguez believes that the rapid screening and identification of human versus nonhuman bone can be demonstrated utilizing this methodology.

## Review of Bone Histology

The composition of bone is a combination of two primary components, collagen and hydroxyapatite, into a matrix. The collagen provides the bone with the flexibility within its structure and the hydroxyapatite offers the strength. As a result, the histological composition of bone is composed of both organic and inorganic components, which improves the structural effectiveness and integrity of the material overall (Shipman, et al. 1985 and White 1991).

When studying bone histology it is essential to have an understanding of the cellular arrangement of the general features. A morphological overview of a long bone allows for a visual representation of the major features (see Figure 1). The overall structure of bone can be divided into 3 types (e.g., compact (C), cancellous (CA), and subchondral (SC) (see Figure 2). In addition, there are two membranes found within bone, the periosteum, which covers the outside surfaces, and endosteum, which lines the marrow cavities

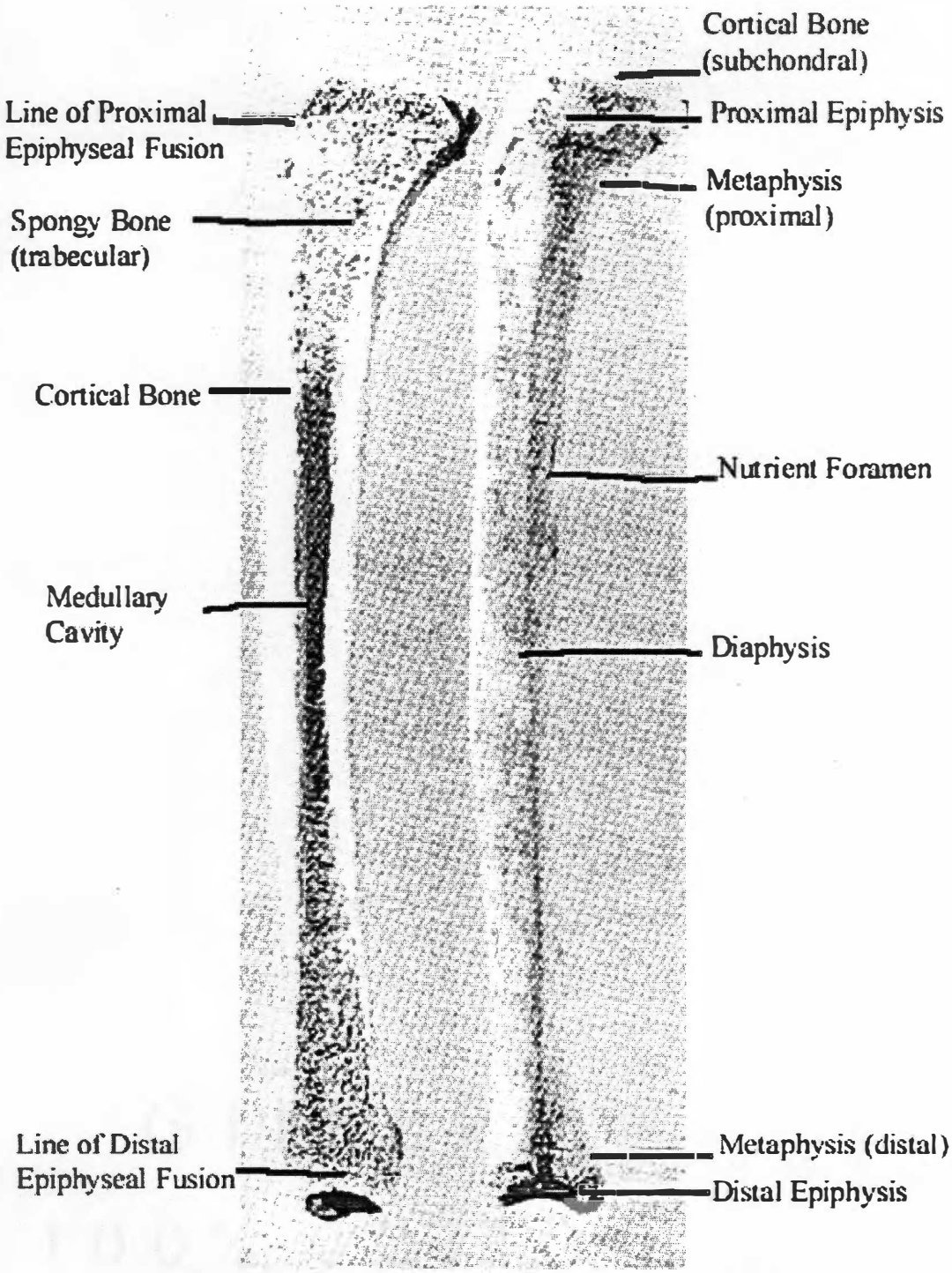


**Figure 1: Left tibia with major features identified.**

Source: White, T. D. 1991. *Human Osteology.* New York: Academic Press, Inc.

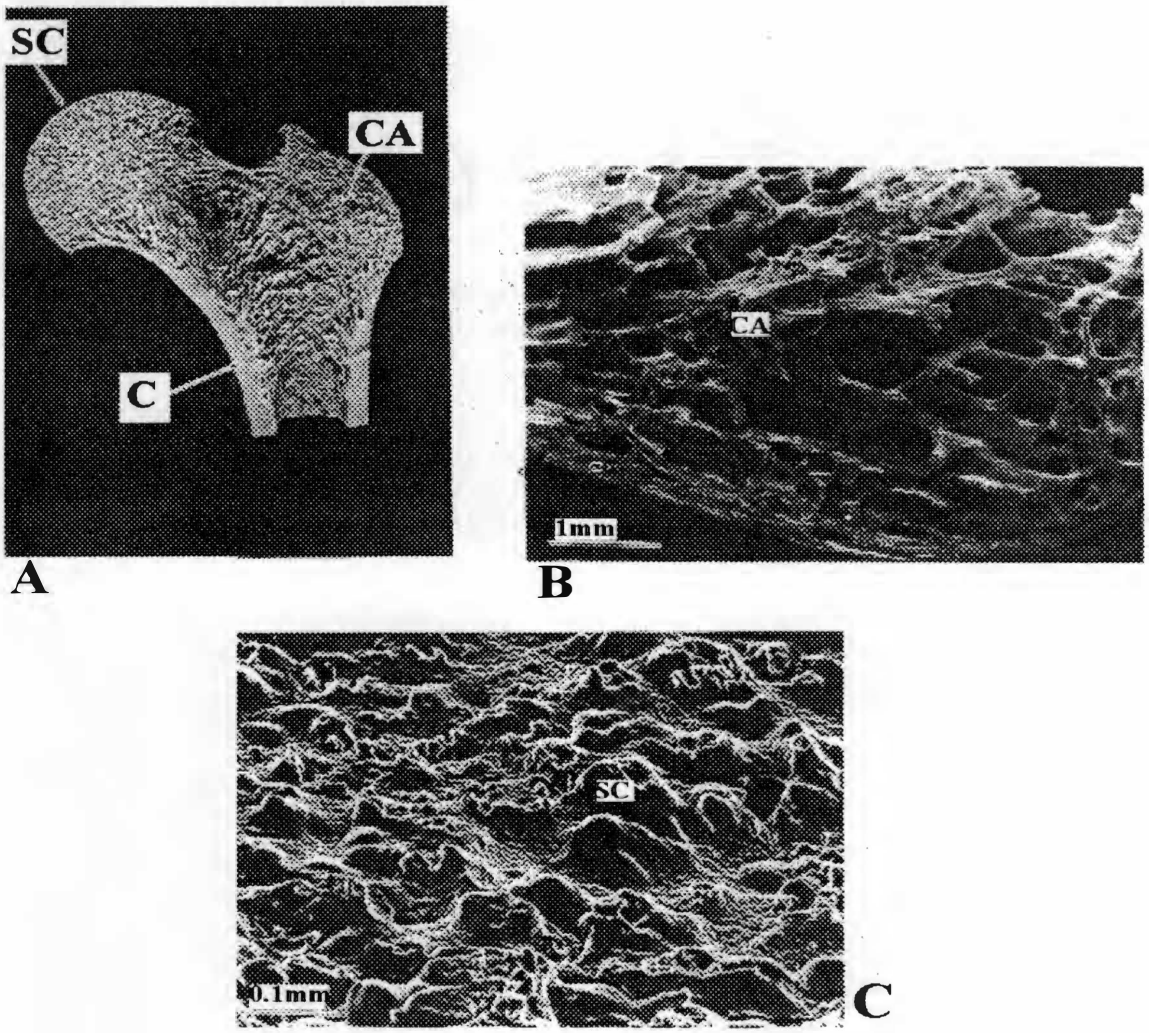


**Figure 2: Three major types of bone identified.**

Source: Shipman, P., A. Walker, and D. Bichell. 1985. *The Human Skeleton*. Cambridge: Harvard University Press.

within the bone (see Figures 3 and 4). The three types of bone are virtually indistinguishable at the microscopic level; except their relationship varies to the blood supply (Shipman, et al. 1985 and White 1991).

The development of new bone is regulated by the maturity and speed with which it is deposited. The new bone is formed from the calcification of cartilage at the epiphyseal plates at the metaphysis by the osteoblasts. During the process osteoblasts produce a protein enzyme which facilitates the calcification of the cartilage. As the process continues, the osteoblast is surrounded by layers and is transformed to an osteocyte. The three forms of immature or new bone are as follows: woven, laminar, and fine cancellous. The process follows with the woven bone being initially deposited in the developing fetus or when expeditious repairs are needed. Woven bone has primary surface characteristics, which have a coarse appearance (Shipman, et al. 1985 and White 1991).

The purpose of laminar bone when it is deposited in sheets or laminae is to facilitate rapid growth which occurs in the development of large animals (for example humans). The sheets of laminae help to incorporate the integral networks of blood vessels (see Figures 3 and 4) (Davis 1987; Shipman, et al. 1985; and White 1991).

The third type of bone, cancellous, is present for rapid growth in bones. It is found where stress upon the bone is requiring the body to reinforce the areas (see Figures 2 and 3) (Shipman, et al. 1985).

Distinctions can further be made between immature and mature bone, which is termed lamellar bone. Lamellar bone is distinctive from the immature bone due primarily to its interrelation between vascular canals and calcified tissue. It is organized into sheets that are 3 to 7 microns thick are organized parallel to one another. Lamellar bone appears in transection to be stratified (see Figures 3 and 4) (Shipman, et al. 1985 and White 1991).

Within the lamellar bone, a group of lamellae could be organized in two possible configurations, depending upon its location within the matrix. The basic unit is the osteon, which is formed by the laminae being laid down during bone growth and surrounding the osteoblast. The composition of an osteon has 15 to 20 sets of lamellae arranged in concentric lines surrounding it. Through the center of the osteon is the

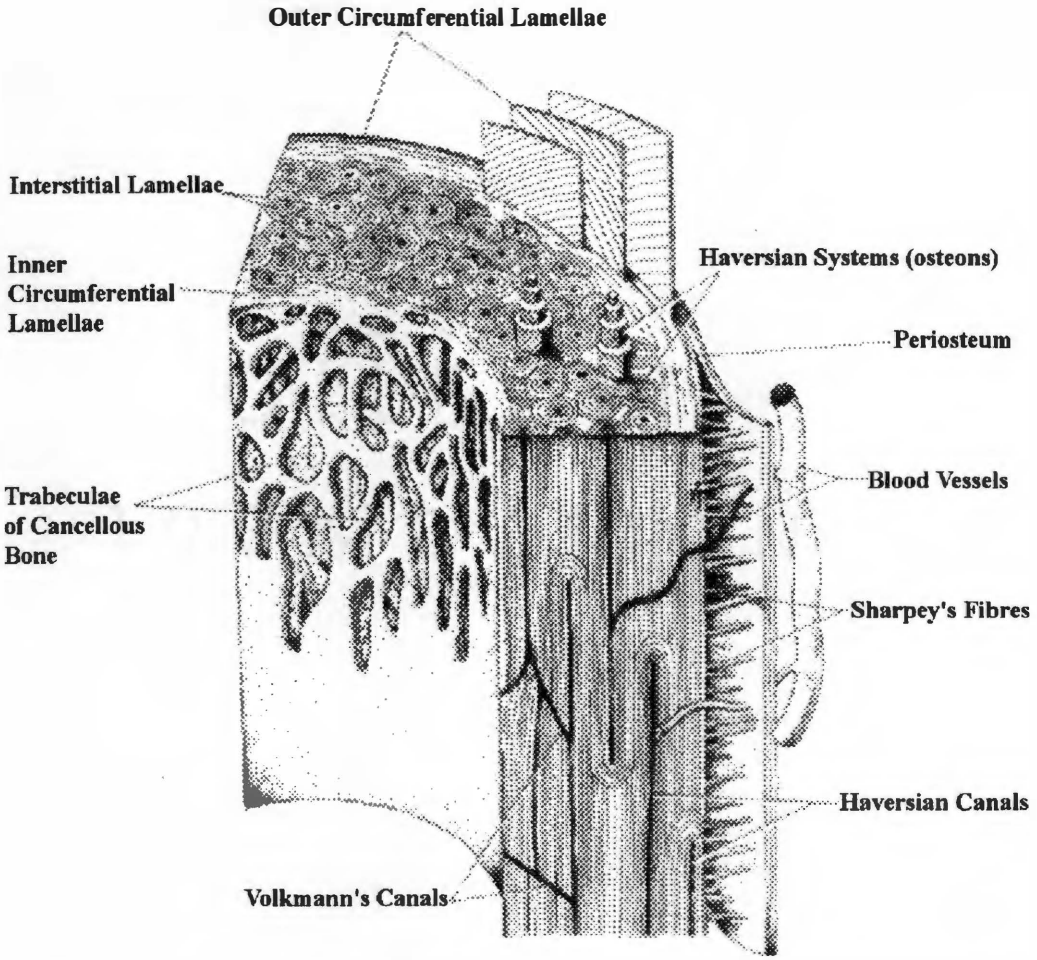


**Figure 3: The cross-section of long bone shaft illustrating the composition.**

Source: Davis, S. J. M. 1987. *The Archaeology of Animals.* New Haven: Yale University Press.

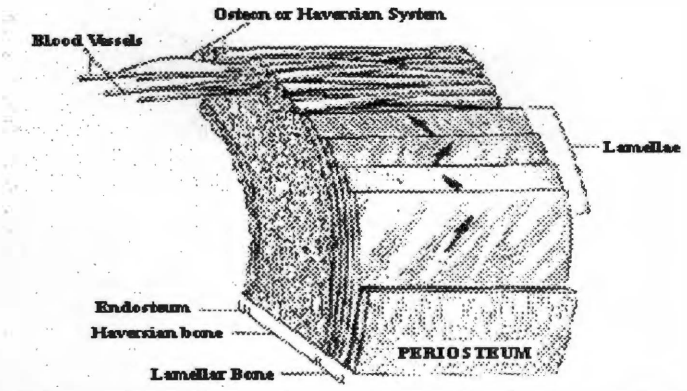


**Figure 4: A cross-section of a long bone shaft illustrating the positions of other structural features.**

Source: Shipman, P., A. Walker, and D. Bichell. 1985. *The Human Skeleton*. Cambridge: Harvard University Press.

vascular canal, which is part of a network known as the Haversian system. Through the vascular canal, a blood vessel carries nutrients within the bone. Surrounding the outer region of the osteon is a boundary or cement line. As an osteon ages, newer osteons will continue to be formed. Some of these newer osteons will cut across the cement line of the older osteon. As a newer osteon cuts the cement line, the older osteon is changed to a fragmentary osteon, which is known as obliteration during the reabsorption process. Some osteons observed microscopically will form an additional cement line surrounding them. These osteons are then considered "double-zoned." The osteons are located within a larger, irregular shaped material called interstitial bone. The interstitial bone is either earlier woven, laminar bone, or older fragmented osteons (Currey 1964; Currey 1984; Shipman, et al. 1985; and White 1991).

Within the Haversian system, two types of canals are found: the Haversian and Volkmann's. The Haversian are aligned parallel to the outer surface of the diaphysis, while Volkmann's canals interconnect the Haversian canals perpendicularly. Volkmann's differ from Haversian by not being surrounded by lamellae and they cut through the lamellae in the matrix (see Figure 3) (Shipman, et al. 1985 and White 1991).

Other structures found within the calcified tissue matrix are the outer and inner circumferential lamellae, which are adjacent to the outer surface of the bone, the periosteum, and the endosteum of the marrow cavity, respectively. Another structure is composed of bundles of collagen fibers which penetrate from the periosteum through the outer circumferential lamellae into the underlying interstitial tissue. These bundles of collagen fibers are known as Sharpey's or perforating fibers and their purpose is to attach the periosteum to the exterior surface of the bone. The Sharpey's or perforating fibers increase in frequency at tendon and muscle attachment sites (see Figure 3) (Shipman, et al. 1985 and White 1991).

The three major types of bone cells are the osteoblast, osteocyte, and osteoclast. The bone cell, which produces the new layers of laminae, is the osteoblast. As the osteoblast becomes enveloped by laminae, it produces a protein matrix, osteoid. The single cells which become embedded within the protein matrix and are single functioning cells called osteocytes. Whereas the function of the osteoblast is to produce new bone growth, the major function of the osteocyte is regulatory and it facilitates

communication with other osteocytes. The osteocyte is found within the lacunae of the osteon or Haversian system. The circumferential rings of the lamellae are composed of the lacunae and the canaliculi. Canaliculi form dendritic connections, a large multi-nucleated cell that link the lacunae within the lamellae. These dendritic connections allow an osteocyte to communicate with other osteocytes to regulate the bone. These circumferential rings surround the blood vessels within the compact bone and these are the osteons or Haversian systems. The osteoclast is located on the endosteal surface of the bone, adjacent to the marrow cavity. The osteoclast is recognizable from its location and scalloped appearance which results from bone being reabsorbed through the remodeling process (see Figure 5) (Cormack 1993; Enlow 1963; Freemont 1989; Hancox 1972; Shipman, et al. 1985; and White 1991).

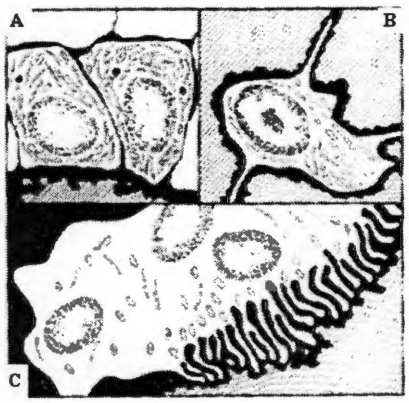


**Figure 5: Three types of bone cells are Osteoblasts (A), Osteocytes (B), and Osteoclasts (C), while the diagonal lines represent bone.**

Source: Shipman, P., A. Walker, and D. Bichell. 1985. *The Human Skeleton.* Cambridge: Harvard University Press.

Bone growth occurs as the process of new bone is created by osteoblasts and the gradual calcification of cartilage at the epiphysis. In addition, osteoblasts are created from cells in the periosteum. Bone growth continues in a process as new bone is deposited, which increases the breadth and the length of the long bone diaphysis increases. The bone growth ceases when the fusion of the epiphyseal plate with the diaphysis and the epiphysis (Davis 1987 and Shipman, et al. 1985) (see Figures 6 and 7).

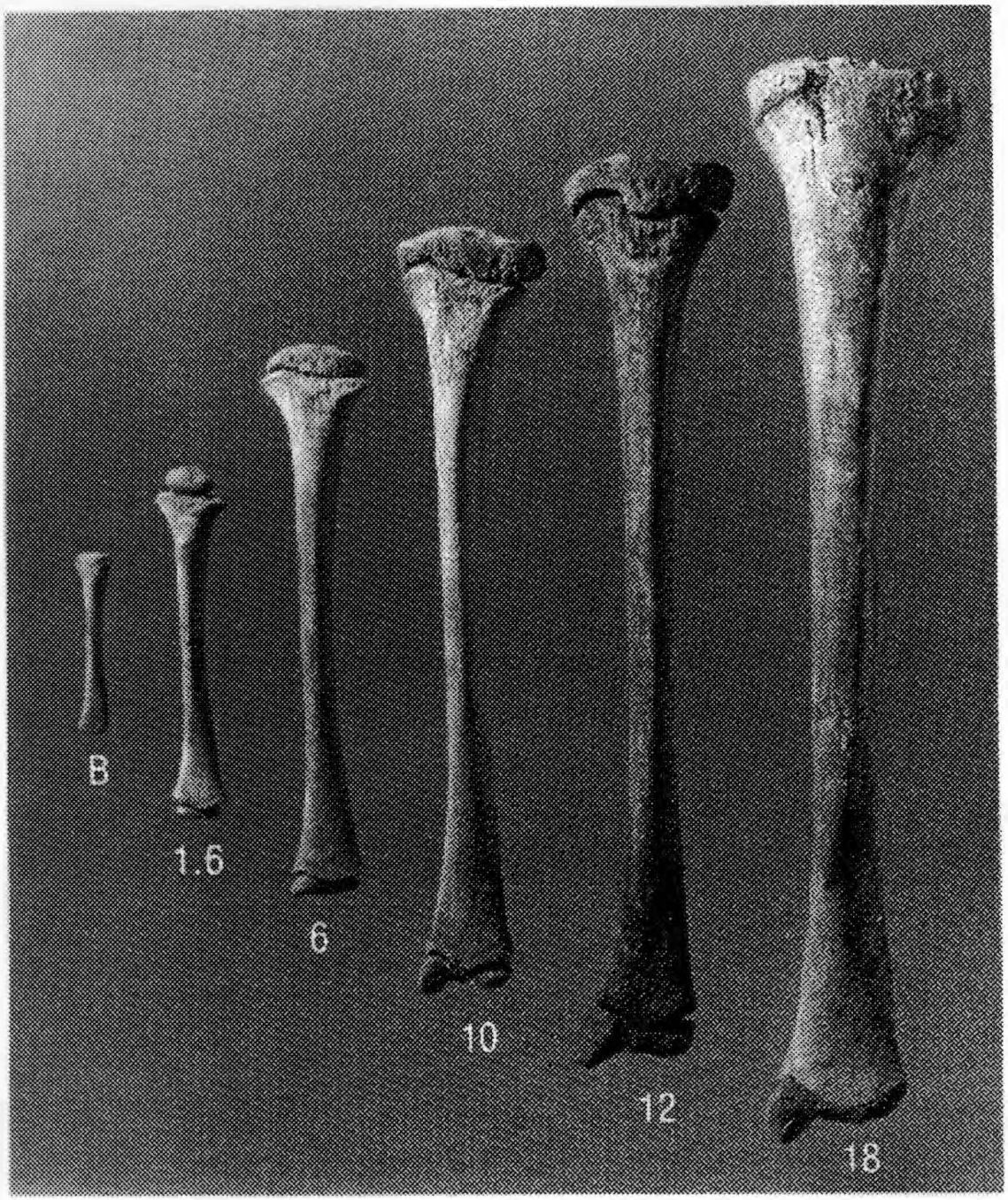


**Figure 6: Growth series of the left human tibia exhibiting the morphological changes from Birth to 18 years of age.**

Source: White, T.D. 1991. *Human Osteology*. New York: Academic Press, Inc.

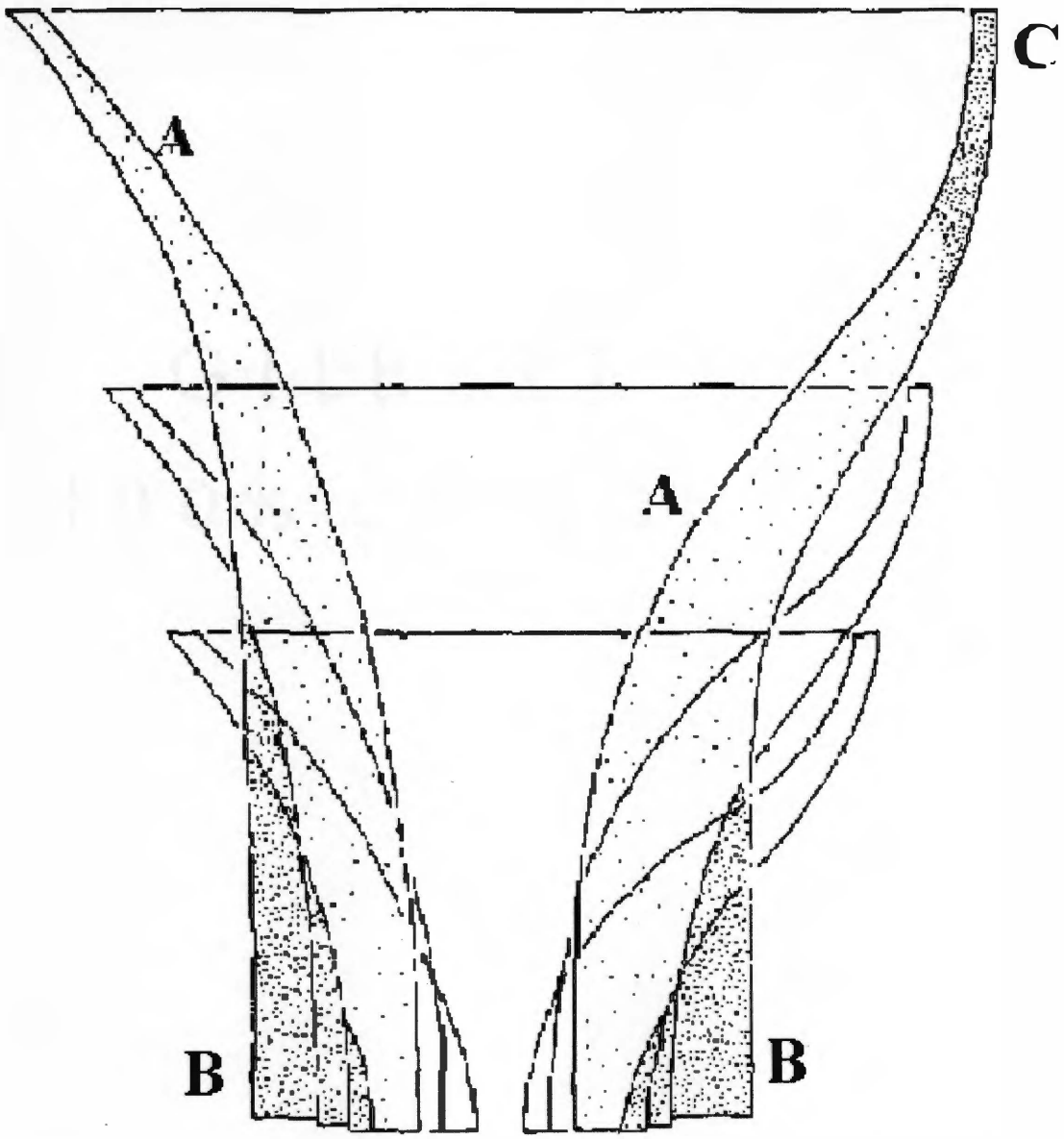


**Figure 7: Diagram illustrating the remodeling process of a long bone. Internal bone is deposited as the bone increases in length, while the circumference of the metaphysis (A) is reduced. At the diaphysis, periosteal bone (B) is deposited, which increases the diameter of the shaft, while periosteal bone formation increases (C).**

Source: Davis, S. J. M. 1987. *The Archaeology of Animals*. New Haven: Yale University Press.

## Review of the Histology Literature for Age Estimation

Kerley pioneered in 1961 the use of bone histology to estimate age in the human skeleton. Kerley's method used ground thin-sections from the human femur midshaft and examined four areas of the cross-section (see Figure 8). Kerley's method relies on four circular sections found in the anterior, posterior, medial, and lateral sections of the femur cross-section. The procedure would entail the counting of the osteons, fragmented osteons, percentage of lamellar bone, and non-Haversian canals in an attempt to estimate age. Absolute counts are made of the number of complete and fragmentary osteons and non-Haversian canals found in each of the four fields, and the percentage of the lamellar bone is calculated. These data are entered into the appropriate regression formula (Kerley 1961 and 1965). To estimate age the lowest of the high estimates and the highest of the low estimates for age are selected and the midpoint established (Kerley 1961 and 1965).

Kerley's (1961 and 1965) was revised to allow for the usage of different microscopes, which could have variations in field size (Kerley and Ubelaker 1978). The correct field size for the microscope can be established by simply dividing into the 2.06 $mm^2$ or 1.62mm diameter, as dictated by Kerley (1961 and 1965) and Kerley and Ubelaker (1978). Knowledge of the particular field of view (FOV) will allow repeatability in age estimation. The Kerley method is still the preferred methodology to follow in a forensic investigation (Bouvier and Ubelaker 1977; Kerley and Ubelaker 1978; and Stout 1992) (see Figure 8).

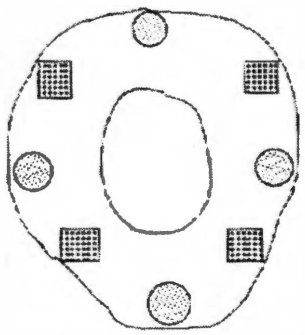

**Figure 8: Microscopic Field of View locations represented by circles (Kerley 1965) and squares (Ahlqvist and Damsten 1969).**

Source: Stout, S. D. 1989a. The Use of Cortical Bone Histology to Estimate Age at Death. In *Age Markers in the Human Skeleton*, ed. M. Y. Iscan, pp. 195-207. Springfield: Charles C. Thomas

In 1969, Ahlqvist and Damsten modified the Kerley methodology. They felt that muscle attachment along the linea aspira would contribute to differences in osteon and osteon fragments within the sampled areas of the femur. They selected regions using a square grid rather than a circular sample area for the femur (see Figure 8). Within the region they counted the Haversian versus the primary lamellar bone and averaged these percentages over the four fields. The standard error of estimation which Ahlqvist and Damsten (1969) achieved is slightly higher than Kerley achieved in 1965, and thus it is not as precise a method at determining ages.

Singh and Gunberg (1970) examined undecalcified and calcified thin sections in the mandible, femur and tibia and calculated the numbers of osteons and the average number of lamellae per osteon and the Haversian canal diameter. They indicate that close approximations of age can be obtained through regression analysis of multiple variables. Further, they conclude that larger studies need to be performed to determine if more accurate regression equations with histological evidence can be formulated. Unlike the imprecision due to subjective interobserver judgments, statistical statements could be performed upon defined structures of a histological sample. They indicated that the test of the reliability and validity of any methodology would need to allow different observers to arrive at comparable conclusions.

Ericksen (1991), Stout and Gehlert (1982), and Kerley and Ubelaker (1978) indicated that the size of the field of view is a potential area of methodological error. Kerley and Ubelaker (1978) address the concern of field size for employing Kerley's (1961 and 1965) regression formula by indicating the corrective factors which researchers should multiply osteons, fragmentary osteons, and non-Haversian canals. They indicate that the lamellar bone is unaffected by field size when estimating the percentage present within a sample. Stout and Gehlert (1982) investigated the field size suggested by Kerley (1961 and 1965) and the revised regression equations (Kerley and Ubelaker 1978) and they determined that the best scenario for accurate analysis was when the field size approximated Kerley's definition of field size. They indicated that the degree of accuracy was probably due to a close approximation of defined histological structures at that level of magnification. Additionally, structures are not uniformly distributed throughout the bone's cortex.

Stout and Stanley (1991) examined the merits of percentage counts of osteons versus osteon counts. They concluded that the preferred method for a sample would focus upon actual counts of osteons rather than percentage of osteons for the development of regression formula for age determination. However, they indicated that their study was to merely test the merits between the two techniques and a larger sample would be necessary to indicate whether their results were statistically significant.

Problems which have occurred within the Kerley methodology (1961 and 1965) are associated with the modification of the cross-section of tissue during grinding. The problems are the subjective decisions based on determining whether a osteon should be counted as a secondary osteon, a fragmentary osteon, or a drifting osteon. The main identifier of a drifting osteon is an elongated shape of its cementum border that appears to travel away from the center of the osteon. The difficulty of the defining characteristics and the percentage of an osteon present to be considered complete versus fragmentary is present. The method is manual, which requires a period of time to collect the data for analysis. The potential problem of inter-observer error also must be considered as the definitions for borderline osteons may differ between two observers (Stout 1989a; 1989b; and 1992).

Stout (1989a; 1989b; and 1992) presented an overview of the history of bone histomorphological investigations and methods of age estimation. The best method for age estimation was Kerley (1961 and 1965) and the revised method from Kerley and Ubelaker (1978). Cautionary advice was presented concerning factors which influence the reabsorption and remodeling rates of calcified tissue. These different factors are spatial variance, incoherence, temporal variance, interpersonal variance, metabolic disease, and methodological factors. Spatial variance refers to differences in metabolic disturbances that effect the rates of remodeling and the numbers of osteons. Stout indicates that metabolic changes could occur with Piaget's disease (Stout 1989a). Another factor concerns differences which might exist within the same sample. If a large enough area was not sampled, incoherence could result. Similar to incoherence, temporal variance is a broader factor which focuses upon overall changes that might have impacted the individual. For instance temporal variance might be related to alterations in diet, physiology, or metabolic rates. The temporal variance might be expressed differently in various portions of the bone histology

depending upon the skeletal element. Differences in interpersonal variance are related to differences between subjects. The factors that might occur due to physiological changes in one subject versus another subject. For example, differences in nutrition could lead to differences in skeletal structure (i.e., rickets). Metabolic diseases can act as factors which influence the remodeling rate within the bone. An example of a metabolic disease would be hyperparathyroidism, which would lead to overestimating age. The methodological factor is concerned with the proper selection of methodological procedure. The preparation of thin-sections, field of view (FOV) size differences, and selection of the sample areas. These are the difficulties that Stout (1989a) indicated could cause discrepancies in histological methodologies. By being aware of these potential influences, it assists the observer in minimizing error. Additional recommendations were the usage of complete cross-sections from a sample and the suggestion of using imaging technology to count the percentage of Haversian canals (Stout 1989a).

Ericksen (1991) researched the use of bone histology techniques in age estimation. The study determined that the best regression equations for estimating age were sex-specific equations based upon observable differences in patterns of osteons and fragmentary osteons. Ericksen acknowledges the criticisms of Stout (1989a) that inter-observer error due to methodological errors. However, Ericksen indicates that the problems can be solved through the creation of a permanent record of photographs which could be reexamined at a future date by other researchers. The positive benefits of a photographic record that Ericksen indicates include the ability to catalog, define, and classify the samples.

The proceedings of the Paleohistology Workshop held 3-5 October 1990 at Gottenberg indicate several suggestions and information in performing histological investigations. Garland (1993) indicated that the usage of histological samples from buried environments does not seriously compromise the calcified tissue. The cells were still observable for the purposes of examination. Further, the cremated bones of animals and humans were still distinguishable at the cellular level; except when the temperatures exceeded 700 degrees Celsius for longer than an hour (Harsanyi 1993). Hummell and Schutkowski (1993) investigated the ability of cross-sections of the midshaft of the femur to survive temperatures of between 400 to 500 degrees Celsius. Their conclusion is in agreement with Harsanyi (1993) that the shape and size

of the microstructures were still distinguishable after exposure to temperatures between 400 to 500 degrees Celsius. Thus, one potential source for the use of bone histology samples could be fire victims. The typical house fires occur generally between approximately 300 to 650 degrees Celsius (Mercyhurst College 1993). In addition, it has been found through cremation studies that microstructures do not undergo shrinkage until after 700 degrees Celsius (Ubelaker 1978). Thus, samples from burned bone fragments should be viable for analysis.

Uytterschaut (1993) indicated that a comprehensive comparison between Kerley (1965) and Ahlqvist and Damsten (1969) was still needed to ascertain which method is more reliable. An advantage that Uytterschaut addresses is microscopic methods utilizing fragmentary samples. The use of histological samples examined microscopically is useful in determining the presence and extent of bone pathologies. The techniques available have a range from manual to computer semi- and automated procedures (Uytterschaut 1993). However, during the same Paleohistology meeting, image analysis by computer was reported to be unable to identify calcified cells (Boivin and Meunier 1993).

## Review of Digital Image Technology: Development and Applications

Digital image analysis processing developed originally from the early 1960s when the National Aeronautics and Space Administration (NASA) was engaged in mapping the lunar surface for the Apollo Program. The technology has continued to advance with the advent of faster, smaller and more economical computers. Other applications were originally developed in the 1970s and 1980s for military use in image analysis from high-altitude photography, satellites, and improved navigational systems for aircraft. A timeline illustrates the development of computers as digital analysis systems (see Figures 9 through 13). Digital image systems first originated during the 1960s as part of the NASA (see Figure 9). These basic systems were expanded in the late 1970s with a transition to microcomputers and digital image processors (see Figure 10). In the early 1980s, frame grabber boards made their first appearances along with the microcomputer (see Figure 11). Image processing boards appeared in the late 1980s (see Figure 12). The 1990s technology increased efficiency and modular design (see Figure 13) (Baxes 1994).

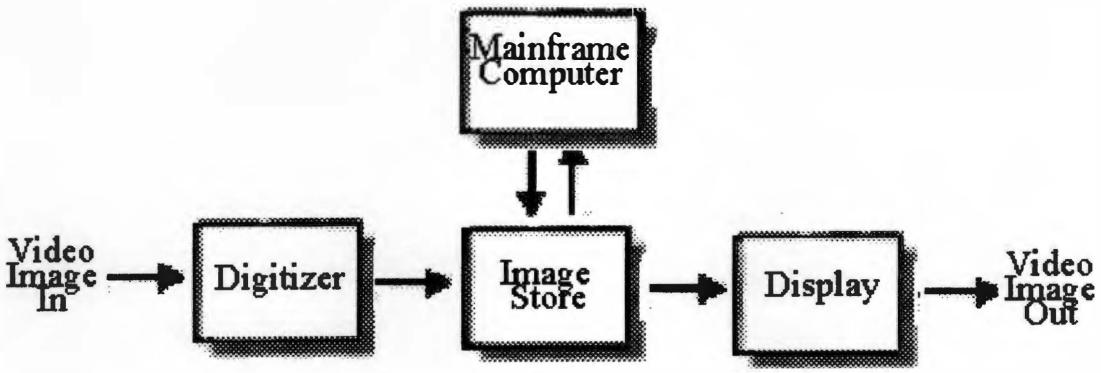


**Figure 9: Digital Image Systems existing during the 1960s.**

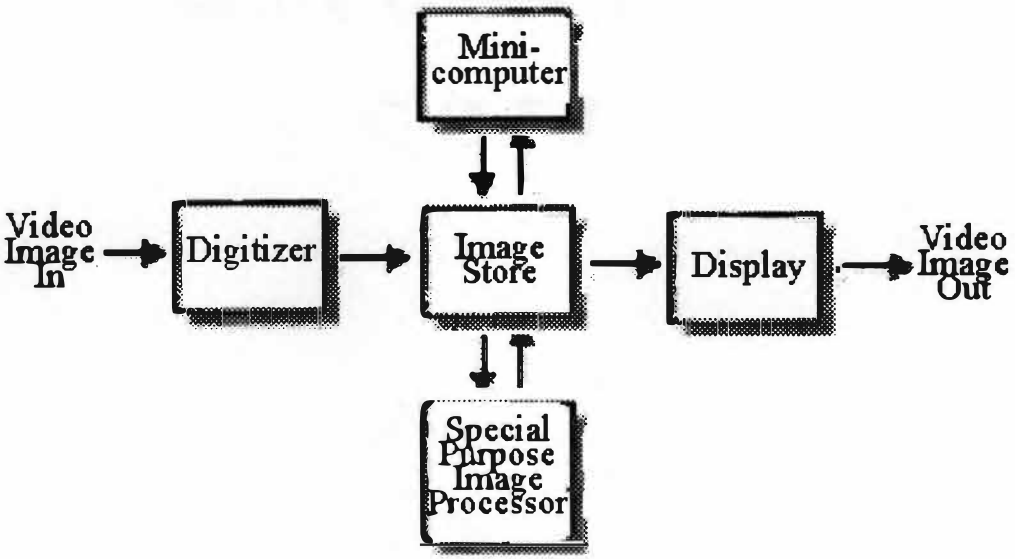


**Figure 10: Digital Image Systems during the Late 1970s**

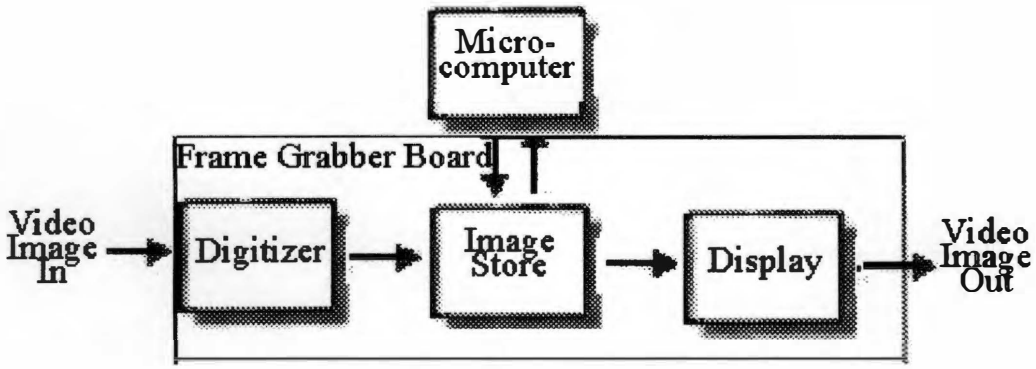


**Figure 11: Digital Image Systems during the Early 1980s**

Source: Baxes, Gregory A. 1994. *Digital Image Processing: Principles and Applications.* New York: John Wiley & Sons, Inc., pp. 248-50.

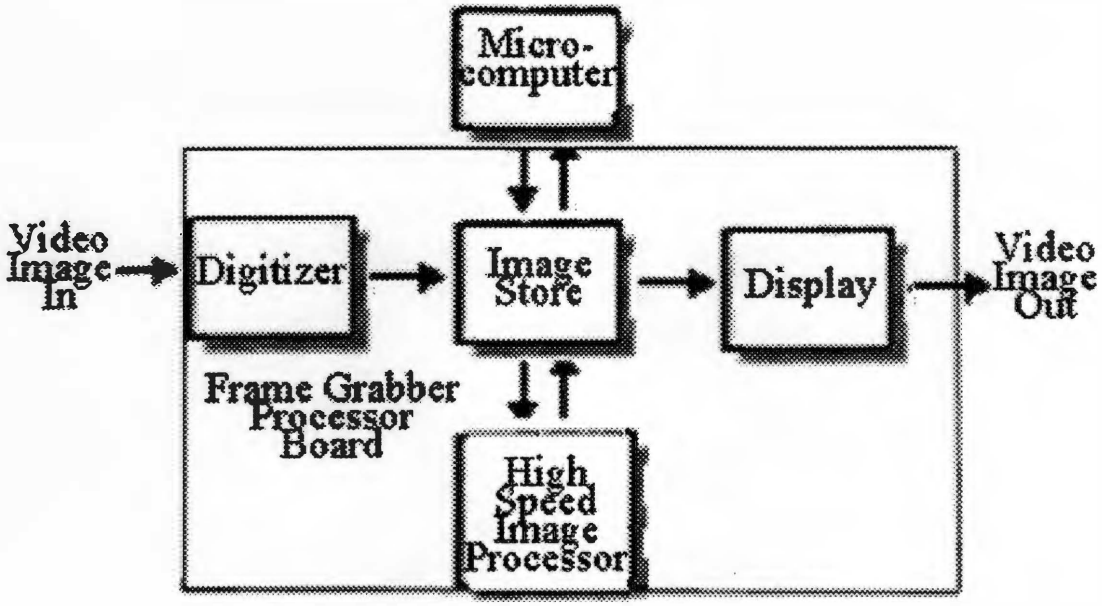


**Figure 12: Digital Image Systems during the Late 1980s**

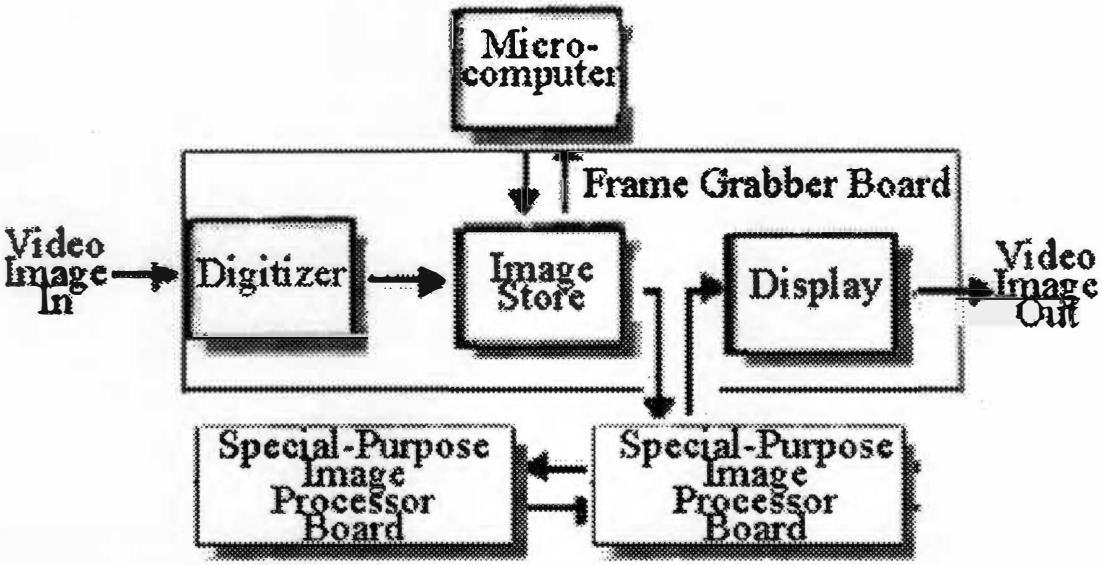


**Figure 13: Digital Image Systems during the 1990s**

Source: Baxes, Gregory A. 1994. *Digital Image Processing: Principles and Applications.* New York: John Wiley & Sons, Inc., pp. 248-50.

The advantages of utilizing digital image analysis have increased with the decreasing technological costs, time saved, and the increasing capabilities of the microcomputers and storage devices. Through the years, the use of computers to analyze analog signals, which have subsequently changed to digital, has been employed in a number of fields of research. These fields of research include the defense industry, medical technology, forensics, film, special effects, publications, resource management, weather forecasts, etc. (see Table 1) (Baxes 1994).

The advancements in the field and its applications will continue as technology is developed and better equipment is designed. The projects that utilized new technology at their inception are now faced with equipment that may be already obsolete. Until the late 1980s, controlling financial restrictions generally forced compromises within a research project which was focusing on digital image processing. However, high quality image processing boards and software are available at economical levels, which has permitted an increase in digital image research. Research applications based off existing digital image technology are now feasible without requiring development of the equipment for the research.

Early in digital image development the need for large mainframe computers was a necessity. However, the development of the silicon chip has lead to the development of portable, faster computers, which are also economical. The predictions for the late 20th and early 21st century are that new imaging technologies will help drive research in various fields. The question of whether or not a particular task can be performed using digital imagery or optics is no longer in question. The purpose of research now is how shall applications in a particular field be approached? If necessary data is incorporated into a machine vision process, what procedures for differentiating distinct objects will be available to researchers? The question is already being applied in forensics in the analysis of fingerprints. Medical research is using the technology to facilitate the automatic counting, analysis, and classification of biological structures (such as healthy versus cancerous cells, differentiating different shaped blood cells, or distinguishing between two or more types of bacteria) (Baxes 1994). Thus, it should be possible to utilize these technologies in the field of forensic anthropology.

**Table 1: The Current Applications for Digital Image Analysis**

| | | |
|---|---|---|
| 1. Biological Research<br>a. Image Enhancement<br>b. Bone, Tissue, and Cell Analysis<br>c. DNA Typing | 2. Defense/Intelligence<br>a. Image Enhancement<br>b. Reconnaissance Photo-Interpretation<br>c. Target Acquisition and Guidance | 3. Document Processing<br>a. Scanning, Archiving, and Transmission<br>b. Document Reading |
| 4. Factory Automation<br>a. Visual Inspection | 5. Law Enforcement Forensics<br>a. Image Enhancement<br>b. Fingerprint Feature Analysis<br>c. DNA Matching | 6. Materials Research<br>a. Image Enhancement<br>b. Material Feature Analysis<br>c. Surface and Structural Rendering |
| 7. Medical Diagnostic Imaging<br>a. Image Enhancement<br>b. Digital Subtraction Angiography<br>c. Computed Tomography | 8. Photography<br>a. Image Enhancement<br>b. Mulitiple-Object Scene Compositing<br>c. Special Effects | 9. Publishing/Prepress<br>a. Image Enhancement<br>b. Layout Compositing<br>c. Color Separation |
| 10. Remote Sensing/Earth Resources<br>a. Landcover Analysis<br>b. Terrain Rendering | 11. Space Exploration/Astronomy<br>a. Image Enhancement<br>b. Imaging System Deficiency Correction<br>c. Automatic Event Detection<br>d. Terrain Rendering | 12. Video/Film Special Effects<br>a. Multiple-Object Scene Compositing<br>b. Scene Creation<br>c. Special Effects |
| 13. Video Programming Distribution.<br>a. Video Archiving and Transmission | | |

Source: Baxes, Gregory A. 1994. *Digital Image Processing: Principles and Applications.* New York: John Wiley & Sons, Inc., pp. 7-11.

## The Development of Digital Image Analysis

In 1994, Dr. Sam D. Stout reviewed an Australian research paper which investigated the uses of digitized images in "A Morphometric Study of the Cortex of the Human Femur from Early Childhood to Advanced Old Age" by P. K. Bertelsen, J.G. Clement, and C.D.L. Thomas. In the study, Dr. Stout discovered an inability to differentiate osteons from canaliculi. In 1995, I communicated through e-mail with Dr. Stout to learn what his exact criticisms were. He explained that the 1994 research had fallen short due to its inability to differentiate between similar shaped histological cells. He also informed me that such research using digitized images is not completely ruled out, as long as it can differentiate between different cell types successfully (Stout 1995 Personal Communication).

Although the 1994 Australian study mentioned previously had current technology, the resolution of the camera (CCD) was 700 lines and the frame grabber that they were employing only had a resolution of 512 by 512. Another difficulty was that the software counted an absolute count of holes in the image without differentiating them (Bertelsen, et al. 1994). Both of these would appear initially adequate. However, based upon Dr. Stout's comments concerning their results, it would appear that more advanced imaging equipment was needed (Stout 1995 Personal Communication). The potential use of the microcomputer for analysis and data storage/retrieval cannot be underestimated by the rate at which computer technology has advanced even in the last year. Technology necessary for successfully examining digital images has existed since 1990. However, refinements within the program software have allowed for greater flexibility for researchers to create programs for data analysis. The ability to perform detailed examination on microscopic structures has now decreased in cost to make it cost effective and practical for use in the forensic setting. The different storage devices, such as magnetic-optical storage devices and hard drives acting as cartridges, allow the preservation of large amounts of digital imagery data. Further, their base cost, storage capacities of the types of drives, and price of storage media have reduced in price. One difficulty is being able to keep aware of new technical solutions to solve current problems with equipment. For instance, Sorbothane® which has dampening characteristics for vibrations is a recent development on the market in the last few years. One use of Sorbothane® is to eliminate vibration noise that might effect video signals (Sorbothane, Inc. 1996 Personal Communication).

However, the technology which Boivin and Meunier referred to at the 1990 workshop and was later published in 1993 are inadequate and focus on information which is out of date from the 1970s (Boivin and Meunier 1993). The technology, which will be used, made its first appearance in Global Image Lab™ version 1.0 in 1990 to early 1991. Global Image Lab™ version 1.0 contained a core program that specifically focused upon morphological and microscopy examination of digitized computer images. The present research project will employ Global Image Lab™ version 3.0, which became available in June 1994. The new version increased the statistical capability of the program and allowed the user to create module programs and macro-based programs (Pouliot 1994 Personal Communication).

The use of microscopy and photomicrography are entering a new field of analysis that holds several advantages over the traditional microscope photography. Through the new technology of electronic imaging, the specimen being examined no longer requires the use of chemicals or a darkroom (Smith 1994). A live image can be recorded through the use of a digital camera or CCD. The data collected for analysis is then entered into the computer via the graphic image analysis of a framegrabber card, and software will allow for efficient, accurate, and detailed analysis. The digital images can be stored for future reference on a magnetic-optical drive, a standard hard drive, or similar storage media. The most economical storage method is the usage of a ZIP™ Drive from IOMEGA, Inc., or a similar device. The color balance and contrast can also be handled electronically using the software package, as can filtering of the image to improve the resolution or imaging of particular details of interest. Other advantages which are present include the permanency of digital image storage, reproduction of the images, transportability of the system, and ability for future refinements by training the image identification macros with each additional specimen added to the database. Alternatively as new capabilities in software are developed, the existing data can be reexamined beyond the initial research.

The ability to examine bone histological samples still requires one to manually count or compare ratios of BSUs. However, if one were able to import data into a PC using a video frame grabber and image analysis software, one would be able to begin to automate the process. The continued advancement in expert system technology in software is also an important consideration. The software used in a forensic investigation would be beneficial if it could be calibrated and programmed to recognize individual and

particular patterns of objects (such as secondary osteons, fragmentary osteons, non-Haversian canals, and the percentage of lamellar bone) using known samples. Through the use of known samples, one could constantly refine the reliability of the software, which would allow increased validity of the results. The refinement of the software would be a gradual calibration of the macros to recognize the morphology (size and shape) of secondary osteons, fragmentary osteons, lamellar bone, and non-Haversian canals. Once the calibration was finished the software macros would enhance the efficiency of the absolute counts of the (secondary osteons, fragmentary osteons, and non-Haversian canals), as well as the calculation of the percentage of lamellar bone present in the FOV. The accumulation of scanned images would allow for the construction of a digital image database, which would allow for comparisons using statistical analysis in the future. Until the software was calibrated, such a system could act as a valuable instructional tool in the field and classroom.

## Digital Analysis Procedures and Techniques

There are four main procedures that are accomplished by a digital analysis system. These operations include the digitization, storage, displaying, and transfer of images. In addition, the images become the data, which can be manipulated to follow different classes of operations that include image enhancement, restoration, analysis, compression, and synthesis (Baxes 1994).

Among the procedures for image enhancement and restoration are modifications and manipulations of the image data known as filters. These mathematical alterations of data by the computer software allow for images, which suffer from noise, distortions, obscure features, etc., to be corrected. One procedure, which can be employed, is brightness slicing that allows the operator to perform a brightness histogram on the data. The data can then be examined to where the lower brightness values can be separated spatially from the higher brightness values. A similar method is used to obtain the optimal gray threshold of pixels for an image. Thus, an image that has faded due to higher pixel frequencies is adjusted, which will allow obscure features to become more easily discernible (Adobe Systems, Inc. 1994; Data Translations, Inc. 1994; and Baxes 1994).

Two filters that are commonly used in image analysis are the high-pass and low-pass filters. The high-pass filter highlights higher frequency pixels, which allows for a sharper image, a possibility of obscure or hazy elements to be easier to identify. The bright pixels are expanded slightly to create the effect. An alternative is a low-pass filter which alters the image by subduing higher frequencies, which might tend to obscure the low frequency details within the image. However, the edges of the image and broader details, such as distinctions between objects would become more apparent (Adobe Systems, Inc. 1994 and Baxes 1994).

Another procedure follows a general format of producing outlines of the objects within the image. Through the use of these procedures, it enhances the ability to measure, count, and classify different objects. Two of these operations are the Laplacian edge enhancement and the Binary skeletonized image. The Laplacian edge enhancement creates a highlight of the edges where they can be distinguished from all other aspects of the image. It has an appearance of a brass drawing found in art classes. The Binary skeletonized image is identifiable by the lines appearing to be elongated ovals. Other details are obscured using the procedure but overlapping objects are easier to distinguish (Adobe Systems, Inc. 1994 and Baxes 1994).

Other processes for distinguishing and highlighting the images are termed erosion and dilation procedures. Erosion allows for the subtraction of single pixels from an image, to reduce noise and increase the major features. On the other hand, dilation affects the image by dilating objects within the image. Thus, whereas letters under erosion might have noise holes removed from their interiors, the dilation would increase the relative size of the same letters in an image (Adobe Systems, Inc. 1994 and Baxes 1994).

Alternatives to these procedures allow for cleaning up the image, by doing both procedures sequentially. Thus, the opening, closing, top hat, and well transformations follow this general pattern. Their main purpose is to remove noise, while retaining object integrity within an image. The gray-scale opening procedure alters the image by erosion followed by dilation, while the gray-scale closing procedure alters the image by dilation followed by erosion. Both the opening and closing procedures function to remove noise spikes and improve the clarity of the image, while retaining the original shape. Major differences, however, exist between the top hat and well transformations. The top hat transformation allows the image peaks to be enhanced (i.e., the edges and line details), while the well transformation

enhances the valleys (i.e., the spaces between the edges and interior line details) (Adobe Systems, Inc. 1994 and Baxes 1994).

Functions that are available include the ability to perform feature extraction based on the color and brightness of features, texture, morphological measurements, boundary descriptions, and arrangement and relation of pixels. Image analysis can use these different aspects of an object within an image to classify and sort different categories. Further, these different functions allow for different styles of recognition to match a particular object with a particular category. Moreover, if practical object recognition and sorting into categories occur, one needs to go beyond defined, known features, so it would recognize a particular orientation and resolution of object. These categories can be programmed into macros which operate within the parameters of the software. By using image analysis tools to calibrate the morphological macros, the object identification can be based upon guidelines for specific objects that are of interest in the digital image. Thus, if a similar shaped object was depicted in an image but it has smaller dimensions, the software will recognize the object as it falls within a particular range, which is established by the researcher (Adobe Systems, Inc. 1994; Data Translations, Inc. 1994; and Baxes 1994).

The use of image compression is possible, but a low possibility of data corruption or loss due to the compression exists. By not compressing images, it is possible to retain the information without running a potential loss of data. Though depending upon the size and/or numbers of the image file(s), it may be a necessity to compress the image(s). Compression software should be used when transmitting data over internal networks or the Internet (Adobe Systems, Inc. 1994 and Baxes 1994).

## Conclusions

The review of the relevant literature indicates that a computerization of histological analysis would be definitely beneficial to age estimations based upon bone thin-sections. The difficulties, which have hampered such research in the past, have been associated with either the cost or the existence of adequate equipment to perform the analysis in this manner. The reason that the problem can now be addressed is that the equipment is available and is now affordable. Further the image analysis literature indicates that the question is not so much can it be done but when will it be done. The other aspect of the

research is still to prove how adequate digital analysis technology is in performing the task, but in addition what other related problems can be addressed and applications developed out of this research.

# CHAPTER III

# METHODS

## Equipment for the Research

The research equipment included a micrometer slide, 2 different computer systems, an IOMEGA Zip™ drive with 100 Meg disks, a 1600x flat field microscope, a PC Concepts flat surface mouse, an Edmund Scientific Video Coupler System, a SONY XC-75 (B&W) CCD camera, the Fidelity 200™ Frame Grabber card and Global Image Lab™ ver 3.0 software by Data Translations, Inc., the Adobe Photoshop™ ver 3.0 by Adobe Systems, Inc., and a sheet of Sorbothane® by Sorbothane, Inc (see Figure 14).

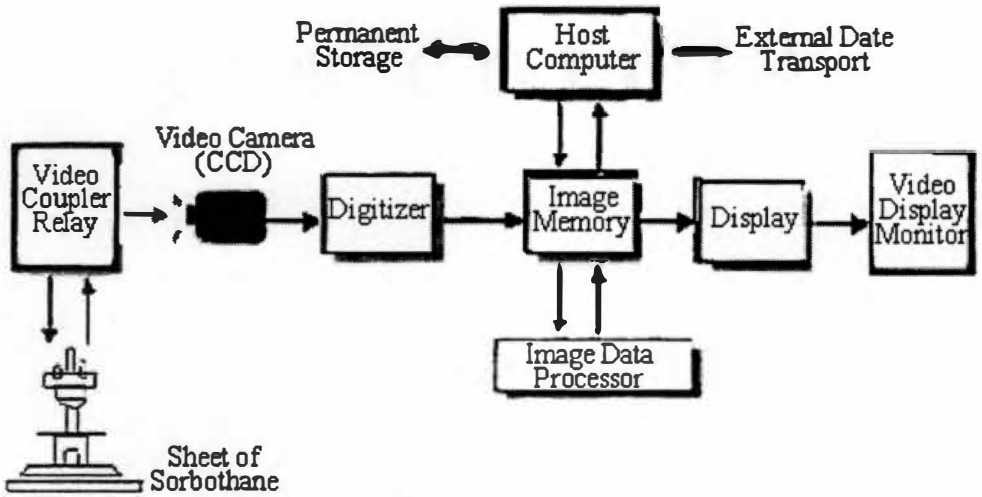


**Figure 14: Diagram illustrating research equipment setup.**

Modified Source: Baxes, Gregory A. 1994. *Digital Image Processing: Principles and Applications.* New York: John Wiley & Sons, Inc., p. 33

The micrometer slide was used in creation of a digital FOV to overlay across the FOV area, which was created by combining two of the images from one of the sample areas of a single slide (anterior, posterior, medial, or lateral). The FOV mask was created based on the article by Kerley and Ubelaker (1978).

The two computer systems used are referred to in the research as system 1 and system 2. System 1 is a 486DX4 100MHz with 16 Megs of RAM, which operates under Windows 3.1™, and it houses the Fidelity 200™ card with 2 Megs of memory. It also is used to operate the Global Image Lab™ software package. System 2 is a Pentium 120MHz with 24 Megs of RAM, which operates under Windows 95™ and uses the Adobe Photoshop™ software package.

## Digital Image Microscopy and Global Image Lab™ v3.0

The Data Translations, Inc., Global Image Lab™ software, is able to interface with a frame grabber card to allow for the analysis of digitized images. The capabilities of the software-hardware combination will allow for a practical application of the computer in the study of bone histological thin-sections. The software is able to do precise measurements of microscopic samples, alter the image and reduce noise that obscures details of the image, statistical tests can be performed, and macros can be written for automating the analysis procedure. Other features built into the program are an ability to use filtering procedures, which can separate overlapping objects, count objects detected automatically, and allow for user-defined searches of particular classified and sorting of structures.

One of the first Add-on Modules for the Global Image Lab™ will be a Densitometry application package, which will allow the measurement of optical density. Dr. Steve Symes during March 1994 agreed that densitometry could be useful at differentiating cells in an image (Symes 1994 Personal Communication). It will also allow for the correction of uneven illumination, which will increase the ability to improve the background of images. The Densitometry Add-in Module, was scheduled for release between the 2nd to 3rd quarter 1995, will be a simple matter to add to the proposed research procedure. A secondary purpose is its potential use in the forensic setting as a method of further differentiating human verses nonhuman remains. Currently, other software packages have been released as of 1998, which are similar in cost to the Global Image Lab™ but have more features built into their platforms, including densitometry.

## Adobe Photoshop™ v3.0

The Adobe Photoshop™ v3.0 by Adobe Systems, Inc., allows for the improvement of the image quality of the data captured by the CCD camera. Through importing the image file into the Adobe Photoshop™, it becomes possible to have the program process edge detection, sharpen the image, invert the image, remove noise, etc. Additionally, the size of the image file as presented on the screen can be manipulated to overlay with additional images for a larger overall image. The resulting data can then be saved as a single file to be exported to the Global Image Lab™ software for analysis and/or imported into a document as plates for illustration.

The difficulty normally associated with the overlaying of images is based on the inability to decrease the size of the image and increase the background surface that the image is presented. However, the Adobe Photoshop™ allows the researcher the ability to manipulate both of these variables, which makes the overlaying of entire sections a possibility.

Another difficulty, which occurs even utilizing a flat-field microscope, is that the field of view is often not illuminated to the same degree across the entirety of the image. Thus, the researcher needs the capability to equalize the lighting of the data through the manipulation of contrast and brightness. The Adobe Photoshop™ and other similar image processing packages can equalize lighting across the image, if needed. However, these operations can also lack some of the ability to equally examine the features of importance. As a result, the image will be improved to allow meaningful data to be analyzed, even if illumination of features was initially inadequate. Additionally, edge detection can be performed either independently or in conjunction with one of these operations, described above. Then the observations by both observer and software analysis can be performed with greater expediency and efficiency.

The morphological differences between the secondary and fragmentary osteons could be managed using the Global Image Lab™ by knowing what the changes are and training the software to recognize differences in morphological changes. In addition, Adobe Photoshop™ or similar image processing software could be used to lessen image problems that might result.

## Other Equipment

The IOMEGA Zip™ drive was necessary to communicate the data files efficiently between Systems 1 and 2. The Data Translations' products were discovered to be incompatible with Windows 95™ operating system.

Initially, two products manufactured by E. G. & G. Reticon were considered in the original research design, the E.G. & G. Reticon MC2013 Analog Camera and its controller board. However, due to lengthy and unresolved technical difficulties and incompatibilities with the Data Translations' products, a SONY XC-75 CCD was used for acquiring the image data. The Sony XC-75 is similar in characteristics to the E. G. & G. Reticon CCD initially considered for the research. Whereas the E.G. & G. Reticon CCD would need to have the light and dark settings calibrated using frame averaging, the SONY CCD had an automatic gain setting of the video signal. Additionally, the SONY XC-75 is more economical in cost, dimensions, and setup time.

A sheet of Sorbothane® is placed under the microscope to eliminate the vibration noise, which is generated by the computer systems due to their proximity to the microscope and CCD. Sorbothane® was developed with a unique combination of physical properties, which consist of viscous damping and elastic memory elements. These characteristics allow the Sorbothane® to withstand structural changes, as well as minimize vibrational frequencies transmitted through its structure. Its original development was within the electronic and computer industries as a development against shock and vibration for equipment (Sorbothane, Inc. 1996 Personal Communication).

The procedure for acquiring the images will employ the use of a 1600x Flat-Field Trinocular microscope, which is fitted with an Edmund Scientific Video Relay system to the Sony XC-75 CCD camera. Its purpose is to securely connect the microscope to the CCD, while at the same time helping to focus the light from the microscope onto the sensors of the CCD. The XC-75 CCD is capable of 768 by 494 resolution.

These images are then delivered via an RS-170 cable to the Fidelity 200™. From the Sony XC-75 CCD camera, cables carry the analog signal to the 486-DX4 100Mhz (System 1), where the Fidelity 200™

frame grabber card translates the analog signal from the camera to a digital signal for the computer. The images captured are stored to disk and analyzed utilizing Data Translations' Global Image Lab™ v3.0, a software package for image analysis. The images which are captured in sections with the camera are imaged enhanced using the Adobe Photoshop™ v3.0, where the images are saved for analysis by the Global Image Lab™ software routines. The Adobe Photoshop™ manipulates the image data on a Pentium 120 MHz with 24 Megs of Ram (System 2).

The advice of Dr. Dwayne C. Savage, the Department Head in Microbiology at the University of Tennessee, was sought as to the type of microscope for the research. He indicated that the key difference between an achromatic microscope and a flat-field microscope was based on the correcting of the prismatic effect at the field of view boundary. The flat-field microscope will have more precise lenses, and the samples viewed will not be distorted at the boundary of the field of view, as in the achromatic (Personal Communication 1995). Thus, one's ability to successfully obtain a flat, nondistorted image is possible, which is crucial for digital image research. If one uses an achromatic, then one can control the distortion with mathematical manipulation of the acquired image, but it can be time-consuming.

The research utilized a microscope equipped with illumination controls, which include an adjustable condenser, iris diaphragm, and illuminator rheostat, which will help ensure that high quality images were examined due to proper illumination of the sample. It also employs parfocal quadruple objective nosepiece to allow for changing the power without refocusing the microscope, which allowed for viewing of details in the same field of view without losing the targeted region of the sample. The importance of maintaining the same viewing conditions between samples, due to illumination and maintenance of the target FOV, is important to maintain a specific FOV between different samples.

The sample examined will have its image fed directly to the System 1, which has the frame grabber card. As entire cross-sections will be eventually scanned, the individual digitized images would be linked and merged to form a complete cross-section with the aid of the computer and the image processing software. The current research combined two images by overlaying them to create an area, which would contain the FOV, as described by Kerley (1961 and 1965) and revised by Kerley and Ubelaker (1978). The

Fidelity 200™ will allow for the analysis of the image by the Adobe Photoshop™ and Global Image Lab™. As the images are accumulated, the research will allow for calibration of the image recognition software and the creation of macros to perform the tasks with increased precision and efficiency. Thus, one of the eventual goals of the present research will be the eventual elimination of manual counting and comparison of histological samples.

The current focus of the research will simply employ the 4 FOV indicated under Kerley (1961 and 1965) and Kerley and Ubelaker (1978) (see Figure 8). The correct field size for the microscope can be established by simply dividing into the 1.62mm. Knowledge of the particular field of view will allow one to follow the identical procedure used for age estimation. The primary reasons for using the Kerley (1961 and 1965) and Kerley and Ubelaker (1978) methodology are based upon the literature that it is the most accurate and the amount of time and storage media required for an entire cross-section for each sample is not practical at this point in the research. Though the technology is now becoming more accessible, the image storage for archival purposes would recommend the use of recordable CD-ROMs and the memory for displaying the images would exceed 64 Megs of RAM.

As the database obtains a larger sample size population, it will be possible to perform regressional statistics upon the calibrated data and compare these results with the current regression equations (e.g., Kerley 1961 and 1965; Ahlqvist and Damsten 1969; and Ericksen 1991). The field size for the video-microscope will employ the revised methodology for field size adjustment (Kerley and Ubelaker 1978). Although based upon the literature review that the Kerley and Ubelaker method is the most accurate, a future focus will be in comparing the other methods to it, when a larger sample has been assembled. These methods will be compared to the results obtained from a regressional study of the data from the database in order to see if the standard deviation in these other methodologies can be refined to a greater precision. Once the databank has been calibrated to recognizing known samples, contributors could then use the calibrated database for analysis of unknown samples.

## Selection of the Sample

The procedures and morphological discrimination, counting, and management of the images was first performed on thirty (30) prepared slides from the Anthropology Forensic Center at the University of Tennessee Knoxville (see Table A-1). In addition, sample data was received and permission given to use the data from Dr. Sam D. Stout, which consisted of eight-four (84) records of known ages (Table A-2). These known samples assisted in the initial creation of a base line from which the research could expand. One of the current points, besides testing the age estimation techniques, is to determine the most efficient methodology for handling larger samples via collecting, storage, and analysis of the data.

## Procedure for Additional Samples

Once the system is calibrated, one could test it on additional known samples to determine how accurate age estimations from digital images are, when compared to the manual counting method. Previous communication with Dr. Steve Symes in Memphis offered the opportunity to obtain known cross-section samples of the human femur for a sample population (Personal Communication 1994). Further samples could be added through donated samples from other institutions, forensic scientists, medical hospitals, and samples prepared by the researcher. For these submissions as well as samples prepared by the researcher, a standardized protocol would need to be established for location, physical dimensions of the unprepared cross-section, and method/manner of shipment. With a protocol established variation between submitted samples might be controlled better. Further preventive measures will include that submitted samples be from the midshaft of the femur and approximately 10 to 20 mm in thickness to add protection during transit and allow for the preparation of two cross-sections from the same known sample. The nondecalcified thin sections will be prepared according to the literature (Ubelaker 1974; Ubelaker 1978; and Stout 1989b). The procedure will attempt to control for spatial variation with which Stout and others have expressed concern.

Future contributions initially would begin with a cross-section from the femur's midshaft to the previously mentioned dimensions. The section is first cleaned using an ultrasonic cleaner and exposed to an oxidizing agent, Decal. The section is immersed in water in an ultrasonic cleaner for approximately 5 minutes and allowed to dry overnight. The section is placed within an embedding agent, which

impregnates the block within a vacuum chamber. The previous process helps prevent the specimen from developing indistinguishable features. Once impregnated, the section is dried overnight at approximately 55 degrees Celsius. Afterwards the embedded section can be prepared on a microtome, using a sectioning blade. The cut sections are then polished using a polishing compound. The polishing allows for a greater uniformity to the surface thickness to the prepared sample. After polishing, they are mounted and a cover slip is secured over the sample (Ubelaker 1974 and Stout 1989b).

## Description of the Method

The location of the sample from the femur was noted from the description on the slide. The correct facing and orientation was determined by notation on the slide or due to lack of notation by the shape of the curvature, whether posterior or anterior. Thus, all the samples could be positioned in the same manner. All the slides indicated that they were from the left femur of subjects, which was noted on the research notes from the Anthropology Forensic Center and the slide labels. The areas were noted in the positioning of the samples on the microscope stage (see Figure 8) (Kerley 1965 and Kerley and Ubelaker 1978). These 4 FOV areas, corresponding to the tangential sections, were aligned under the microscope.

Each selected area was focused using both the microscope and the computer monitor. Initially the microscope was used to focus on the target area of the sample. Then the fine adjustments were performed using the microscope, while observing the computer monitor. Once the image was successfully positioned and focused, a screen image of the displayed area was captured using the camera and the file was saved to the ZIP™ drive on System 1. Later these images could then be transferred to System 2 for the image manipulation under Adobe Photoshop™.

After the first image of the selected area was captured for a particular sample, the stage was moved slightly until it was positioned so that 75% of the displayed area was different from the initial image. This was found necessary as the FOV determined by Kerley and Ubelaker (1978) is slightly larger than would be displayed on the computer monitor. Since 25% of the first image's structures are found on the second image, it allowed for their successful overlap later in the image analysis process. The best

method was found utilizing the Adobe Photoshop™ program by using different layers and overlaying them to obtain a blended image (see Technical Note 1).

## Technical Note 1: Procedure to Combine Images

1. The first image, which is to be combined with the second image, is opened and then determine where the location of the image should be positioned on the enlarged canvas (see Plate 1).
2. The canvas size of the base image is increased to 11" by 11", while maintaining the image size positioning with the 1st image in the center-top of the canvas (see Plate 2).
3. Open the 2nd image to be added to the canvas (see Plate 3).
4. Outline the area with the Magic Wand tool, copy the image and paste layer as normal (see Plate 4.
5. Use the DIRECTIONAL movement tool to align the images over each other, the opaqueness scale between the two images can be lessened to make sure of the positioning of the two images (see Plate 5).
6. Once the two images are positioned correctly, then the mask, which has a diameter of 1.62 mm., can be positioned over the merged image. The FOV mask file (see Plate 6) is opened, copied, and pasted in a similar manner as with the 2nd image; except that OVERLAY is selected.
7. Position the FOV mask over the two images, which have been combined, by using the DIRECTIONAL movement tool (see Plate7). The image is then darkened, by decreasing the brightness of the image, to allow for the details to be visible (see Plate 8).
8. Save the image of the two blended images with the overlay of the FOV mask under a different file name.

The process of combining the images by overlay is important. Although System 2 was able to manipulate any of the images due to its greater memory capacity, System 1 has a maximum of 2 Megs on

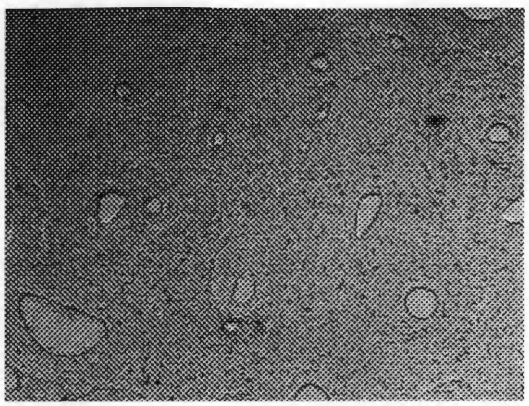

**Plate 1: The first image is opened in the combination sequence.**

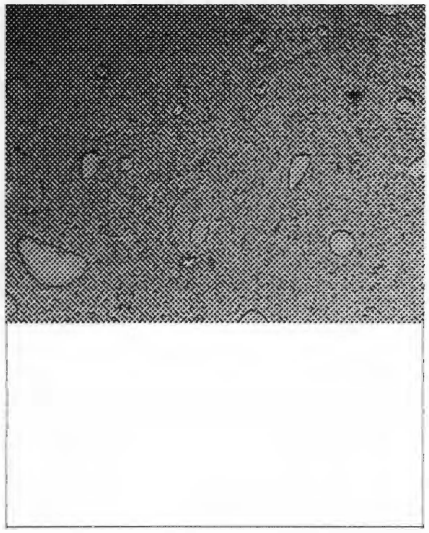

**Plate 2: The canvas area is enlarged with the first image present.**

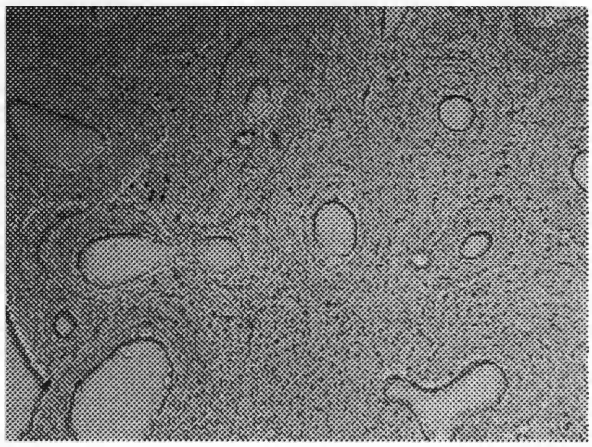

**Plate 3: The second image is opened in the combination sequence.**

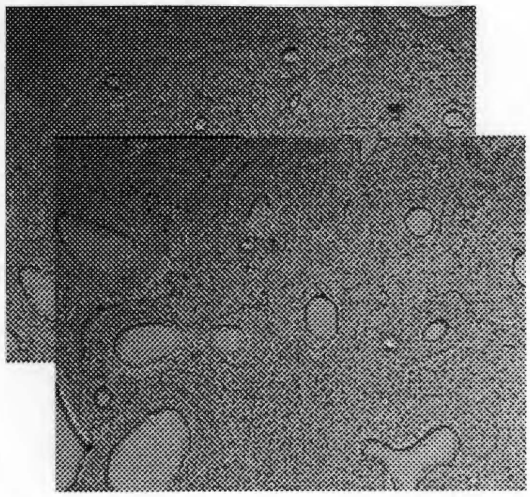

**Plate 4: Overlaying the first and the second images in the operation.**

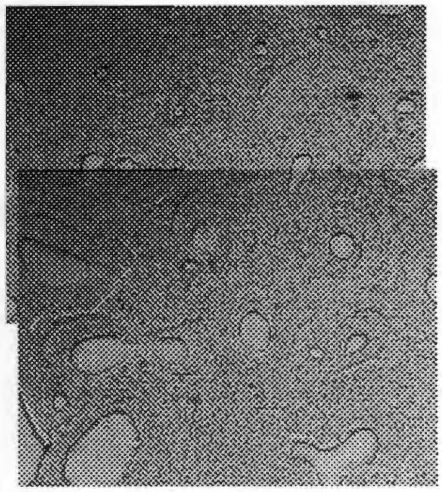

**Plate 5: The first and second images are aligned properly.**

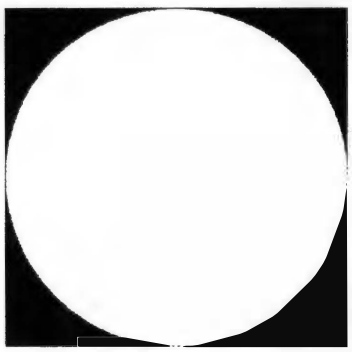

**Plate 6: The FOV Mask is opened.**

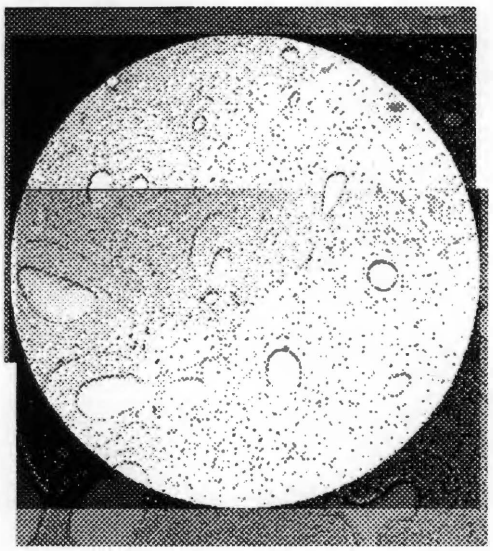

**Plate 7: The FOV Mask is positioned.**

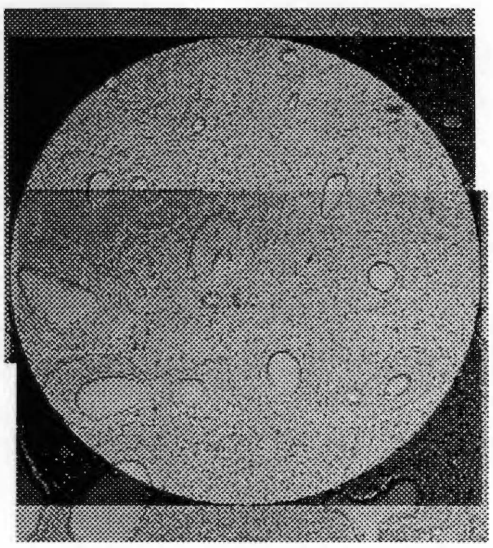

**Plate 8: The brightness is altered.**

the Fidelity 200™ for image manipulations. To obtain increased flexibility an upgraded video capture card and software package are required for future expansion of the data (see Technical Note 2).

## Technical Note 2: Procedure for Acquiring the Images.

1. Each sample has two images, which overlap each other taken in each of the following locations of the slide (anterior, posterior, medial, and lateral). These locations follow the procedures defined by Kerley (1965) and Kerley & Ubelaker (1978).
2. These overlapping sections are carefully combined together and a circular FOV mask was positioned over them, then the combined image is saved in this configuration (see Technical Note 1).
3. In order to have the Global Image Lab™ analyze these combined images, it is necessary to reconvert the PSD file format (e.g., Adobe Photoshop™) to the TIFF file format (e.g., Global Image Lab™). The description of the acquiring the image is mentioned earlier under the beginning of the Description of the Method section.
4. To see the entire image using the Global Image Lab™, it is necessary to select under the preferences of the program that the dimensions of the displayed image be set to 1240 by 780 with the software acting as the controller.
5. A negative image is then taken of the displayed location of each sample and saved.
6. Through the use of minimum and maximum ranges of gray scale it is possible to gain a better distinctive image of the particular section of the sample.

An alternative method using Adobe Photoshop™ is to select the tool under the IMAGE menu called Adjust, then select the Brightness/Contrast tool. Then the user can modify the image displayed on the monitor by varying degrees of brightness and contrast, either in the positive or the negative direction. During the procedure, it was found that most of the images appeared over exposed, which meant that the brightness had to be reduced. For most images it was found necessary to decrease the brightness of the image by selecting -100 on the brightness scale. The following are two images showing a before (see Plate 9) and after (see Plate 10) of the same image.

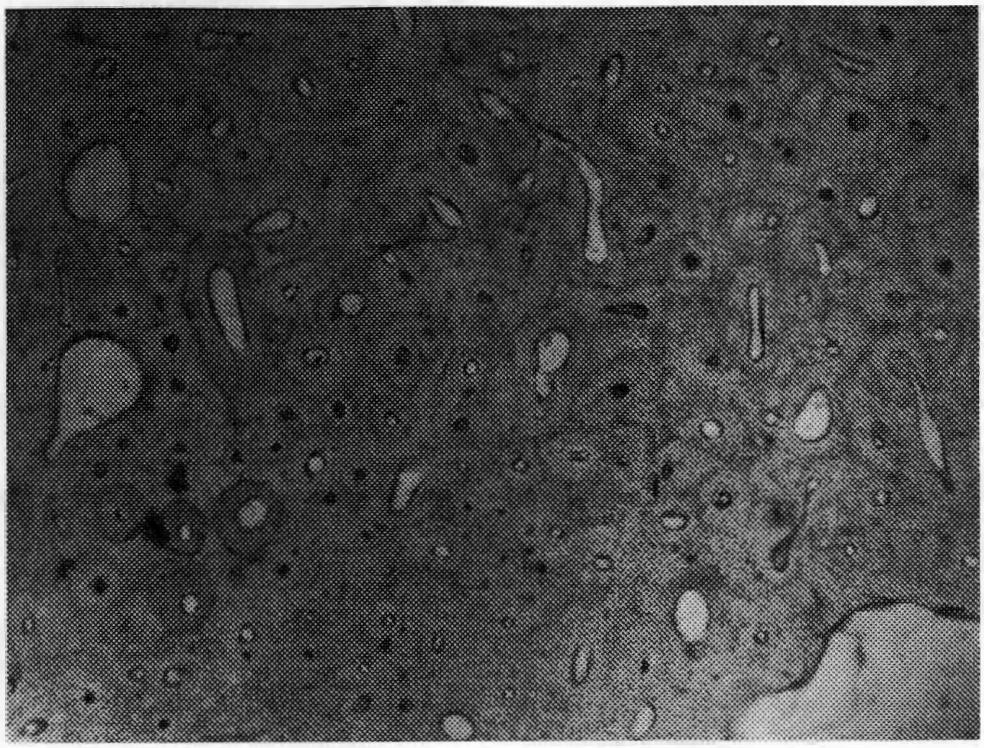

**Plate 9: An image displayed without modification at 100x.**

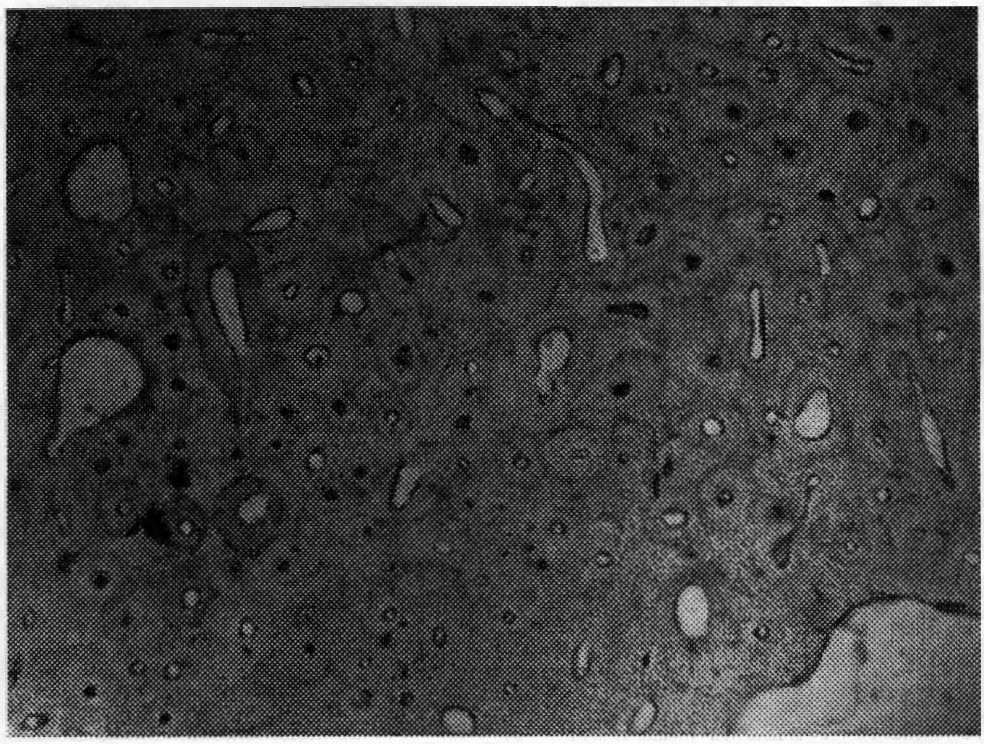

**Plate 10: The image from Plate 9 with illumination adjusted.**

One can use the Adobe Photoshop™ to obtain a better indication as to the structures by increasing the magnification of the image on the monitor. The process will maintain the majority of the detailed features of the FOV. However, if the image was focused to greater than twice normal viewing on the screen, then details were less visible and appeared blurred. It appears only possible to use the magnification tools on current images that have been saved as files. However, live shots can be set to a higher magnification on the microscope to achieve a similar effect.

## Field of View (FOV)

The creation of the proper FOV for the combining of the overlapping images was achieved by using a calibrated micrometer scale on a microscope slide (see Technical Note 3). The image of the line was taken and then transferred to Adobe Photoshop™ on System 2. During the process, special care was taken to maintain the same scale between the images. The line was extended using the copy and paste function of Adobe Photoshop™, and the copied section was positioned at the end of the line to extend the line to the required length. The required length is dictated by following Kerley and Ubelaker (1978) recommendations as to the FOV. With a known diameter of the FOV, it makes it possible to determine the area for the total FOV as it relates to the pixels of the image. The comparison process later is used to determine the correct percentage of lamellar bone in the images during the data collection.

### Technical Note 3: FOV Mask Procedure

1. The procedure requires the use of a micrometer slide, which has one centimeter measured out in calibrated units of 100 microns. An image was made of the slide (see Plate 11).
2. The second step was to utilize the magnification tool and copy and paste features found within the Adobe Photoshop™. The line was thus extended out to 1.62 mm. The diameter of the circle is from the work of Kerley (1965) and Kerley and Ubelaker (1978) (see Plate 12).
3. The image was saved with the extended ruler measurement. The image was then imported into Corel Draw™, where a circle was placed over the exact ends of the ruler. Thus, the FOV circle was created to the exact diameter of 1.62 mm. The image was saved (see Plate 13).

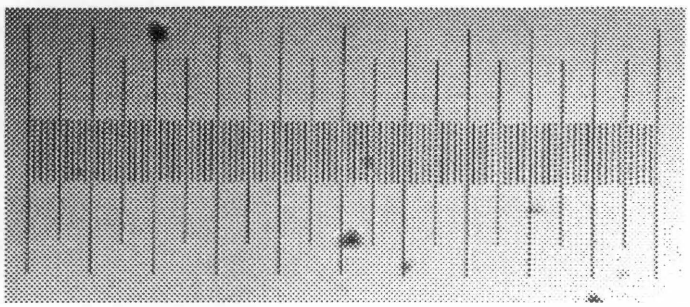

**Plate 11: An image of the micrometer slide used with calibration marks.**

**Plate 12: An image displaying the extended ruler measurements to 1.62 mm.**

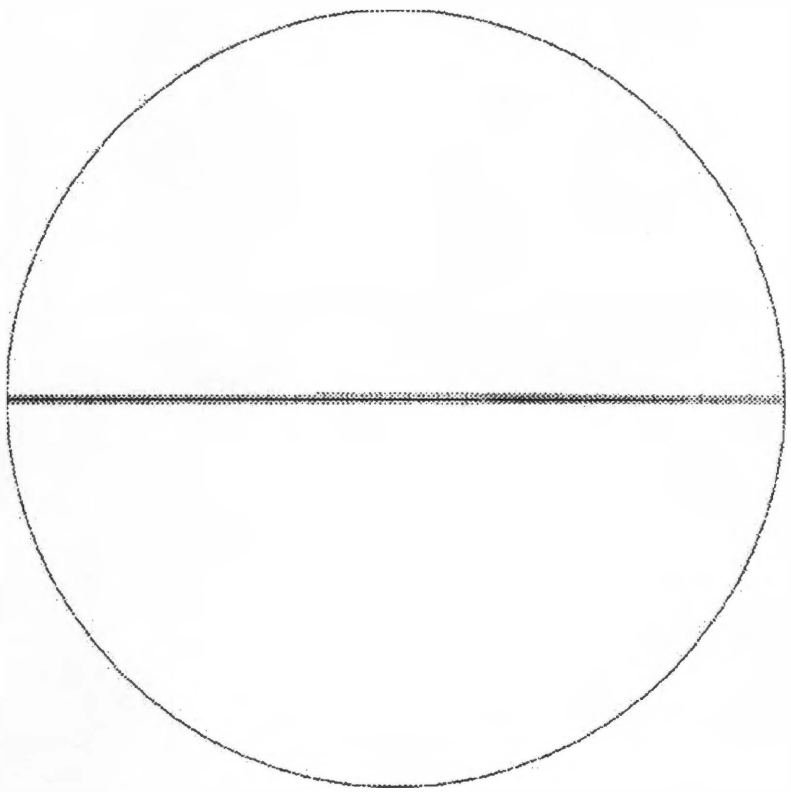

**Plate 13: FOV circle aligned with the extended ruler to create the FOV mask.**

4. The image was imported back into Adobe Photoshop™ and the ruler was removed from the interior of the circle using a digital eraser, and the image was saved again. It was found that if the ruler image remained within the confines of the circle that the MASK feature would not function properly (see Plate 14).
5. When the procedure requires the FOV mask, open FOV mask file. Then the WAND feature is used to highlight the edges of the circle, and the quick MASK feature is used, which results in the exterior of the circle turning black, while the interior of the circle remains white (see Plate 15).
6. The FOV mask is then copied and pasted onto the image, where the selected paste layer is that of an overlay. The FOV mask can then be positioned over the object beneath it. And the only sections, which will appear, are where the white part of the circle is over it (see Plate 16).

## Procedure to Eliminate Extraneous Variables

The extraneous variables, which were detected by the image analysis software, were minimized through a process of trial and error as to the best settings for images. These areas focused on gray scale thresholds, recognition of different BSUs, and positive versus negative images.

One approach focused upon the minimum and maximum thresholds of the gray scale. Using these thresholds, values were excluded above and below these levels, which allowed the software to detect the features within the image that were sought. From within the Global Image Lab™, one method attempted to highlight features with different selections of gray scale thresholds. The gray scale thresholds are ranges in pixel coloration values ranging from white (0) to black (200). These values were used to determine the best range to analyze the image FOV for BSUs. The selection of the MINIMUM and MAXIMUM THRESHOLD for measuring of different osteons was followed by the FIND PARTICLES. The use of the threshold allowed the FIND PARTICLES tool to highlight the BSUs (secondary osteons, fragmentary osteons, non-Haversian canals, and percentage of lamellar bone) in the FOV. Initially a minimum gray-scale threshold of 45 and maximum of 188 was used as a baseline. From this point the threshold values were manipulated until noise was eliminated from the highlighted overlay. Eventually, it was determined

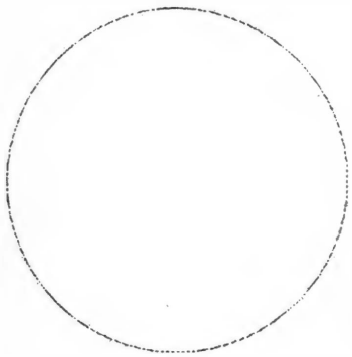

**Plate 14: FOV circle displayed without the calibration marks.**

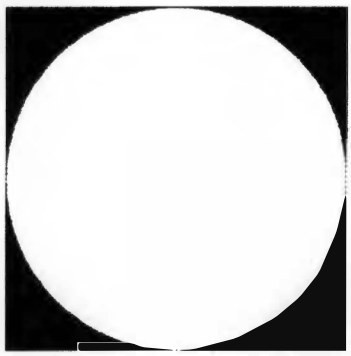

**Plate 15: The FOV mask displayed.**

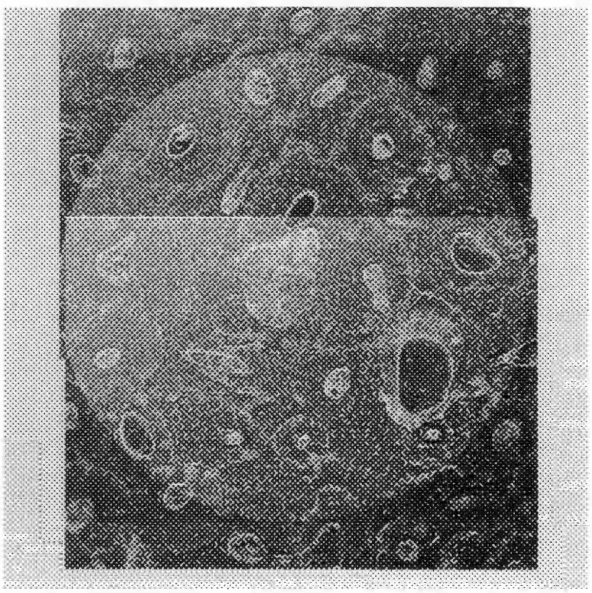

**Plate 16: Two combined images displayed with the FOV mask.**

that a gray-scale base minimum value of 32 and a maximum value of approximately 130 to 135 were best suited when viewing the samples without any other filtering.

The problem with using only the gray-scale is that the software will not differentiate between features. If one marks or highlights features, either through the use of filters or digitally marking different features with different thickness of lines, the problem can be solved. Thus, the software highlights the area but it still requires that the observer be able to recognize distinguishing features of the BSUs. The advantage is that the highlights assist in discerning obscure features in the image more quickly and efficiently. By being able to determine these areas of the image it was found that counting of the different osteons (secondary and fragmentary) could be done. A similar method in the Global Image Lab™ was used with Adobe Photoshop™ to a greater degree of success.

By far the most dramatic change in the FOV image (see Plate 17) is when the negative image is displayed (see Plate 18). In Plate 18, the boundary lines and reversal lines, which help distinguish the osteons (secondary and fragmented) can be seen more clearly. Through the use of these two images (e.g., positive and negative) the process of counting the number of osteons and osteon fragments is simplified. It is possible through the use of just the negative image and the DRAW and PARTICLE tool to be able to determine and separate different structures within the FOV in the process of absolute counts of the secondary osteons, fragmentary osteons, non-Haversian canals, and percentage of lamellar bone.

The two images (positive and negative) were compared, as to which operations and filters would allow for the best view of the FOV. However, the important point is that the procedure is a tool and its use is beneficial to individuals who can recognize the different features of the BSUs. Utilizing the proper settings for minimum and maximum gray thresholds allows one to be able to perform the counts eventually by using only the negative image.

An advantage with digital image software is it can help distinguish different sections of the FOV or objects within it by digital overlays using distinct colors. As a result, less time was necessary for noting differences and identifying key features. However, the problem with the overlay lines in GLI is that they do not become part of the image. Thus, one cannot archive identified features, which leads to the usage of image software to mark the identified features for archiving purposes.

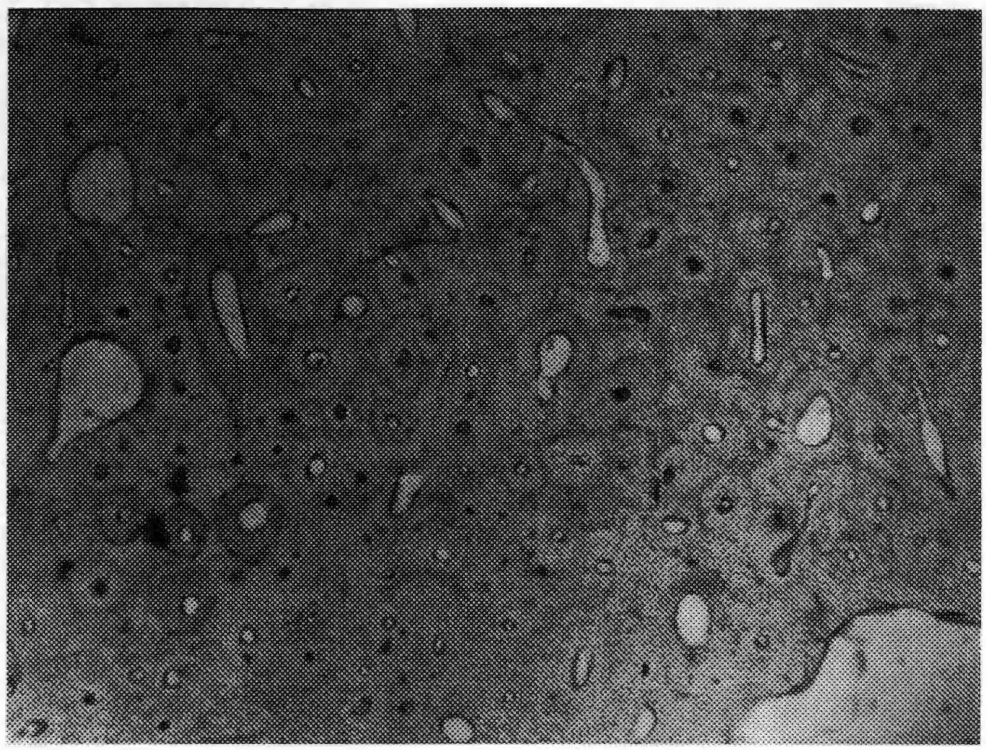

**Plate 17: Positive view of an image displayed.**

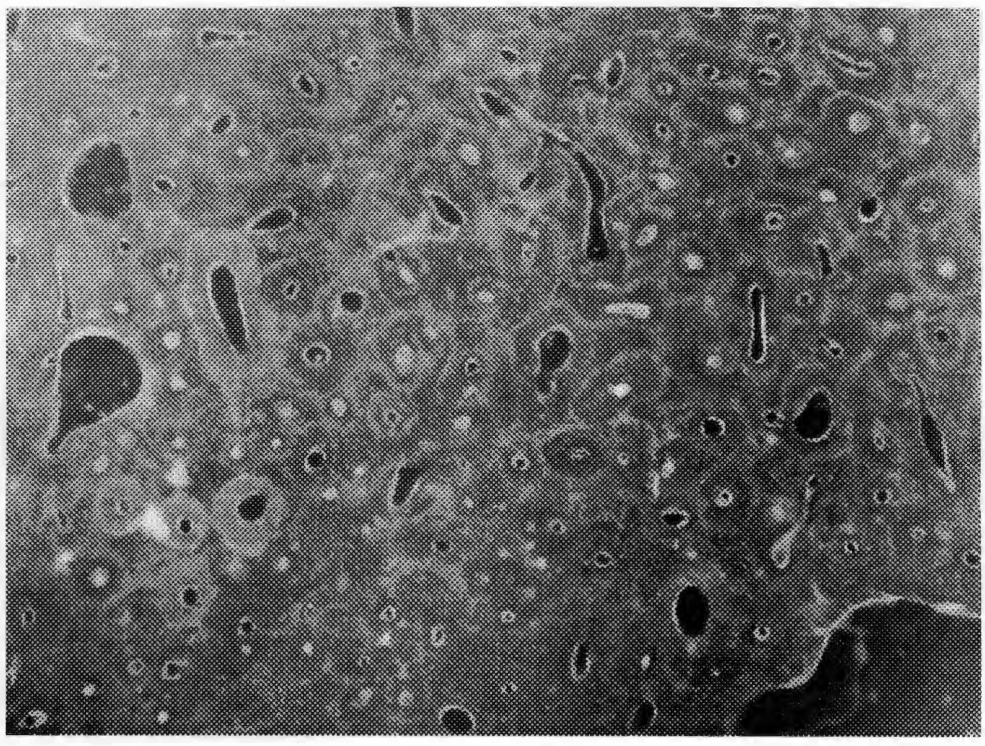

**Plate 18: Negative view of image from Plate 17 displayed.**

## Technical Solutions for Data Image Processing

One of the problems that became observable when the negative image of the section was viewed is a pattern of noise, which speckled and caused difficulties in the Global Image Lab™ software to recognize sections of the image. These difficulties once discovered in 1996 were traced to the vibrations originating from the computers operating on the same desk as the microscope. The solution was a polymer material of Sorbothane®, which was ordered from McMaster Carr after communicating to Sorbothane, Inc.

The sheet of Sorbothane® that was ordered is 12 by 12 inches by 3/4 inches in thickness. After the material was placed under the microscope, it isolated the microscope from external vibration, which caused the noise in the video signal to disappear. The benefit allows the user to receive a better view of the image, and the software has a better opportunity to capture a satisfactory image. It appears that the use of Sorbothane® layers in the reduction of noise under laboratory equipment may be recent, as it was part of an exhibition in England in 1995. The material itself appears to have existed since the early 1980s. Although a distinct year when the material was first used for this particular application was not released by the manufacturer (Sorbothane, Inc. 1996 Personal Communication).

Another problem, which has been a technical difficulty, is that the Global Image Lab™ will only work under Windows 3.1™. The software package at present will not work under Windows 95™ without the possibility of internal settings running the risk of being corrupted. Even though GLI was created to operate under Windows 3.1™, the possibility exists that setup setting can be corrupted, which causes the software to not operate correctly and refuse to load. Unfortunately, both Windows 3.1™ and GLI do not have uninstall routines which can simply be selected (see Technical Note 4).

### Technical Note 4: Repairing the Corruption of Program Files

The solution to this problem, which has occurred more than once during the project is the following:

1. Under the Windows™ directory, delete all GL.INI files, as these were found to be the region of system corruption within the computer environment.

2. In order to change the Windows™ setup, a different graphics setting would need to be selected, or Windows™ would not load properly until the problem was resolved.
3. Reinstall the Global Image Lab™ software package and run setup. For the Fidelity 200™, one needed to select 3152-2 with interrupt setting 290 and UNDO setting. Additionally, the TIGA Large fonts were chosen.
4. If the Windows™ program, refuses to run or fails to recognize that the TIGA adapter drivers have been loaded, then within the AUTOEXEC.BAT file, the following changes need to be added to the PATH extension, C:\GL; C:\GL\DT3851\WIN. These steps are mentioned as they are not covered in the software manual and technical assistance from the product manufacturer will not be able to supply these solutions.

Another problem that caused technical difficulties was when the frame grabber card ceased functioning. The solution, which the technical engineer suggested, was that the computer chips on the Fidelity 200™ were becoming overheated. The solution that was initiated was to move the board closer to the CPU fan within the computer case. The problem with the overheating chips then ceased.

One reoccurring problem is the occasional loss of the program through a conflict with the GDI module, a software package within GLI, which maintains part of the operation of the program's environment. The possible solution to this problem was solved by the addition of extra memory, as the memory buffer of the program may be causing integrity problems. Alternatively, another solution has been to simply reboot the machine and attempt to execute the program again. However, the process can at times take several attempts. As with other technical challenges with the research project, the problem is often not intuitively obvious at first inspection. Another indication has been that the GDI module has technical problems due to the memory on the board being exceeded by the size of an image file.

Researchers need to consider that software and hardware need to work together without conflicts. The difficulty is that often programs may initially perform together without difficulty, then conflicts arise. One program, which was utilized in combining the images, is Adobe Photoshop™. However, Adobe Photoshop™ and Global Image Lab™ conflict with each other. The solution uses a Zip™ Drive to

transport the data files between the two computer systems. The Zip™ Drive is a portable storage device, which is external and can connect to any parallel port on a computer. One of the tasks is to attempt to make the system portable for field applications. Each of the Zip™ diskettes can hold 100 megabytes of information. In addition, these disks are only slightly larger than standard 3.5" floppy disks.

For continuing the research a different video capture board and program have been located that operate under both Windows 95™ and Windows NT™. One recommendation based upon cost and utility is the Dimension Pro™ and Ultra II™ board. These items would increase the overall efficiency for processing images and the maximum size of the data which could be processed for analysis. Generally, IBM™-compatible computers have access to a wider array of high-quality video capture technology than Macintosh™ computers. In addition, if the researcher is computer literate, then technical problems can be deciphered rather than depending upon licensed technicians. One definite recommendation is that data and computers which research is performed be equipped with virus protection software that is updated on a regular schedule.

## Usage of Filters and Morphological Transformations

Different morphological filters can alter pixels composing features within an image. By carefully selecting and managing the filters used, data from images can be observed under optimum conditions. The types of filters used included strategies that used dilation and erosion techniques, as well as methods that sharpened contours and edges.

These different morphological filters were found useful when uncertainty was experienced early within the experiments with the image processing procedure. However, the negative image allowed distinctions between the cells due to the ability to see the lacunae and layers of lamellae. Under the normal image, these different morphological tools were investigated to determine if they would be beneficial in distinguishing between different aspects of the image. However, a technique or combination was required to minimize the noise without eliminating defined features. Noting the relative position of lacunae as they related to cementum and reversal lines assisted in noting where the different features occurred in the FOV. However, a single filter was often not sufficient in the data collection procedure.

Adobe Photoshop™ has a variety of digital filters and image manipulation tools. Different possible filters and effects upon the images were investigated. The observations are described for the high pass filter, Laplacian edge enhancement, brightness and contrast modifications, Fast Fourier Transformation, pixilation, median noise reduction, and sharpen edges. Through careful experimentation on the effect of using different filters and combinations the most optimum image was acquired

One possibility was using a high pass filter to sharpen the details in the image, while another was using a Laplacian edge enhancement to sharpen the edge detection of the object. The result was that the details needed to distinguish the finer characteristics of the image are lost. Although secondary osteons. fragmentary osteons, and non-Haversian canals might be distinguished, the cementum borders and lacunae were better observed by applying a negative image.

Through the use of filters and the use of brightness/contrast tools it is possible to enhance the image quality of the data. However, if the sample is correctly scanned with a digital camera, the most useful and efficient methods of differentiating the elements in the image are through GLI negative image process or Adobe Photoshop™ brightness/contrast tool. Either of these methods will bring out sharp distinctions between the different elements in the FOV.

Different approaches to producing the best image were performed using both Global Image Lab™ and Adobe Photoshop™. When using the Global Image Lab™, these operations included optimizing the ILUT settings, the illumination settings allowed for the selecting of a negative or inverse image, which would enhance the distinctions of BSUs in the FOV. Another one was using a median filter to reduce noise, while using the sharpen filter to increase the remaining definition of the image. However, the problem of eroding of the distinction between BSUs in the FOV occurred.

Another method, which was attempted with a Fast Fourier Transformation (FFT) followed by an inverse FFT. The FFT performs a mathematical algorithm on the image which allows the areas of noise or interference to appear as bright spots on the FFT of the image. Using a masked FFT the noise spikes are removed from the image to improve the clarity of the image. The procedure is complete by using an inverse FFT provide an transformation of the original image without the noise spikes.

The FFT was selected for the area of interest then using the circular area of observation before particle counting of the FOV. The lacunae and lamellae are the key features, which allow the observer to distinguish the different BSUs (e.g., secondary osteons versus fragmentary osteons) within the FOV. Although the lacunae act as key features for identification of BSUs within the bone matrix, they also were a source of noise in data analysis by the software. Though both operations removed noise without losing detail from the cell structures, the inverse FFT appears to be better with the current samples. Initially, noise reduction was thought possible through the use of frequency tools (FFT). However, the best method was a combination of three operations (Pixilation, Median Noise Reduction, and Sharpen Edges), using the Adobe Photoshop™.

Under Adobe Photoshop™ the images can be brought into clearer definition by several different methods, which included sharpening the edges, adjusting the contrast/brightness, and edge tracing. One operation attempted initially to sharpen the edges, then adjusting the contrast (+42) and brightness (-85). It was possible to increase the contrast of the lamellae within the bone structure to the extent that under the magnification tool, it was able to accurately trace the lines of cementum separating the different cells within the FOV.

When digital overlays had to be traced manually, the most accurate method was using a mouse touchpad. The best method for keeping track of different features is to mark them using Adobe Photoshop™ or a similar program (see Plate 19). Two key points are satisfied, which are keeping a tally of the features already counted, while the second allows for another observer to double check the identified features. Although the GLI could differentiate the secondary osteons, fragmentary osteons, and non-Haversian canals with different colors, these overlay marks were not permanent. Once the procedure is refined, it would be recommended to use the edge tracing features along with the nonpermanent overlay feature for counting the secondary osteons, fragmentary osteons, non-Haversian canals, and the calculating the percentage of lamellar bone.

The highlighting of the different features with the touch pad has enough control that it is possible to accurately count the total number of whole osteons, fragmentary osteons, and non-Haversian systems. Due to its accuracy, it is able to mark the outlines of the lamellar so that the percentage of lamellar bone

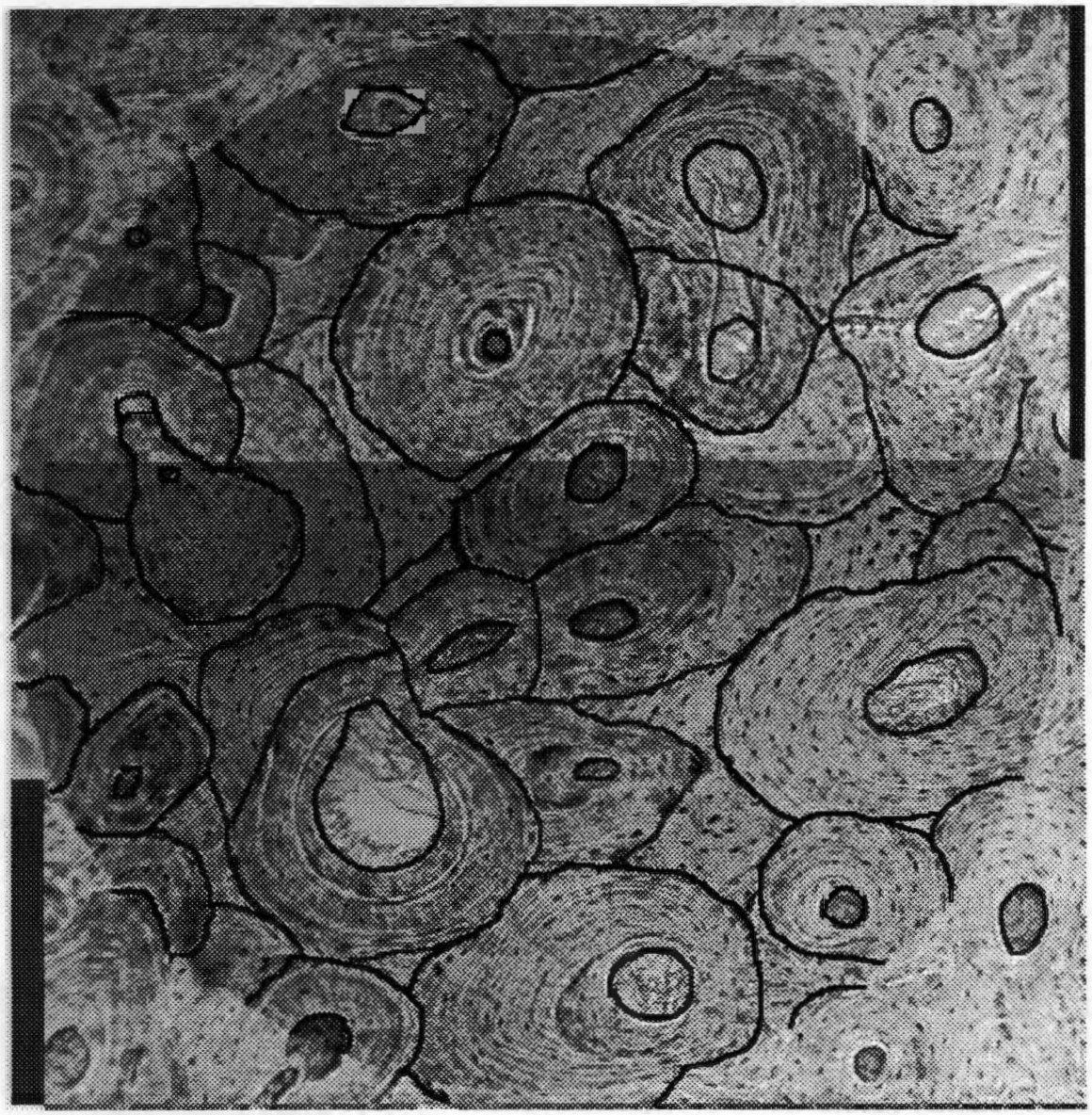

**Plate 19: An image displayed with marked structures for identification.**

can be determined. Once the lamellar bone is outlined in this manner, then the Global Image Lab™ particle tool will be able to give a calculation of the area of the lamellar bone in pixels. Since both the area of the lamellar bone and FOV are calculated, it is possible to determine the total percentage of the area that is composed by the lamellar bone through comparison.

Following the above procedure the image needs to be SAVED AS A COPY as a TIFF file format. The GLI will not recognize the PSD file format, which is used by the Adobe Photoshop™. To determine the percentage of the lamellar bone, it is simply necessary to set the PARTICLE tool for GLI on Statistics mode. The area of interest with the Global Image Lab™ is defined by selecting the ROI, then using the maneuvering arrows to position the ROI in relation to the image and FOV. Once the ROI is positioned on the image the particle tool can simply count the area. The data for the pixels is displayed as output. The area in pixels for the lamellar bone is then divided into the total area of pixels for the FOV, which gives the percentage of the area that excludes the lamellar tissue. The percentage found is subtracted from 100 percent to get the percentage of the lamellar bone in a particular FOV.

## Basic Structural Identification Definitions

The following definitions were used when classifying BSUs (e.g., secondary osteons, fragmentary osteons, non-Haversian canals, and lamellar bone) in the images. Other descriptive information indicates what structures should be counted. Another feature that is necessary to recognize is the lacunae.

Secondary osteons are more than 80% complete, show little if any remodeling from older fragmentary osteons, and have a complete Haversian canal. The secondary osteons have a reversal line (see Figure 15). The secondary osteon may have other secondary osteons crossing its cementum boundary but will be recognizable as a secondary osteon by still being at least 80% complete. The lacunae are essential in helping to trace the lamellae to distinguishing the borders of the secondary osteons from the fragmentary osteons. Kerley's method utilizes an absolute count of the secondary osteons present within each FOV. Once all secondary osteons have been observed in each of the four FOV, the absolute counts are entered into the femoral osteon equation.

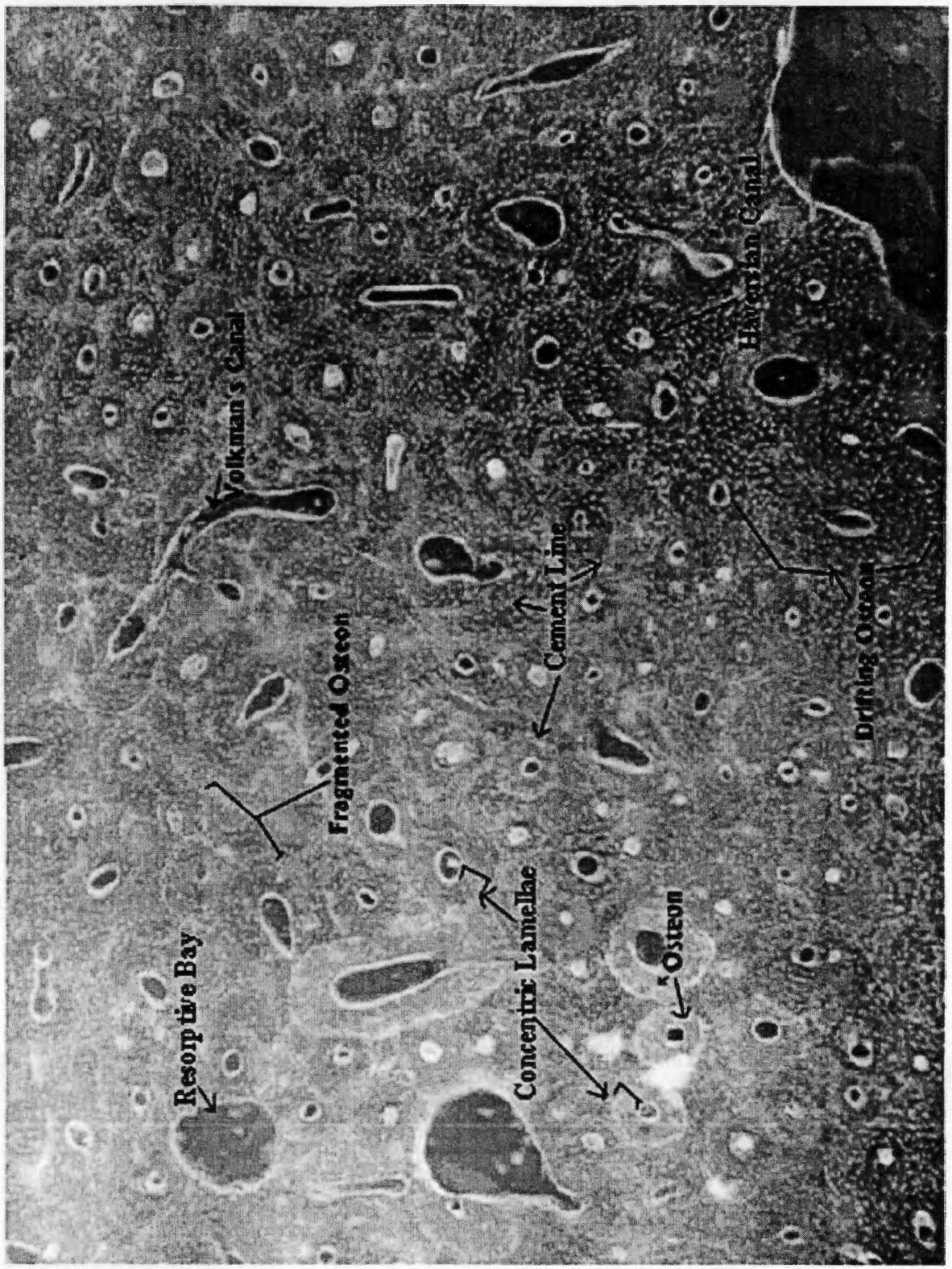


**Figure 15: A femoral histological section displayed with identified BSUs.**

Lacunae house the osteocytes of the osteon or Haversian system. They are also located within the layers of lamellae which are deposited around an osteon. The lacunae are connected by fine canals, the canaliculli and are embedded within the bone matrix and are located within the cementum line marking the boundary of the osteons (fragmentary and secondary) (see Figure 15).

Femoral fragments resemble incomplete secondary osteons as they have a scalloped appearance and appear overlapped by secondary osteons (see Figure 15). The best method in distinguishing different fragmentary osteons is by following the lacunae and layers of lamellae. These lacunae can be traced to determine the center of a fragmented osteon. These structures will be found generally along the edge of secondary osteons, and will be distinguished by appearing to be overlapped by them. In addition, the dashed lines of the lacunae will help in determining the direction of the former shape of the fragmented osteons, as they relate to the current cross-sectional bone matrix. It takes a longer amount of time to distinguish the fragmented osteons than secondary osteons, as they can be confused with femoral lamellar bone or interstitial tissue, which is also present within the bone matrix. Once the fragmented osteons have been observed in all four FOV the absolute counts are entered into the femoral fragments equation.

Femoral lamellar bone is measured by the amount of circumferential growth rings which surrounds an osteon or fragmented osteon (see Figure 15). It was difficult to determine every instance when an osteon had experienced drift or was simply a indication of the thin-sectioning process occurring.

Non-Haversian/Pseudo-Haversian canals include all vascular canals not included among the Haversian and Secondary Osteons. No reversal line is found near them. They simply appear in the FOV as canals which are surrounded by interstitial tissue. The lack of a reversal line or cementum line is an indication that they are not secondary or fragmented osteons. Once the non-Haversian canals have been observed for the four FOV the absolute counts are entered into the non-Haversian equation (see Figure 15).

## Counting Procedure

Initially, the procedure for automating the counting process was more practical as a method to assist in distinguishing between different features within the image using colored highlights in the FOV.

Later, the method was modified to assist in the calculation of the percentage of lamellar bone. An additional benefit is that borderline cells on the edges of the FOV are recognizable, which helps to determine if they are BSUs, which need to be included in the regression formula without switching between magnifications, as Stout indicates (1989a; 1992).

However, an automating of the process for calculation the percentage of lamellar bone was successful. The method had to minimize the noise within each of the secondary osteons, fragmentary osteons, and non-Haversian canals and then sharpen the edges of the cementum boundaries. The noise within the FOV was the lacunae. Although the lacunae help in distinguishing the secondary and fragmentary osteons, they act as interference for the software when the percentage of lamellar bone is being calculated. The elimination of the noise used the following sequence:

1. An initial image is used to perform the Pixelation operation, which allows pixels to be reduced in appearance within the image (see Plate 20).
2. Median Noise Reduction is an operation which can remove pixels if they are of a certain size or smaller from the image entirely. For the lacunae, the size of the pixel was determined to be a value of 2 (see Plate 21).
3. Sharpen Edges is an operation, which locates the edges of lines within an image and increases the number of pixels along the structure of the lines (see Plate 22).

## Calibrating the Counting Procedure

Calibration of the system is an ongoing process in determining the best methods. One point which lead to the process described above was recognizing minimum and maximum circular objects. As long as the BSUs or features of interest in the FOV are distinguishable either through marking them or through the use of filters, the software can be trained to recognize them. In accordance with the software manual, all one has to do is select three to five similar structures and the software package will make the necessary corrections so that other images which fall within these confines will be the only ones selected for that classification.

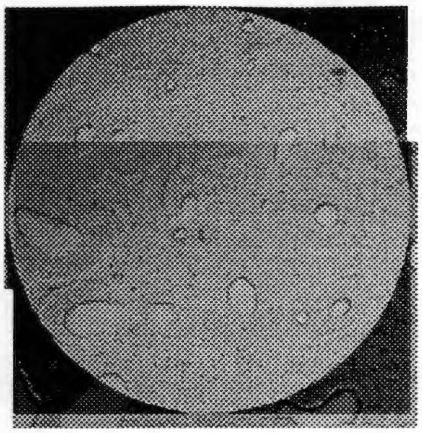

**Plate 20: An initial image is displayed prior to modification.**

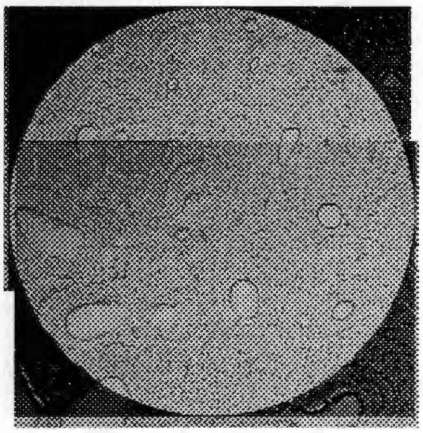

**Plate 21: The initial image displayed after the pixelation operation.**

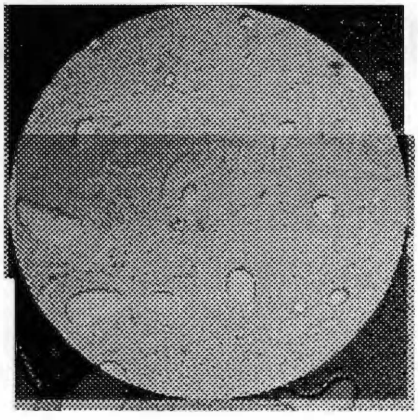

**Plate 22: The initial image from Plate 21 displayed after sharpen edges operation.**

One problem has been to determine the best method for the image software to recognize BSUs for the estimation of age. The current research helps improve the ability for the trained researcher to detect the distinctions between the types of cells displayed. However, at present, the most expedient method is to outline the structures, which are osteons, fragmentary osteons, and non-Haversian systems. The reason being the most expedient method at present is for storage of the marked areas. The digital overlays within Global Image Lab™ are nonpermanent under the PARTICLE TOOL. While using Adobe Photoshop™, one can create marked FOVs to test and refine the digital counting procedure. The Global Image Lab™ can be used to help in the counting procedure by marking secondary osteons, fragmentary osteons, and non-Haversian canals with different identifiable colors. Currently, distinctions between secondary osteons, fragmentary osteons, and non-Haversian canals can be created within the system by marking them with different thickness of lines. The use of a flat surface mouse was found to be the most accurate and efficient device for drawing the outlines. Other methods to outline the defining features were found to not be as easy to manipulate. Once these structures had been outlined, it was then possible to determine the percentage of the FOV, which is composed by the lamellar bone. It was found that noise reduction had to be performed, otherwise lacunae would also be counted. The edges of the osteons and non-Haversian canals had to be sharpened to distinguish their morphology within the image. The other benefit of outlining the different features is that the image can be saved as a separate file. Later the separate file could be reviewed for accuracy by other researchers. The overlay file, as it is an digital layer to the image, can also be selected and removed for determining the percentage of area that the lamellar bone comprises of the total FOV (see Plates 23 and 24).

The previous procedure, which utilizes an overlay of selected areas, relies on the Particle Tool of the Global Image Lab™ for one of its key functions. The Global Image Lab™ has the ability to calculate the total number of pixels, which comprise the interior area of a selected particle. The method to determine the area accurately is to simply call up the calibration table, then use the DRAW Freehand tool about the areas which are part of the lamellar bone layers. Use a width of three (3) and full White coloration on the setting of the Freehand tool, then follow this with the PARTICLE tool, using the setting SELECT and SINGLE. As each area of interest is highlighted the program will automatically calculate the area for that

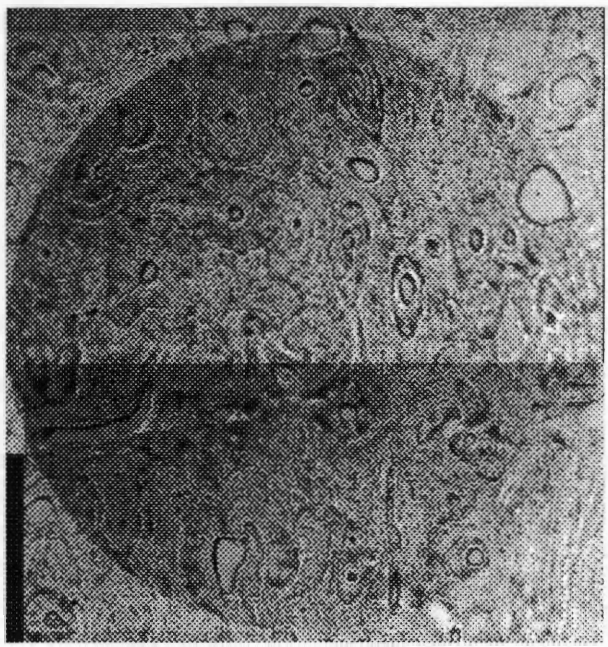

**Plate 23: An image displayed.**

**Plate 24: Image displayed after marking.**

selected area. For larger samples and to allow for evaluation, Adobe Photoshop™ was used to mark the same areas permanently, then saved as a different file name. The different files allow for interobserver comparisons for accuracy in identification of features and help highlight features for the computer to process. These results are then compared to the known percentage of the area of the FOV in order to determine the femoral lamellar percentage. Since the total pixel area and the real world area of the total FOV are known, the percentage of the lamellar bone can be calculated. The difference between the FOV total area and percentage computed indicate the percentage of lamellar bone. By using this method it eliminates the problems described by using only the Global Image Lab™ for analysis.

## Time and Image Requirements for Data Collection

Each field of view of a sample is composed of two images or eight images for the entire slide. It generally takes approximately five minutes to record a complete FOV per section of a slide (i..e., anterior, posterior, lateral, and medial). To translate the images within the Global Image Lab™ takes approximately 15 minutes. To process the images from positive to negative formats takes about 5 minutes total. By using the particle tool to keep track of the secondary osteons, fragmentary osteons, and non-Haversian canals with different highlighted colors, it is possible perform faster absolute counts. The time required is about 15 to 20 minutes. To calculate the percentage of lamellar bone, it is either necessary to use a macro or manually mark the FOV digitally. Once the FOV is marked the percentage of lamellar bone can be calculated in a few seconds for each FOV. It takes a total of 2 to 3 hours to perform all the steps of the procedure on a prepared slide. The process time includes the image capturing, processing, and counting the secondary osteons, fragmentary osteons, and the non-Haversian canals. The current time limit may be possible to substantially decrease when a macro is finished which will mark everything but the lamellar bone in the FOV. The time estimate could decrease by fifty percent. If only the absolute counts of the secondary osteons and fragmentary osteons are required, then the time is approximately 30 to 45 minutes. Two suggestions should be followed when marking data images. One is that the marked and unmarked images should be saved under different files, while the other is the use of a standardized hierarchy of file names to ensure that necessary control is maintained over the images. A checklist of the hierarchy to adopt

was created when combining the initial images. A similar method was utilized in keeping track of original images from modified images after they were marked for identification.

## Data Collection Procedure

One necessary item is a checklist, which matches slides with their corresponding images, while the images are being collected. With the checklist, it is possible to keep track of each particular file name that corresponds to each image and what stage of the procedure the image represents.

For example, the numbers represented the assigned Case # of the sample, while the letter meant the Anterior, Lateral, Medial, or Posterior side of the sample. The numbers located after the letter code (A, L, M, or P) represent whether it is first (1) or second image (2) of a combination, (3) being the combined image, and (4) being the image after it has been identified with marks. By using the code, it is possible to call up a particular file pertaining to any particular stage of the procedure (see Figure 16).

80-6A1 + 80-6A2 = 80-6A3; 80-6A4
80-6P1 + 80-6P2 = 80-6P3; 80-6P4
80-6L1 + 80-6L2 = 80-6L3; 80-6L4
80-6M1 + 80-6M2 = 80-6M3; 80-6M4

**Figure 16: A sample of the data checklist used when combining images.**

## The Formulas for the Data Collection

After reviewing the literature, these regression formulas were determined to offer the best age estimation with an overall field of view setting at a magnification of 100 power (Kerley 1965; Bouvier and Ubelaker 1977; Kerley and Ubelaker 1978; Stout 1989a; and Stout 1992). As a result, if any improvement or test using digital imaging can be done for age estimation, then it should be based on these earlier sources.

Regression Formulas

| Factor | Predicting Equation | SEE |
|---|---|---|
| Femoral Osteons | $Y = 2.278 + 0.187X + 0.00226X^2$ | 9.19 |
| Femoral Fragments | $Y = 5.241 + 0.509X + 0.017X^2 - 0.00015X^3$ | 6.98 |
| Femoral Lamellar % | $Y = 75.017 - 1.790X + 0.0114X^2$ | 12.52 |
| Femoral non-Haversian | $Y = 58.390 - 3.184X + 0.0628X^2 - 0.00036X^3$ | 12.12 |

## Procedure for Determining the Age Estimation Midpoint

Kerley (1961) described the method as using the highest minimum age and the lowest maximum age from the regression formulas that overlap. The regression equations generated four age ranges which were associated with either the femoral osteons, femoral fragments, femoral non-Haversian, or the percentage of femoral lamellar bone. To determine the midpoint of the estimated age, only the generated age ranges within five years of each other were used. However, if all the age estimates generated were equally distributed, then all were included to estimate the midpoint of the estimated age. The midpoint for age estimation was calculated by the average of the estimated ages from the equations included. The estimated midpoint was recorded as the estimated age for each slide on the data record sheet.

In addition Kerley (1961) plotted Age Range Curves for different BSUs found in the femur, tibia, and fibula. The age range charts for the BSUs of the femur illustrate the graphical relationship of age to the regression formulas (see Figures 17-20). These age range charts also give an indication as to the upper and lower ranges of scores, which could be expected to result from the regression formulas. The charts were used to assist in the inclusion of borderline age ranges for estimating the midpoint age. Another variable for borderline cases is the difference between the age estimations of three equations. Two equations that were compared to each other were the fragmented osteons and percentage of lamellar bone and the osteons and non-Haversian canals. A third set was comparing the difference between osteons and fragmented osteons with the difference between the fragmented osteons and the lamellar bone. By comparing the differences between these three sets of equations, a generated age range was either included or excluded from calculating the midpoint for age estimation.

The data was entered into a Microsoft's Excel™ spreadsheet and the regression equations were performed. The estimated ages generated for the femoral osteons, fragmentary osteons, lamellar bone, and non-Haversian systems were examined. Each of the estimated age ranges was compared and the procedure to select the most probable midpoint for age estimation was completed. For the estimated age, the estimated age midpoint was recorded twice with decimals and rounded to the nearest whole number.

Three tables (see Tables 2-4) have been included to illustrate the procedure to calculate the midpoint for age estimation. The three examples illustrate different situations that can occur when

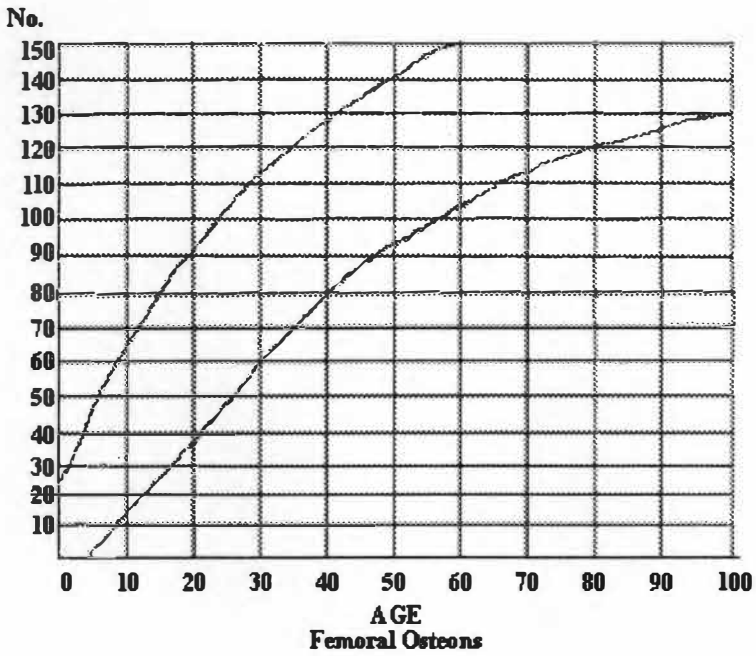


**Figure 17: Age Range Chart for Femoral Osteons (Modified from Kerley 1961)**

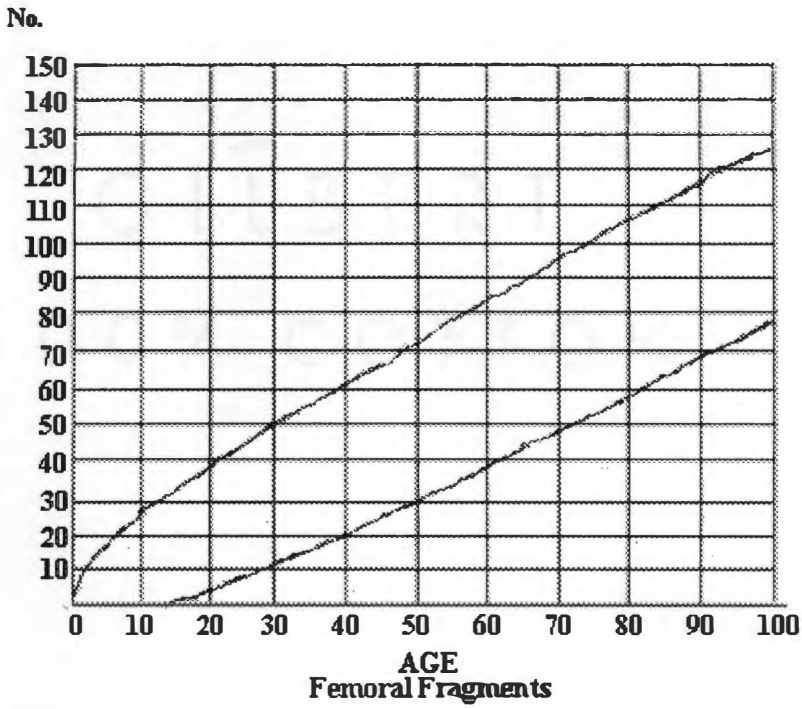


**Figure 18: Age Range Chart for Femoral Fragments (Modified from Kerley 1961)**

Source: Kerley, E. R. 1961. *The Microscopic Determination of Age in Human Bone.* Dissertation. University of Michigan.

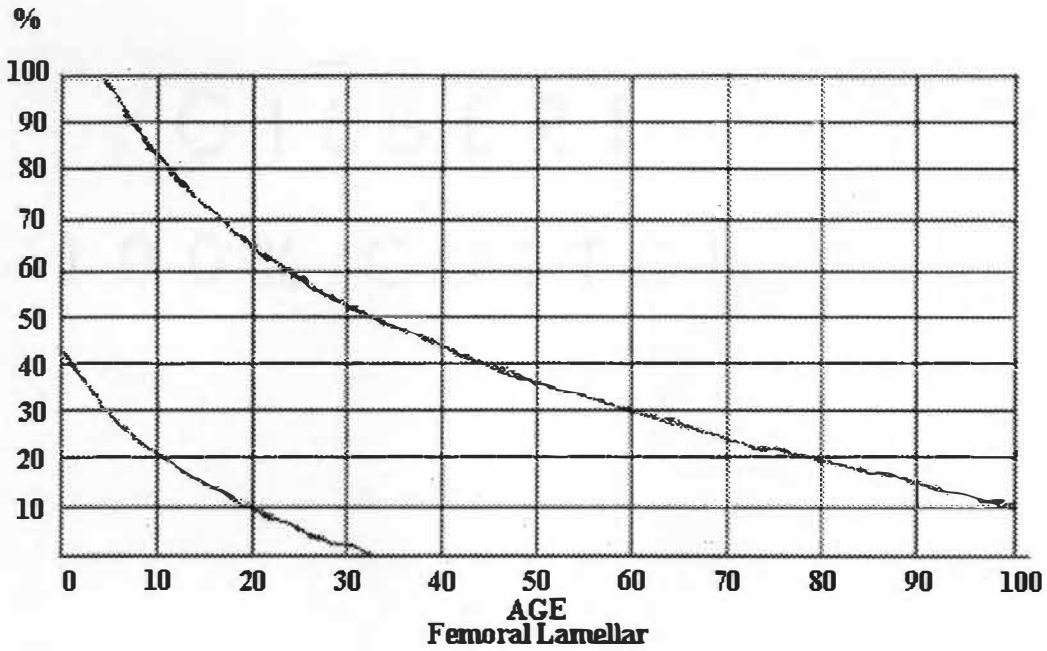


**Figure 19: Age Range Chart for Femoral Lamellar (Modified from Kerley 1961)**

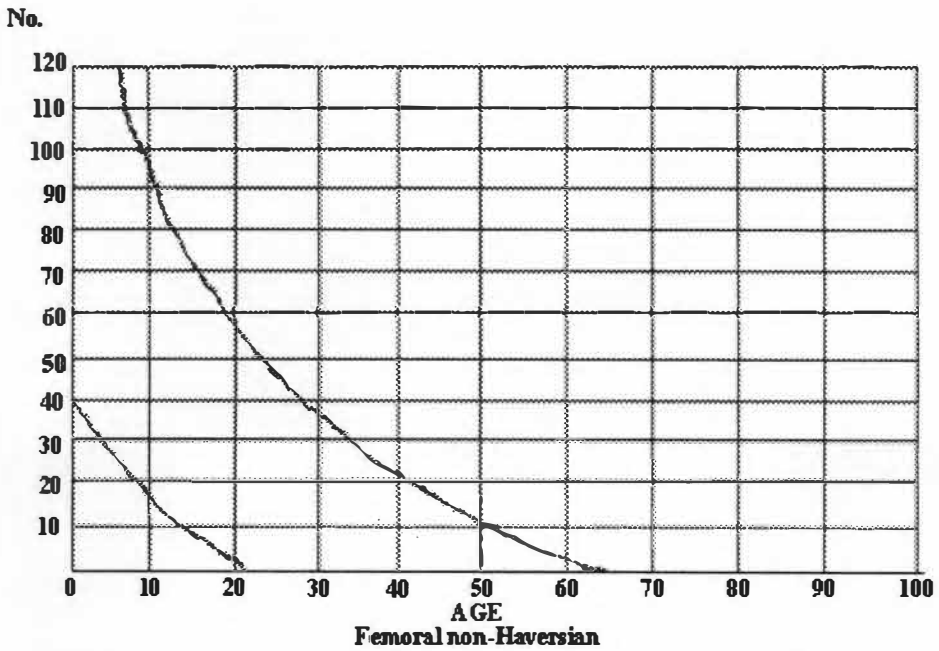


**Figure 20: Age Range Chart for Femoral non-Haversian (Modified from Kerley 1961)**

Source: Kerley, E. R. 1961. *The Microscopic Determination of Age in Human Bone*. Dissertation. University of Michigan.

**Table 2: Case #2 (ID 72-3)**

| Regression Equation | Estimated Age | SSE- | SSE+ |
|---|---|---|---|
| Femoral Osteons | 26.442 | 17.252 | 35.632 |
| Femoral Fragments | 47.7714 | 40.7914 | 54.7514 |
| Femoral % of Lamellar Bone | 74.57042 | 62.05042 | 87.09042 |
| Femoral non-Haversian | 20.64252 | 8.52252 | 32.76252 |

**Table 3: Case #9 (ID 80-3)**

| Regression Equation | Estimated Age | SSE- | SSE+ |
|---|---|---|---|
| Femoral Osteons | 37.414 | 28.224 | 46.604 |
| Femoral Fragments | 56.5858 | 49.6058 | 63.5658 |
| Femoral % of Lamellar Bone | 74.47811 | 61.95811 | 86.99811 |
| Femoral non-Haversian | 10.09092 | -2.02908 | 22.21092 |

**Table 4: Case #10 (ID 80-6)**

| Regression Equation | Estimated Age | SSE- | SSE+ |
|---|---|---|---|
| Femoral Osteons | 44.21926 | 35.02926 | 53.40926 |
| Femoral Fragments | 70.54255 | 63.56255 | 77.52255 |
| Femoral % of Lamellar Bone | 74.3407 | 61.8207 | 86.8607 |
| Femoral non-Haversian | 12.415 | 0.295 | 24.535 |

calculating the midpoint of age estimation. The first example is when three age estimates overlap and a one is excluded. The next example describes a group of estimated age ranges which are evenly distributed. The final example illustrates a situation where age estimations that are borderline are examined to include or exclude, one or both from averaging the midpoint.

For example, Case #2 (ID 72-3) had an actual age of 34 years. The regression formulas generated the following age estimations (see Table 2). The femoral osteons and non-Haversian have age estimated ranges which overlap each other. The femoral fragments estimated minimum age is 40.7914 which is within 5 years of the maximum range of the femoral osteons at 35.632 and it was included in calculating the age midpoint. However, the femoral lamellar bone generated age estimate was not within five years and was excluded from the calculation of the age midpoint. The estimated age was 31.62 years, which is rounded up to 32 years. The estimated age is two years from the known age of 34 years.

Another example is Case #9 (ID 80-3). The Forensic Center records indicated a skeletal age between 30 and 40 years. The regression formulas generated the following age estimations (see Table 3). The generated age estimates were approximately the same number of years separating each range from the next range. The estimated ages were compared and were approximately twenty years between each generated age range. As a result, the femoral non-Haversian was included when calculating the average midpoint. Thus, all the age estimates were included to calculate the average midpoint. The estimated age was 44.64 years, which is rounded up to 45 years. The estimated midpoint is five years from the skeletal age range of 30 to 40 years.

A final example is Case #10 (ID 80-6). The Forensic Center records indicated a known age of 65 years. The regression formulas generated the following age estimations (see Table 4). The age ranges generated from the femoral fragments and the percentage of lamellar bone overlap. The other two age ranges estimated, the femoral osteons and the non-Haversian, were compared. The femoral osteons were closer to the age estimates for the fragmented osteons and the lamellar bone, and the osteons were included in estimating the age midpoint. The non-Haversian estimate was 32 years below the age estimate generated by the femoral osteon equation, and the non-Haversian estimate was not included to estimate the age midpoint. The estimated age was 63.03 years, which is rounded down to 63 years. The estimated midpoint is two years from the known age of 65 years.

## Data Record Sheet

As the data is collected it will be entered onto a record sheet (see Figure 21). Data from the thirty (30) slides was recorded (see Table A-3).

| Case # | ID: | Actual Age: | Lab Age: | Estimated Age: | | | |
|---|---|---|---|---|---|---|---|
| FOV | | | | Results of Regression Equations | | | |
| | Osteon | Frag. Osteon | % of Lamellar | Nonhaversian | | Est Age | SSE- | SSE+ |
| Anterior | | | | | O. | | | |
| Posterior | | | | | F | | | |
| Lateral | | | | | O | | | |
| Medial | | | | | % L | | | |
| Total Overall Count | | | | | N H | | | |

**Figure 21: A blank data record sheet illustrating its organizational format.**

## Procedure to Print the Images

Another difficulty was in printing the images. The saved images, which were analyzed, are generally 10 inches by 10 inches which falls outside the printable areas of standard printers. Using the Global Image Lab™, it was not possible to print the entire image onto a single sheet of standard paper nor was it possible to change the dimensions of the image within that program. The program parameters will allow the entire image to be printed so long as the image is on 14 by 14 inch paper. Thus the level of resolution captured by the Fidelity 200™ frame grabber card requires that the image be exported to a image software package to allow for the image canvas to be altered. When the image canvas is altered, the image can then be printed out on standard printer paper. The solution to printing the entire image while adjusting the proportions of the image was solved using Adobe Photoshop™.

The Adobe Photoshop™ was able to change the dimensions of the image, while preserving the details of the original image. Simply reduce the specified size of both the image and canvas size. To

display all 4 FOV (see Plates A1 - A60), it was necessary to decrease the FOV images by the same amount, while maintaining the canvas size. In this manner it is possible to preserve the same space relations of the elements in the image.

# CHAPTER IV

# RESULTS

The research methodology produced digital images based on the four FOV (anterior, posterior, medial, and lateral) for each of the 30 slides, which were selected from the Anthropology Forensic Center collection (see Tables A-4 through A-12). The slides were selected from the clearest of the slides of femur cross-sections. The collection of the data followed the procedure described under the methods section (Chapter 3), which is based on Kerley (1961 and 1965) and Kerley and Ubelaker (1978).

A record of the data collection from Plates A1 to A60, where the odd numbered plates represent the images prior to marking features and the even numbered plates represent the images after marking features. The recorded data is listed in Table A-3.

After the data was recorded it was observed that a possible relationship might separate different age clusters. Dr. Sam D. Stout was contacted to provide data to investigate the possible relationships between the age clusters (see Table A-2). The SAS program was used with a step-wise regression of the data to determine if better equations could be generated based on an apparent interaction between similar age groups. However, the step-wise regression procedure indicated the statistical interaction was an artifact of clustering similar groups only. The r-value without the group clusters only explained approximately 3% of the total variation. As a result, alternative equations were rejected, as the regression equations developed by Kerley (1961and 1965) and Kerley and Ubelaker (1978) are still the most accurate for age estimation.

The regression equations generated age estimations for the secondary osteons, fragmentary osteons, non-Haversian, and percentage of lamellar bone across the four FOV. The midpoint was determined by the results of the equations and comparing equations as overlapping if they were within 5 years of either the minimum or maximum of a particular regression equation. To determine the overlap of estimated age ranges a comparison of between pairs of the estimated age ranges was required. The age estimations for the overlapping equations were averaged to estimate the midpoint for a particular subject.

The age estimation of the thirty (30) slides tested is presented in Table 5. The table indicates the actual age (when known) along with the lab age (when estimated), while the estimated age is the age

calculated using the regression formula from the digital images. Some of the Forensic Center records were incomplete (NA), while others had a skeletal age estimated (SA). Skeletal age was left in the known age, when the Forensic Center record indicated that a positive ID was present but the known age was not recorded on the record card. Some Forensic Center records indicated age estimates with a decimal. These age estimates had not been rounded to the nearest whole number. The age estimations for the current research with the estimated age and the estimated age rounded to the nearest whole number (e.g., inside parenthesis). The age estimates are plotted to illustrate their relationships (see Figure 22).

**Table 5: Summary of Age Estimations**
**Key: NA = Not in Record and SA = Skeletal Age**

| Case # | Case ID | Actual Age | Lab Age | Estimated Age |
|---|---|---|---|---|
| 1 | 22781 | NA | NA | 29.26 (29) |
| 2 | 72-3 | 34 | NA | 31.62 (32) |
| 3 | 73-1 | 18-21(SA) | NA | 31.08 (31) |
| 4 | 74-2 | 28 | NA | 32.63 (33) |
| 5 | 74-5 | 43 | NA | 38.72 (39) |
| 6 | 79–13 | 36 | 26-28 (SA) | 38.10 (38) |
| 7 | 80-12 | 27 | NA | 25.57 (26) |
| 8 | 80-15 | NA | NA | 27.96 (28) |
| 9 | 80-3 | 30-40 (SA) | NA | 44.64 (45) |
| 10 | 80-6 | 65 | NA | 63.03 (63) |
| 11 | 81-110 | NA | NA | 41.53 (42) |
| 12 | 81-13 | NA | NA | 39.24 (39) |
| 13 | 812005 | NA | NA | 42.82 (43) |
| 14 | 81-9 | 25 | NA | 32.63 (33) |
| 15 | 82-16 | NA | NA | 17.04 (17) |
| 16 | 82-1 | 60 | 56.50 | 59.09 (59) |
| 17 | 83-10 | NA | NA | 27.82 (28) |
| 18 | 83215 | NA | NA | 22.59 (23) |
| 19 | 83-25 | 26 | 54 | 24.71 (25) |
| 20 | 83-9 | 18 | 18.45 | 24.75 (25) |
| 21 | 84-14 | 45 | 45 | 42.74 (43) |
| 22 | 85-1 | NA | NA | 43.06 (43) |
| 23 | 85-24 | 32.70 | NA | 43.54 (44) |
| 24 | 85-7 | 30-40 (SA) | NA | 41.43 (41) |
| 25 | F83215 | NA | NA | 57.30 (57) |
| 26 | F83539 | 54.40 | NA | 54.52 (55) |
| 27 | FA12 | 48 | NA | 42.82 (43) |
| 28 | O80120 | NA | NA | 59.67 (60) |
| 29 | O81-9 | 25 | NA | 24.31 (24) |
| 30 | 082-2 | 6-7 (SA) | NA | 21.20 (21) |

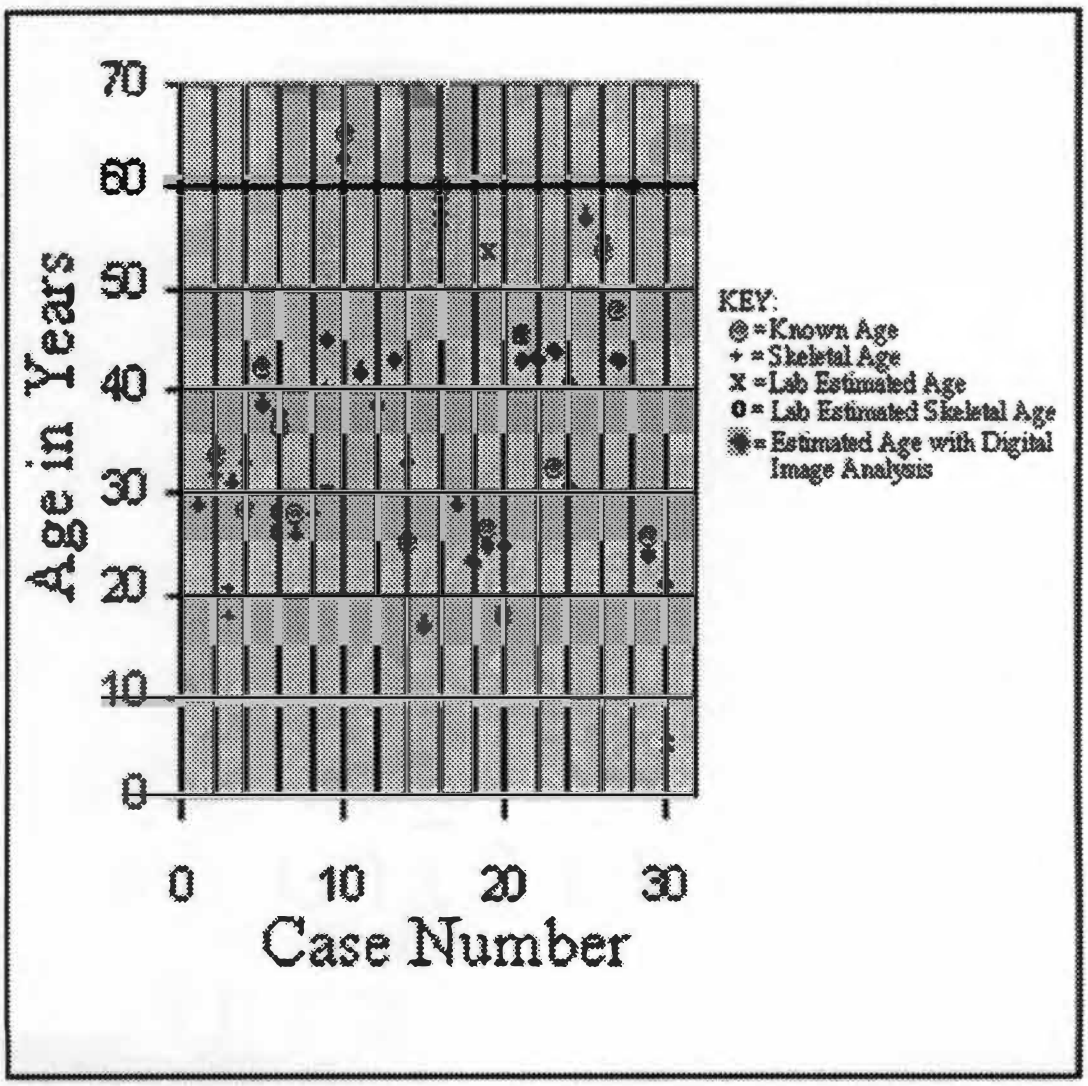


**Figure 22: Plotted Age Estimates from 30 Slides**

# CHAPTER V

# DISCUSSION

The images selected from the histological slides were limited to femur sections that could be sampled clearly with the computer. The digitized images of the 4 FOV for the 30 slides were examined, and the data was recorded in data record sheets (see Figure 21). The estimated ages of the 30 slides are presented in Chapter 4 (see Table 5 and Figure 22).

Kerley (1961 and 1965) describes the procedure for determining the best fitting age estimation. According to Kerley (1961) using his method of age estimation it is easier to determine the age of younger individuals. Only one of the slides with a skeletal age and positive ID without a known age listed was found to differ significantly from the estimated age generated. The exception was Case #30 (O82-2), which had a skeletal age of 6 to 7 years and an estimated age of 21 years. The age ranges generated by the digital image data were within the predicted range for the 30 samples.

The majority of the samples from the Forensic Center provided have known ages or skeletal ages. However, several samples included within the research study are unknown, according to the records provided. By using the known samples and the possible results gained through their estimation, it was possible to obtain a better estimation for the age of the unknowns in the study.

The records from the Anthropology Forensic Center indicated that eleven (11) slides of the sample size (n=30) did not have known ages, whereas twenty-five (25) slides from the same sample did not have lab ages estimated (n=30). Thus, nineteen (19) of the thirty (30) slides had known ages, which made up the sample.

The results of the regression equations helped to clarify the sample records by describing the resulting estimation of ages for the slides, which had known ages (n=19). In eight (8) slides, it was possible to estimate the age of the sample within 2 years of the known age. In three (3) slides, it was possible to estimate the age of the sample within 4 years of the known age. In another three (3) slides, it was possible to estimate the age of the sample within 6 years of the known age. In two (2) slides, it was possible to estimate the age of the sample within 8 years of the known age. For the remaining 3 slides that

had known ages, two (2) were approximately 10 years from the known age and one (1) slide was estimated to be more than 10 years from known age. The greatest error in estimating the age was found when estimating the age of Case #30 (O82-2), which was mentioned earlier. Thus, the estimated ages were within 6 years of the actual ages of the samples in fourteen (14) of nineteen (19) cases. Further, eighteen (18) of nineteen (19) of the slides with known ages were estimated within the standard error of the regression equations.

The general indication from the comparison of the case numbers with the age estimated using the research procedure indicates that the overall investigation was successful. As a result, it appears that the digital record keeping and counting of osteons is possible and effective. Additionally, as long as the slides without known ages from the Forensic Center are not of very young individuals, then the estimated ages for the other eleven (11) slides in the sample are probably accurate.

One key advantage of the digital collection of data from images is the ability to digitally mark features within the images. Once the lamellar bone is marked it is possible to determine the percentage of lamellar bone present accurately. Another advantage is the use of digital colors to keep track of osteons, fragmentary osteons, and non-Haversian canals while counting the structures. As a result, the marked images can be implemented as tools for teaching bone histology. Another benefit is the permanency of the digital records that can be re-examined due to their dynamic nature. The dynamic nature allows data to be entered into other software packages and applications for future corroboration.

Future goals are to continue to apply the procedure to other histological thin-sections to generate other regression formulas. It is believed that alternative regression formulas for age estimation can be generated through continued observations. Further research could be conducted to observe other skeletal elements.

The time requirements for the age estimations based on digital imaging take a slightly longer time to operate. However, Dr. Sam D. Stout indicated that the average time to perform femoral histological counts is approximately 30 minutes to 1 hour (Personal Communication 1999). Thus, it is believed that further refinement of the existing system will allow a more efficient process with increased levels of accuracy for age estimation. Further, the expense is the initial system cost. Since the system is present,

additional costs would not be expensive in maintaining or updating the system. The flexibility of the overall system is worth the effort and time investment as the potential returns are worth consideration.

# CHAPTER VI

# CONCLUSIONS

The results support the conclusion that a digital image database can be used in the estimation of age from femoral histological samples. The regression formulas selected in estimating the ages of the sample slides were deemed the most accurate based upon an extensive literature review.

Of the slides with known ages, the data collected from the images is able to place eighteen (18) of nineteen (19) subjects within the standard error of the regression formulas (Kerley 1965 and Kerley and Ubelaker 1978). In addition, as fourteen (14) of nineteen (19) subjects were estimated within 6 years of the known age, it is believed that the image database is supported in estimating the ages accurately. Further, the eleven (11) slides, which had unknown ages, have probably been estimated using the image database to their actual age. The previous conclusion is probably accurate as long as the unknown ages are not young.

During the research the digital analysis was able to help to distinguish secondary osteons, fragmentary osteons, non-Haversian and calculate the percentage of lamellar bone. It should be possible to use the software to identify plexiform bone. Thus, one potential use of a digital image library would be in differentiating human from the remains of other species when investigating complex sites. Other potential uses would be large-scale disasters, where fires are involved or fragmentary. As it could assist the identification process, one possibility could involve the identification of victims of airline disasters.

The procedures presented indicate an advantage which should not be overlooked nor underestimated as it applies to the collection, analysis, and storage of data. The image database is a practical augmentation to the field of forensic anthropology. The images are not simply data, which can only be viewed as reference material. Rather, the image data can be re-examined by other researchers who may have either different procedures and/or better equipment. The use of the data to train future observers and students in the field is also possible. In addition, the communication of data between researchers can be done with compressed files. For instance, the average size of most of image files can be compressed to approximately 50 bytes with little difficulty, which could be additionally protected by encryption software for sensitive data. One such encryption program is PGP™, which is readily available to users.

Other avenues are possible following the general principles outlined under the image analysis. The application of digital databases in forensics is initially an expensive undertaking when compared to manual counting and age estimation using bone histology. However, once the capability to process and analyze digital images is operational in a laboratory, the cost for the subsequent operations decreases. In addition, upgrades to computer equipment are less expensive than implementing the entire system. One future area of image data techniques is found in digital scans of three-dimensional objects. The area of research focuses on a process called Rapid Prototype Stereo Lithography (RPSL) technology, which can store the data from a three-dimensional object within a database (Walls 1999).

The digital database procedure could be applied to other areas of study due to the fact that the calibration method simply needs a measurement instrument captured as an image. The image of the measurement scale would need to remain stationary as to the distance from the camera, where new objects would be imaged. However, depending upon the situation it is entirely possible that the procedure could become portable and allow the classification and analysis of objects as images. In addition archival images could be made of collections given enough storage space for the data. The advantage of a computerized database of images would not only allow a permanent library of sample data but would allow for rapid dissemination and communication of the databank to other researchers for collaborative efforts.

The refinement of the research is scheduled to occur under the instruction of Dr. Sam D. Stout during the Summer of 1999. It is believed that the efficiency will increase sufficiently to make the method a potential alternative to manual counting. With additional refinements the accuracy for the estimation of age from bone histology will increase. It is hoped that the research presented will encourage other researchers to examine the use of digital image analysis as a tool for assisting in age estimation. In conclusion the objective of the research is possible and obtainable.

# BIBLIOGRAPHY

# BIBLIOGRAPHY


Adobe Systems, Inc. 1994. *Adobe Photoshop version 3.0 Manual.* Mountain View, Ca.: Adobe Systems, Inc.

Ahlqvist, J. and O. Damsten. 1969. Modification of Kerley's Method for the Microscopic Determination of Age in Human Bone. *Journal of Forensic Sciences.* 14:205-12.

Amprino, R. and E. A. Bairati. 1936. Processi do ricostruzione e di riassorbimento nella sostanza compatta delle osa dell nomo. Richerche see cento soggetti della nascita sino a tarda eta. *Zeitschr Zellforsch und Mikr Anat.* 24:439-511.

Baxes, Gregory A. 1994. *Digital Image Processing: Principles and Applications.* New York: John Wiley & Sons, Inc.

Bertelsen, P. K., J. G. Clement, and C. D. L. Thomas. 1994. A Morphometric Study of the Cortex of the Human Femur from Early Childhood to Advanced Old Age. Research Paper.

Boivin, G. and P. J. Meunier. 1993. Histomorphometric Methods Applied to Bone. In *Histology of Ancient Bone: Methods and Diagnosis*, ed. G. Grupe and A. N. Garland, pp. 137-56. Berlin: Springer-Verlag.

Bouvier, M. and D. H. Ubelaker. 1977. A Comparison of Two Methods for the Microscopic Determination of Age at Death. *American Journal of Physical Anthropology.* 46:391-94.

Cormack, D. H. 1993. *Essential Histology.* Philadelphia: J. B. Lippincott Company.

Currey, J. D. 1964. Some Effects of Aging in Human Haversian Systems. *Journal of Anatomy (London).* 98:69-75.

Currey, J. 1984. *The Mechanical Adaptations of Bones.* Princeton: Princeton University Press.

Data Translation, Inc. 1994. *Global Lab Image Manual.* Marlboro, Mass.: Data Translation, Inc.

Data Translation, Inc. 1994. *Fidelity 200 Frame Grabber Cards.* In *Data Translation 1994 Catalog.* Marlboro, Mass.: Data Translation, Inc.

Data Translation, Inc. 1994. *Densitometry Add-in Module.* Marlboro, Mass.: Data Translation, Inc.

Davis, S. J. M. 1987. *The Archaeology of Animals.* New Haven: Yale University Press.

Enlow, D. H. and S. O. Brown. 1956. A Comparative Histological Study of Fossil and Recent Bone Tissue, Part I. *Texas Journal of Science.* 8: pp. 405-443.

Enlow, D. H. and S. O. Brown. 1957. A Comparative Histological Study of Fossil and Recent Bone Tissue, Part II. *Texas Journal of Science.* 9: pp. 186-214.

Enlow, D. H. and S. O. Brown. 1958. A Comparative Histological Study of Fossil and Recent Bone Tissues, Part III. *Texas Journal of Science.* 10(2): pp. 212-20.

Enlow, R. D. 1969. The Bone of Reptiles. In *Biology of the Reptilia vol. 1, Morphology A*, ed. C. Gans, pp. 45-80. London: Academic Press.

Ericksen, M. F. 1991. Histological Estimation of Age at Death Using the Anterior Cortex of the Femur.

*American Journal of Physical Anthropology.* 84:171-79.

Freemont, A. J. 1989. Histology of Mineralized Tissue. In *Calcified Tissue*, ed. D. W. L. Hukins, pp. 21-40. Baco Raton, Fl.: CRC Press.

Garland, A. N. 1993. An Introduction to the Histology of Exumed Mineralized Tissue. In *Histology of Ancient Bone: Methods and Diagnosis*, ed. by G. Grupe and A. N. Garland, pp. 1-16. Berlin: Springer-Verlag.

Green, M., D. H. Isaac, and G. M. Jenkins. 1985. Bone Microstructure by Collagenase Etching. *Biomaterials.* 6:150-2.

Hancox, N. M. 1972. *Biology of Bone.* Cambridge: Cambridge University Press.

Harsanyi, L. 1993. Differential Diagnosis of Human and Animal Bone. In *Histology of Ancient Bone: Methods and Diagnosis*, ed. G. Grupe and A. N. Garland, pp. 79-94. Berlin: Springer-Verlag.

Havers, C. 1691. *Osteologia Nova.* London: Samuel Smith.

Hummell, S. and M. Schutkowski. 1993. Approaches to the Histological Age Determination of Cremated Human Remains. In *Histology of Ancient Bone: Methods and Diagnosis*, ed. G. Grupe and A. N. Garland, pp. 111-23. Berlin: Springer-Verlag.

Jowsey, J. 1960. Age Changes in Human Bone. *Clinical Orthopedics.* 17:210-18.

Kerley, E. R. 1961. *The Microscopic Determination of Age in Human Bone.* Dissertation. University of Michigan.

Kerley, E. R. 1965. The Microscopic Determination of Age in Human Bone. *American Journal of Physical Anthropology.* 23:149-64.

Kerley, E. R. and D. H. Ubelaker. 1978. Revisions in the Microscopic Method of Estimating Age at Death in Human Cortical Bone. *American Journal of Physical Anthropology.* 49:545-6.

Krogman, W. M. and M. Y. Iscan. 1986. *The Human Skeleton in Forensic Medicine.* 2nd ed. Springfield: Charles C. Thomas.

La Croix, P. 1971. The Internal Remodeling of Bones. In *The Biochemistry and Physiology of Bone, Vol. 3*, ed. G. H. Bourne, pp. 119-44. New York: Academic Press.

MacGregor, A. 1985. *Bone, Antler, Ivory and Horn: The Technology of Skeletal Materials since the Roman Period.* London: Croom Helm.

Mercyhurst College. 1993. *Field and Laboratory Methods in the Location, Recovery, and Analysis of Human Remains in a Rural Setting.* Erie, Pa.: Mercyhurst College.

Pouliot, R. 1994. Phone Interview with Data Translation technician concerning the History of the Global Image Lab on 21 October.

Rodriguez III, W. C. 1994. Rapid Screening Procedure for Histological Differentiation between Human and Non-Human Fragmentary Skeletal Remains. Paper presented at the American Academy of Forensic Science 46th Annual Meeting.

Savage, D. C. 1995. Personal communication concerning the characteristics and use of biological microscopes.

Shipman, P., A. Walker, and D. Bichell. 1985. *The Human Skeleton.* Cambridge: Harvard University Press.

Singh, I. J. and D. L. Gunberg. 1970. Estimation of Age at Death in Human Males from Quantitative Histology of Bone Fragments. *American Journal of Physical Anthropology.* 33:373-82.

Smith, R. F. 1994. *Microscopy and Photomicrography: A Working Manual.* 2nd ed. Ann Arbor: CRC Press.

Sorbathane, Inc. 1996. Personal communication with company concerning Sorbothane product information.

Stewart, T. D. 1979. *Essentials of Forensic Anthropology: Especially as Developed in the United States.* Springfield: Charles C. Thomas.

Stout, S. D. 1989a. The Use of Cortical Bone Histology to Estimate Age at Death. In *Age Markers in the Human Skeleton,* ed. M. Y. Iscan, pp. 195-207. Springfield: Charles C. Thomas.

Stout, S. D. 1989b. Histomorphometric Analysis of Human Skeletal Remains. In *Reconstruction of Life from the Skeleton.* ed. M. Y. Iscan and K. A. R. Kennedy, pp. 41-52. New York: Wiley-Liss, Inc.

Stout, S. D. 1992. Methods of Determining Age at Death Using Bone Microstructure. In *Skeletal Biology of Past Peoples: Research Methods,* ed. S. R. Saunders and M. A. Katzenberg, pp. 21-35. New York: Wiley-Liss, Inc.

Stout, S. D. and S. J. Gehlert. 1982. Effects of Field Size When Using Kerley's Histological Method for Determination of Age at Death. *American Journal of Physical Anthropology.* 58:123-5.

Stout, S. D. and R. R. Paine. 1992. Brief Communication: Histological Age Estimation Using Rib and Clavicle. *American Journal of Physical Anthropology.* 87:111-5.

Stout, S. D. and S. C. Stanley. 1991. Percent Osteonal Bone Versus Osteon Counts: The Variable of Choice for Estimating Age at Death. *American Journal of Physical Anthropology.* 86:515-9.

Stout, S. D. 1995. Personal communication concerning 1994 Australian study.

Stout, S. D. 1999. Personal communication concerning data and time requirements for bone histological counting.

Symes, S. 1994. Personal Communication concerning the possibilities of obtaining samples and potential use of densitometry on the 18 March.

Ubelaker, D. H. 1974. Reconstruction of Demographic Profiles from Ossuary Skeletal Samples: A Case Study from the Tidewater Potomac. *Smithsonian Contributions to Anthropology 18.* Washington, D.C.: Smithsonian Institution Press.

Ubelaker, D. H. 1978. *Human Skeletal Remains. Excavation, Analysis, Interpretation.* Chicago: Aldine.

Uytterschaut, H. 1993. Human Bone Remodeling and Aging. In *Histology of Ancient Bone: Methods and Diagnosis,* ed. G. Grupe and A. N. Garland, pp. 95-109. Berlin: Springer-Verlag.

Walls, C. A. 1999. Personal communication concerning Rapid Prototype Stereo Lithography technology.

White, T. D. 1991. *Human Osteology.* New York: Academic Press, Inc.

# APPENDIX

# APPENDIX

| Table A-1: 30 Selected Forensic Slides from the UTK Forensic Histology Collection | |
|---|---|
| **Case Number** | **Subject Number** |
| 22781 | 1 |
| 72-3 | 2 |
| 73-1 | 3 |
| 74-2 | 4 |
| 74-5 | 5 |
| 79-13 | 6 |
| 80-12 | 7 |
| 80-15 | 8 |
| 80-3 | 9 |
| 80-6 | 10 |
| 81-110 | 11 |
| 81-13 | 12 |
| 812005 | 13 |
| 81-9 | 14 |
| 82-16 | 15 |
| 82-1 | 16 |
| 83-10 | 17 |
| 83215 | 18 |
| 83-25 | 19 |
| 83-9 | 20 |
| 84-14 | 21 |
| 85-1 | 22 |
| 85-24 | 23 |
| 85-7 | 24 |
| F83215 | 25 |
| F83539 | 26 |
| Fa12 | 27 |
| O80120 | 28 |
| 081-9 | 29 |
| O82-2 | 30 |

| Table A-2: Data Submitted by Dr. Sam D. Stout (Permission Given)<br>Key: 1 = Male and 2 = Female | | | |
|---|---|---|---|
| **Subject ID** | **Age of Subject** | **Sex** | **Whole Osteons Count** |
| 1874 | 51 | 1 | 25.76 |
| 1730 | 51 | 1 | 25.76 |
| 1825 | 51 | 1 | 19.26 |
| 2490 | 51 | 2 | 12.82 |
| 2851 | 52 | 1 | 17.05 |
| 2269 | 53 | 1 | 23.37 |
| 1744 | 53 | 1 | 28.92 |
| 1803 | 54 | 1 | 19.13 |
| 1681 | 54 | 1 | 24.84 |
| 2297 | 54 | 1 | 19.61 |
| 2310 | 54 | 2 | 17.20 |
| 2842 | 55 | 2 | 17.46 |
| 1797 | 55 | 2 | 23.25 |
| 1783 | 55 | 2 | 25.15 |
| 2354 | 57 | 2 | 26.21 |
| 1885 | 57 | 1 | 24.62 |
| 18.61 | 58 | 1 | 15.24 |
| 2827 | 58 | 1 | 19.93 |
| 1834 | 59 | 2 | 20.97 |
| 1905 | 59 | 2 | 22.03 |
| 1903 | 59 | 2 | 18.75 |
| 2137 | 60 | 1 | 19.28 |
| 2865 | 60 | 2 | 24.58 |
| 2278 | 61 | 2 | 15.66 |
| 1652 | 61 | 1 | 18.03 |
| 2331 | 62 | 2 | 22.55 |
| 1691 | 62 | 1 | 22.95 |
| 1875 | 62 | 1 | 26.80 |
| 1818 | 63 | 1 | 24.27 |
| 1465 | 65 | 1 | 21.34 |
| 1703 | 65 | 2 | 18.91 |
| 2385 | 65 | 2 | 27.85 |
| 2302 | 66 | 2 | 28.15 |
| 1804 | 66 | 2 | 24.06 |
| 1745 | 66 | 2 | 24.59 |
| 2910 | 66 | 1 | 26.89 |
| 2848 | 66 | 1 | 24.42 |
| 2167 | 67 | 1 | 27.52 |
| 1636 | 67 | 1 | 26.36 |
| 1669 | 68 | 1 | 23.41 |
| 2382 | 68 | 1 | 27.57 |

| Table A-2 (continued) | | | |
|---|---|---|---|
| 2371 | 68 | 1 | 20.53 |
| 1782 | 70 | 1 | 19.05 |
| 2292 | 70 | 1 | 19.55 |
| 2633 | 71 | 2 | 29.95 |
| 1786 | 72 | 2 | 28.05 |
| 1665 | 72 | 2 | 29.76 |
| 1608 | 72 | 2 | 32.34 |
| 2346 | 72 | 2 | 41.10 |
| 1631 | 73 | 1 | 27.84 |
| 1620 | 74 | 1 | 21.56 |
| 1657 | 74 | 2 | 24.85 |
| 1759 | 75 | 1 | 22.51 |
| 1743 | 75 | 1 | 21.11 |
| 1675 | 75 | 1 | 18.62 |
| 1709 | 76 | 2 | 24.87 |
| 2274 | 77 | 2 | 27.24 |
| 1693 | 77 | 1 | 21.30 |
| 1617 | 78 | 2 | 24.99 |
| 1685 | 79 | 2 | 23.80 |
| 1642 | 80 | 1 | 22.37 |
| 1760 | 80 | 2 | 28.47 |
| 2158 | 81 | 2 | 32.08 |
| 1635 | 81 | 2 | 26.94 |
| 1671 | 82 | 1 | 20.73 |
| 2199 | 82 | 1 | 25.36 |
| 1643 | 84 | 1 | 24.41 |
| 1680 | 84 | 2 | 20.00 |
| 1781 | 84 | 2 | 24.26 |
| 1699 | 85 | 2 | 17.85 |
| 1645 | 86 | 1 | 23.79 |
| 1673 | 86 | 1 | 21.07 |
| 1639 | 86 | 1 | 26.16 |
| 1780 | 86 | 2 | 25.80 |
| 1646 | 87 | 1 | 24.93 |
| 2144 | 89 | 2 | 27.43 |
| 1640 | 89 | 1 | 26.87 |
| 1623 | 90 | 1 | 23.72 |
| 1747 | 90 | 2 | 26.53 |
| 1674 | 91 | 1 | 19.19 |
| 2620 | 91 | 1 | 26.56 |
| 1789 | 94 | 1 | 25.57 |
| 2622 | 94 | 2 | 32.79 |
| 2595 | 95 | 1 | 28.85 |

# Table A-3: Data Collection Sheets

| Case #1 | ID: 22781 | Actual Age: NA | Lab Age: NA | | Estimated Age: 29.26 (29) | | |
|---|---|---|---|---|---|---|---|
| FOV | | | | | Results of Regression Equations | | |
| | Osteon | Frag. Osteon | % of Lamellar | Nonhaversian | Est Age | SSE- | SSE+ |
| Anterior | 4 | 4 | 0.213305 | 6 | O. | 16.46104 | 7.27104 | 25.65104 |
| Posterior | 10 | 19 | 0.028724 | 5 | F O | 47.7714 | 40.7914 | 54.7514 |
| Lateral | 16 | 12 | 0.050678 | 3 | % L | 74.39103 | 61.87103 | 86.91103 |
| Medial | 18 | 9 | 0.057782 | 1 | N H | 23.545 | 11.425 | 35.665 |
| Total Overall Count | 48 | 44 | 0.350489 | 15 | | | | |
| Case #2 | ID: 72-3 | Actual Age: 34 | Lab Age: NA | | Estimated Age: 31.62 (32) | | |
| FOV | | | | | Results of Regression Equations | | |
| | Osteon | Frag. Osteon | % of Lamellar | Nonhaversian | Est Age | SSE- | SSE+ |
| Anterior | 21 | 15 | 0.107665 | 2 | O. | 26.442 | 17.252 | 35.632 |
| Posterior | 12 | 9 | 0.043356 | 4 | F O | 47.7714 | 40.7914 | 54.7514 |
| Lateral | 17 | 8 | 0.045592 | 7 | % L | 74.57042 | 62.05042 | 87.09042 |
| Medial | 20 | 12 | 0.053271 | 4 | N H | 20.64252 | 8.52252 | 32.76252 |
| Total Overall Count | 70 | 44 | 0.249884 | 17 | | | | |
| Case #3 | ID: 73-1 | Skeletal Age: 18-21 | Lab Age: NA | | Estimated Age: 31.08 (31) | | |
| FOV | | | | | Results of Regression Equations | | |
| | Osteon | Frag. Osteon | % of Lamellar | Nonhaversian | Est Age | SSE- | SSE+ |
| Anterior | 22 | 12 | 0.033542 | 5 | O. | 31.702 | 22.512 | 40.892 |
| Posterior | 17 | 10 | 0.087295 | 6 | F O | 46.63495 | 39.65495 | 53.61495 |
| Lateral | 20 | 10 | 0.081465 | 5 | % L | 74.23448 | 61.71448 | 86.75448 |
| Medial | 21 | 11 | 0.236083 | 6 | N H | 14.90392 | 2.78392 | 27.02392 |
| Total Overall Count | 80 | 43 | 0.438385 | 22 | | | | |

**Plate A-1**

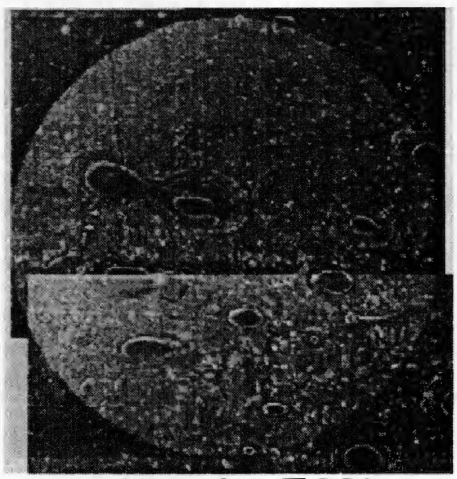

**Anterior FOV**

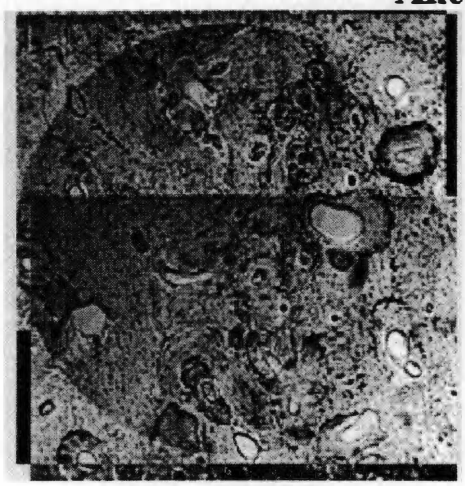

**Lateral FOV**

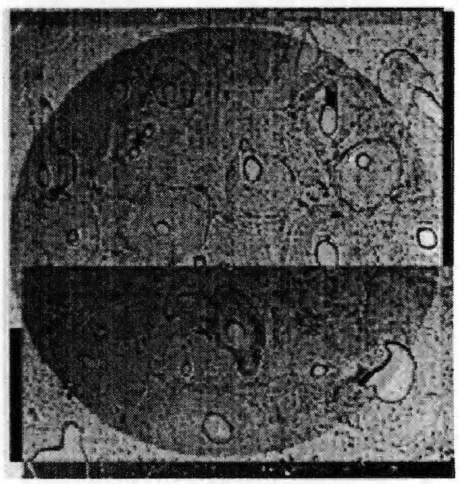

**Medial FOV**

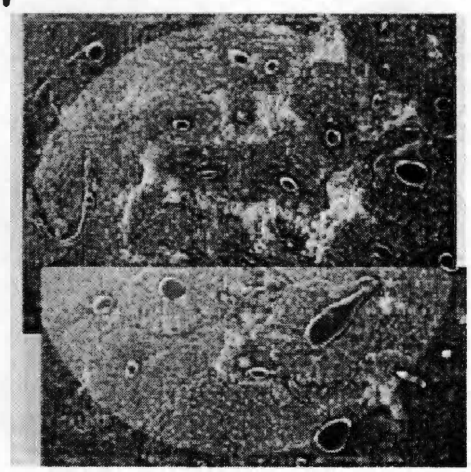

**Posterior FOV**
**Case #1: 22781**

**Plate A-2**

**Anterior FOV**

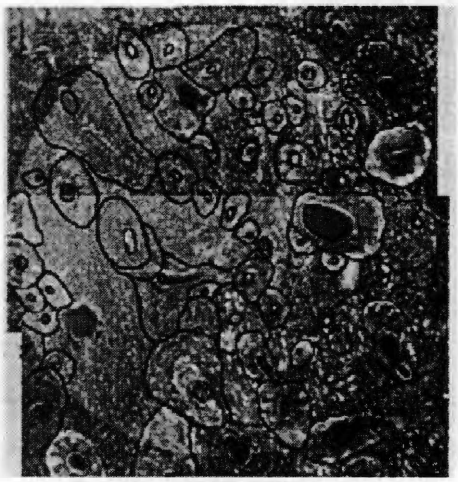

**Lateral FOV**

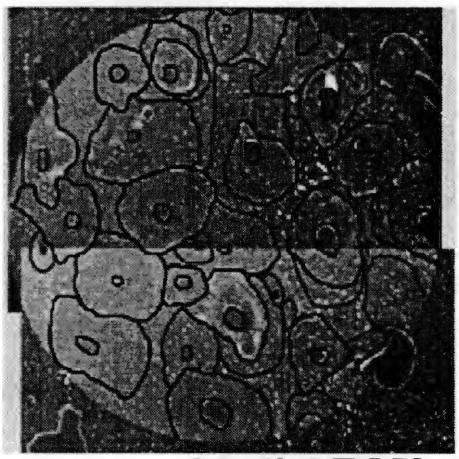

**Medial FOV**

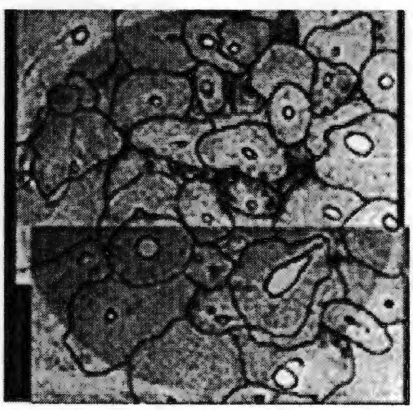

**Posterior FOV**

**Case #1: 22781**

## Plate A-3

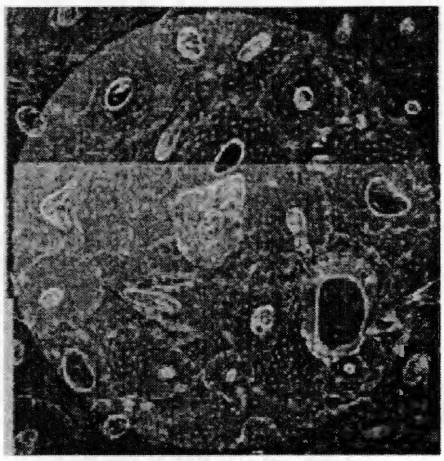

**Anterior FOV**

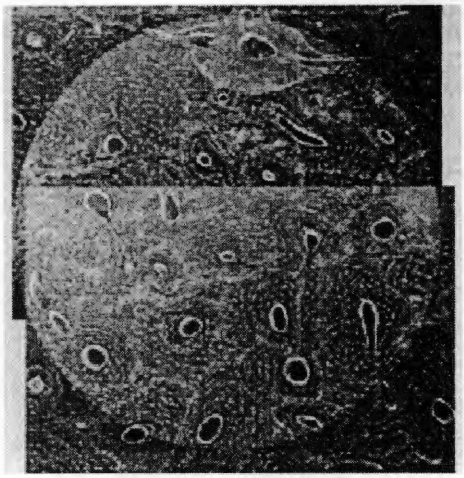

**Lateral FOV**

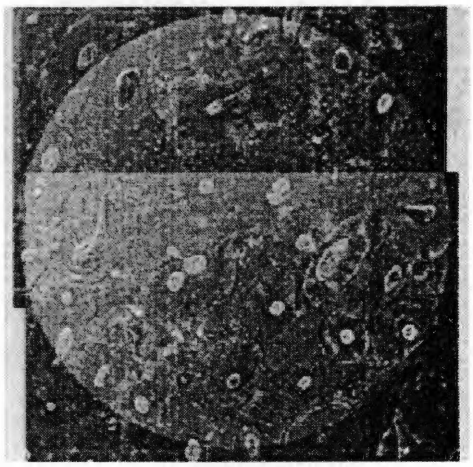

**Medial FOV**

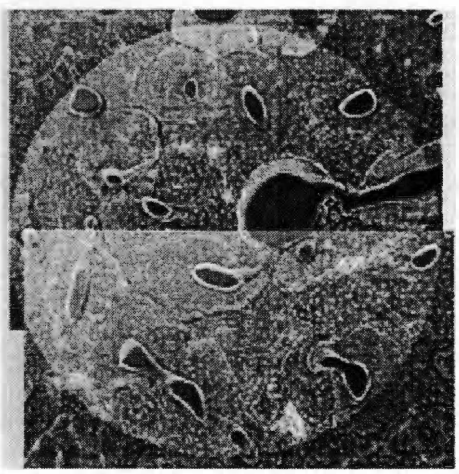

**Posterior FOV**
**Case #2: 72-3**

**Plate A-4**

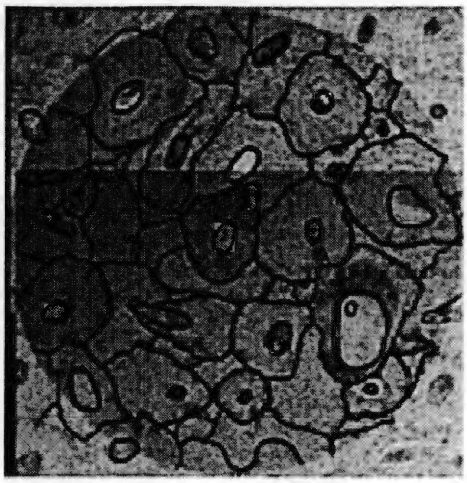

**Anterior FOV**

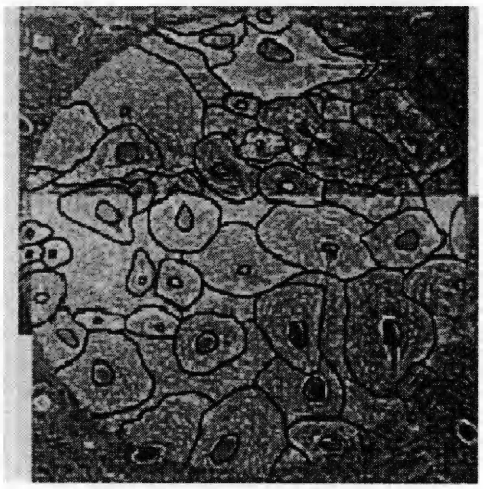

**Lateral FOV**

**Medial FOV**

**Posterior FOV**
**Case #2: 72-3**

## Plate A-5

Anterior FOV

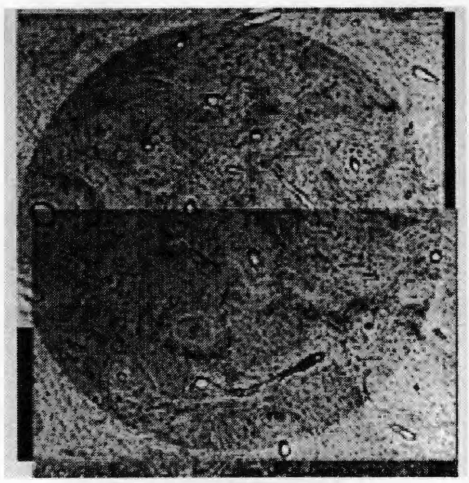

Lateral FOV

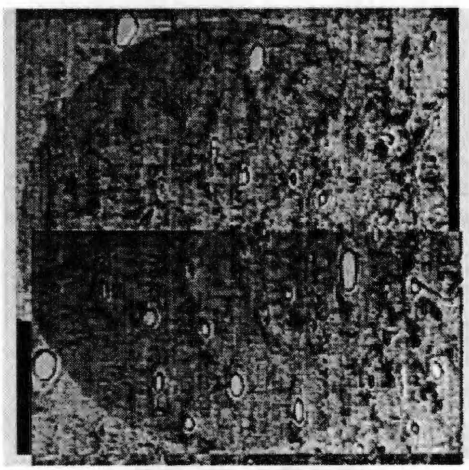

Medial FOV

Posterior FOV
Case #3: 73-1

## Plate A-6

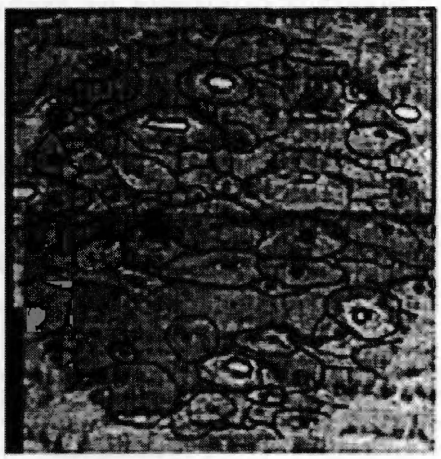

Anterior FOV

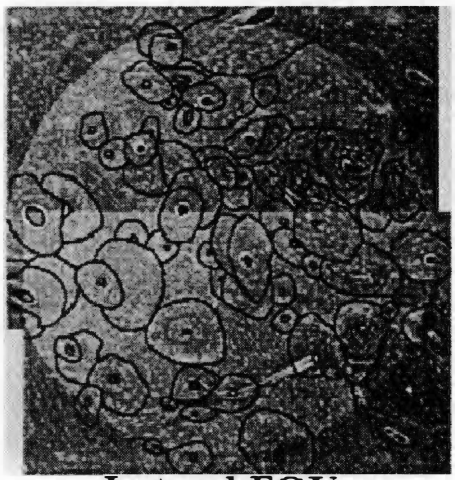

Lateral FOV

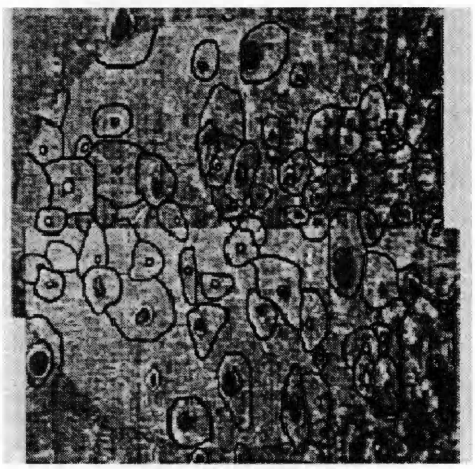

Medial FOV

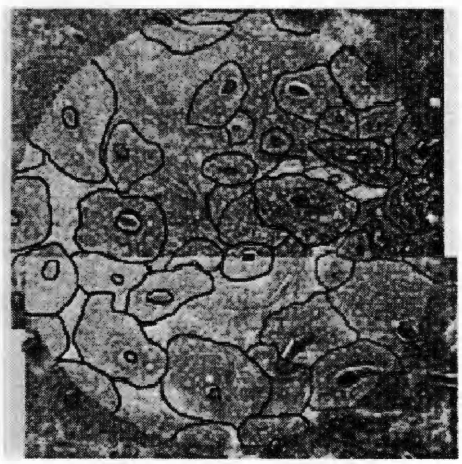

Posterior FOV

Case #3: 73-1

# Table A-3: Data Collection Sheets (continued)

| Case #4 | ID: 74-2 | Actual Age: 28 | | Lab Age: NA | | Estimated Age: 32.63 (33) | | |
|---|---|---|---|---|---|---|---|---|
| FOV | | | | | Results of Regression Equations | | | |
| | Osteon | Frag. Osteon | % of Lamellar | Nonhaversian | | Est Age | SSE- | SSE+ |
| Anterior | 32 | 11 | 0.051188 | 12 | O. | 44.21926 | 35.02926 | 53.40926 |
| Posterior | 25 | 11 | 0.044322 | 7 | F O | 44.34885 | 37.36885 | 51.32885 |
| Lateral | 21 | 6 | 0.055842 | 4 | % L | 74.62292 | 62.10292 | 87.14292 |
| Medial | 23 | 13 | 0.069116 | 8 | | | | |
| Total Overall Count | 101 | 41 | 0.220468 | 31 | N H | 9.31204 | -2.80796 | 21.43204 |
| Case #5 | ID: 74-5 | Actual Age: 43 | | Lab Age: NA | | Estimated Age: 38.72 (39) | | |
| FOV | | | | | Results of Regression Equations | | | |
| | Osteon | Frag. Osteon | % of Lamellar | Nonhaversian | | Est Age | SSE- | SSE+ |
| Anterior | 17 | 5 | 0.089999 | 5 | O. | 20.27974 | 11.08974 | 29.46974 |
| Posterior | 11 | 6 | 0.08097 | 4 | F O | 44.34885 | 37.36885 | 51.32885 |
| Lateral | 12 | 16 | 0.100442 | 4 | % L | 74.37451 | 61.85451 | 86.89451 |
| Medial | 17 | 14 | 0.088344 | 8 | | | | |
| Total Overall Count | 57 | 41 | 0.359755 | 21 | N H | 15.88684 | 3.76684 | 28.00684 |
| Case #6 | ID: 79-13 | Actual Age: 36 | | Lab Skeletal Age: 26-28 | | Estimated Age: 38.10 (38) | | |
| FOV | | | | | Results of Regression Equations | | | |
| | Osteon | Frag. Osteon | % of Lamellar | Nonhaversian | | Est Age | SSE- | SSE+ |
| Anterior | 12 | 10 | 0.040615 | 4 | O. | 20.72664 | 11.53664 | 29.91664 |
| Posterior | 12 | 7 | 0.165517 | 5 | F O | 43.201 | 36.221 | 50.181 |
| Lateral | 17 | 8 | 0.046639 | 9 | % L | 74.47765 | 61.95765 | 86.99765 |
| Medial | 17 | 15 | 0.049125 | 5 | | | | |
| Total Overall Count | 58 | 40 | 0.301896 | 23 | N H | 13.99908 | 1.87908 | 26.11908 |

## Plate A-7

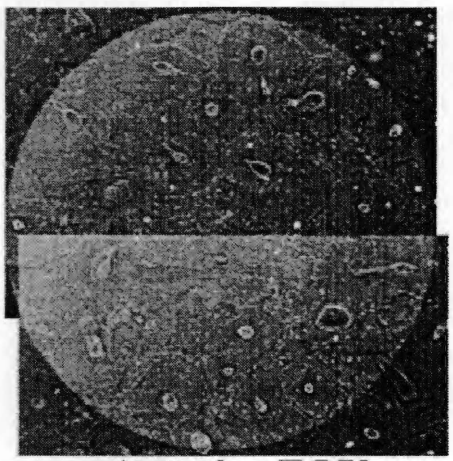

Anterior FOV

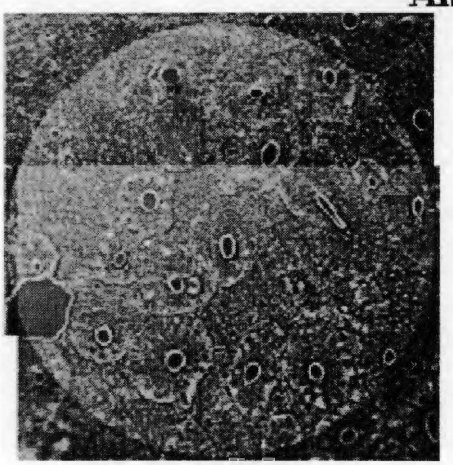

Lateral FOV

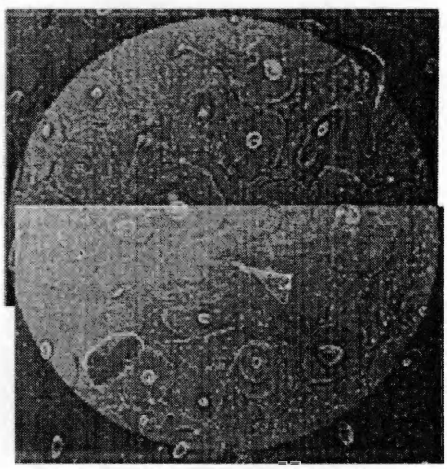

Medial FOV

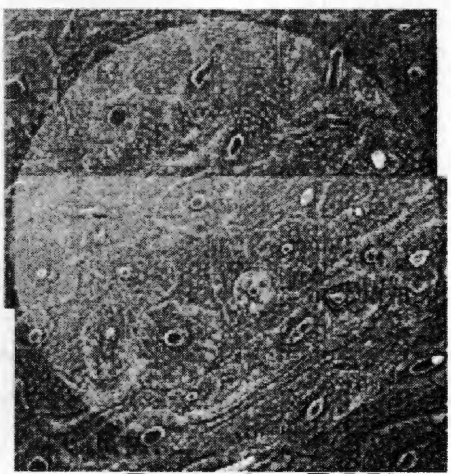

Posterior FOV

Case 4: 74-2

## Plate A-8

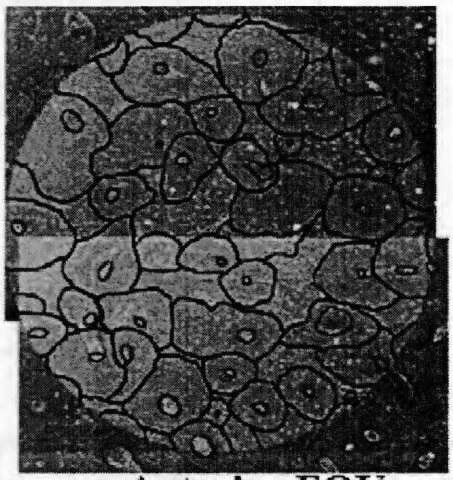

Anterior FOV

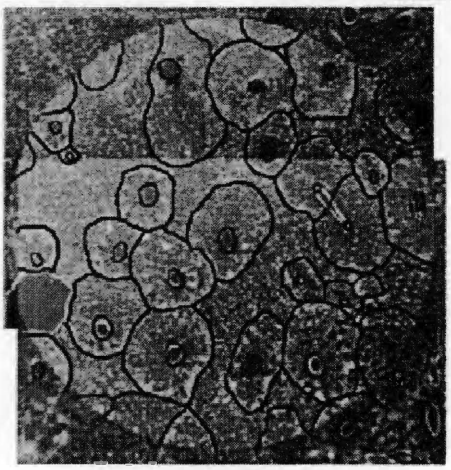

Lateral FOV

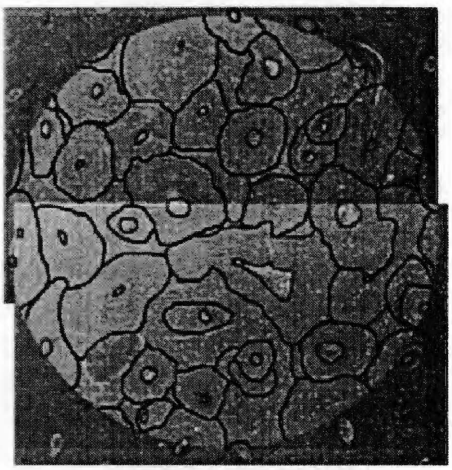

Medial FOV

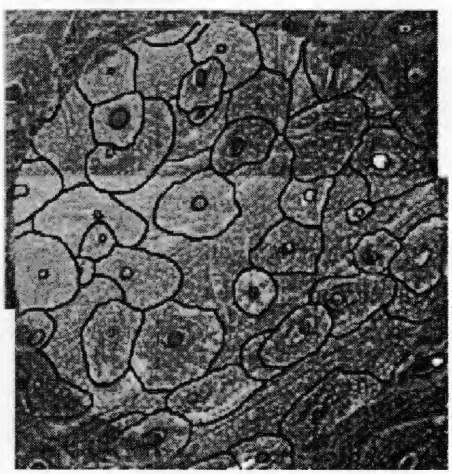

Posterior FOV
Case #4: 74-2

## Plate A-9

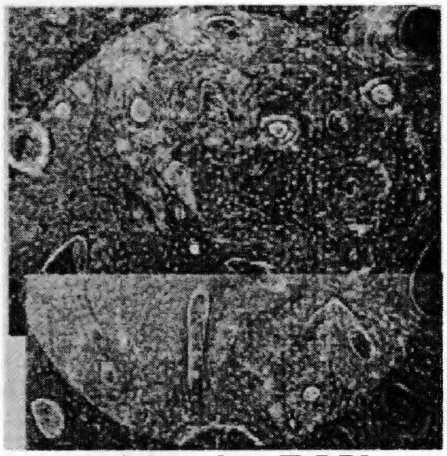

**Anterior FOV**

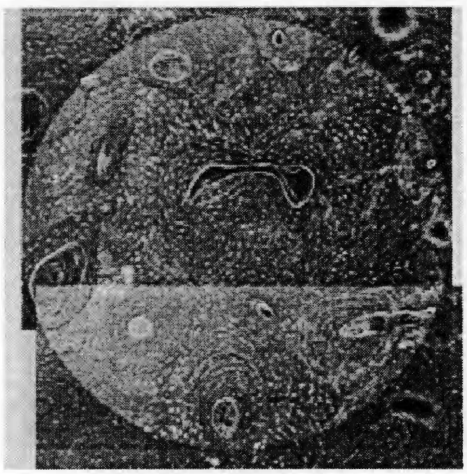

**Lateral FOV**

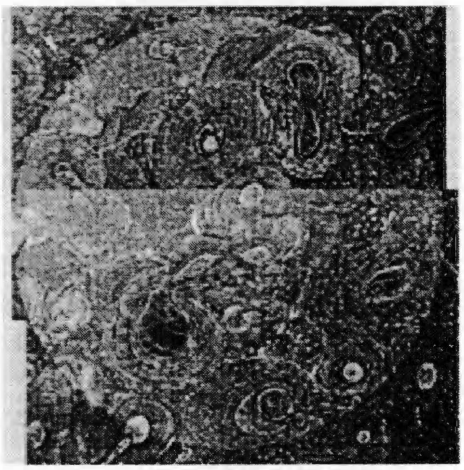

**Medial FOV**

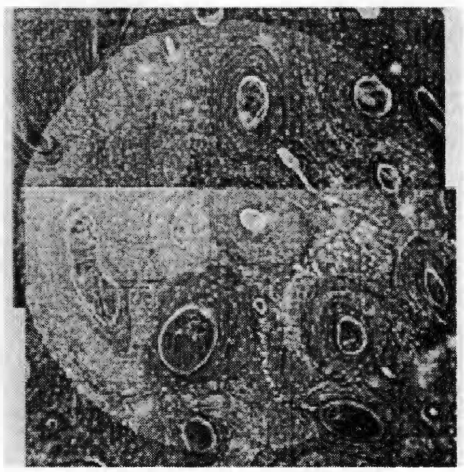

**Posterior FOV**
**Case #5: 74-5**

**Plate A-10**

**Anterior FOV**

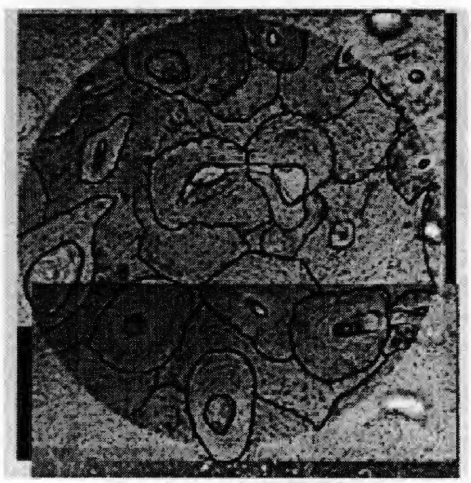

**Lateral FOV**

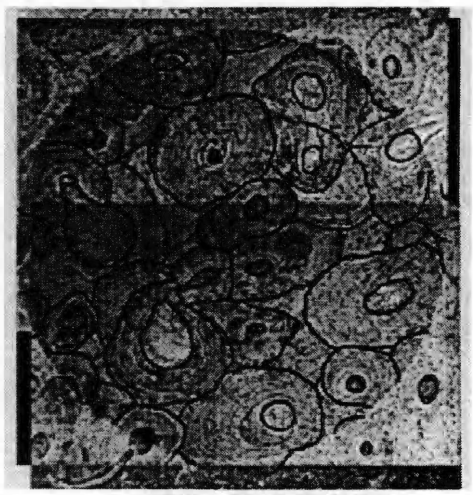

**Medial FOV**

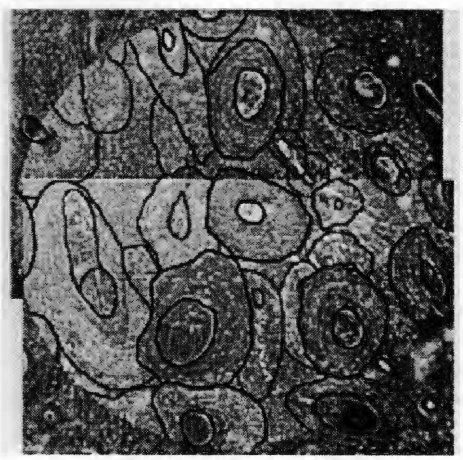

**Posterior FOV**
**Case #5: 74-5**

**Plate A-11**

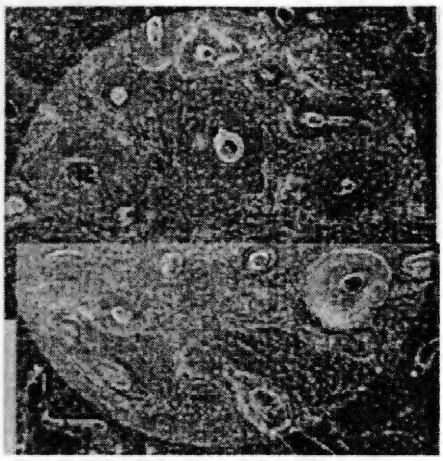

**Anterior FOV**

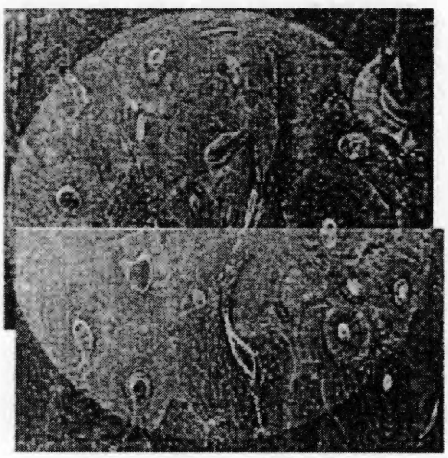

**Lateral FOV**

**Medial FOV**

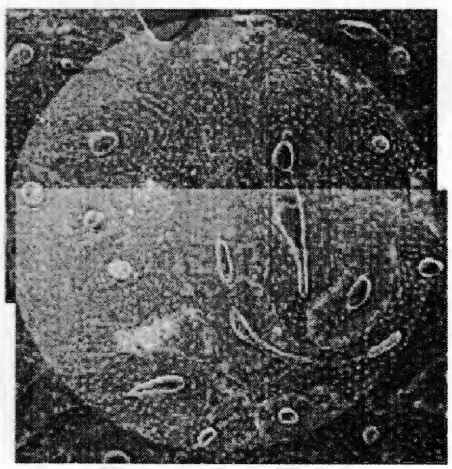

**Posterior FOV**
**Case #6: 79-13**

**Plate A-12**

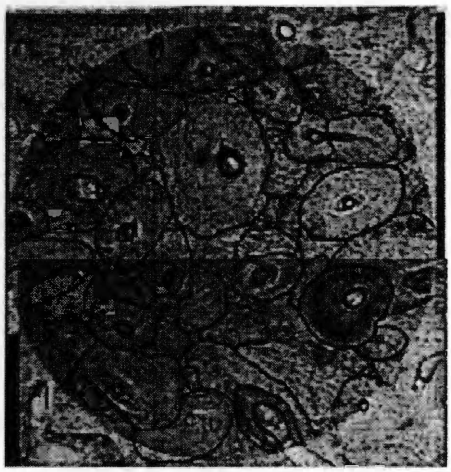

**Anterior FOV**

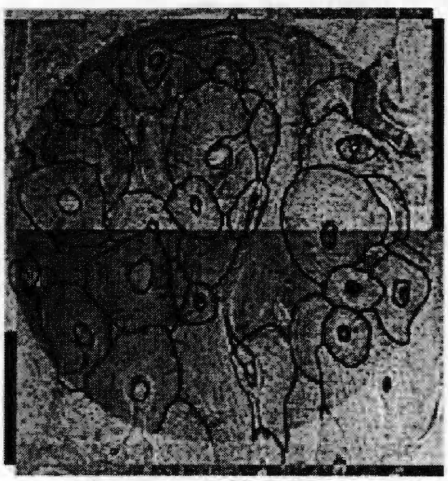

**Lateral FOV**

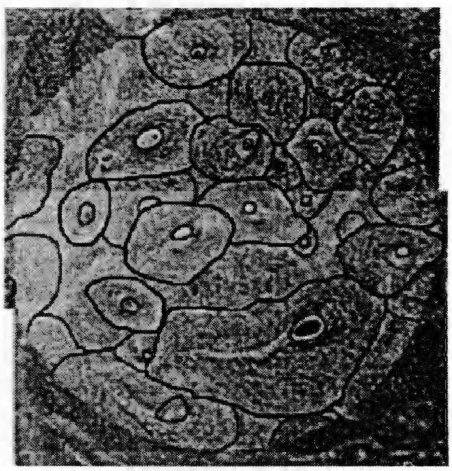

**Medial FOV**

**Posterior FOV**
**Case #6: 79-13**

# Table A-3: Data Collection Sheets (continued)

| Case #7 | ID: 80-12 | Actual Age: 27 | | Lab Age: NA | Estimated Age: 25.57 (26) | | | |
|---|---|---|---|---|---|---|---|---|
| FOV | | | | | Results of Regression Equations | | | |
| | Osteon | Frag. Osteon | % of Lamellar | Nonhaversian | | Est Age | SSE- | SSE+ |
| Anterior | 12 | 11 | 0.230135 | 7 | O. | 24.95214 | 15.76214 | 34.14214 |
| Posterior | 16 | 9 | 0.058981 | 7 | F O | 38.5986 | 31.6186 | 45.5786 |
| Lateral | 18 | 6 | 0.140873 | 6 | % | 74.0579 | 61.5379 | 86.5779 |
| Medial | 21 | 10 | 0.107664 | 4 | L | | | |
| Total Overall Count | 67 | 36 | 0.537653 | 24 | N H | 13.17016 | 1.05016 | 25.29016 |

| Case #8 | ID: 80-15 | Actual Age: NA | | Lab Age: NA | Estimated Age: 27.96 (28) | | | |
|---|---|---|---|---|---|---|---|---|
| FOV | | | | | Results of Regression Equations | | | |
| | Osteon | Frag. Osteon | % of Lamellar | Nonhaversian | | Est Age | SSE- | SSE+ |
| Anterior | 16 | 9 | 0.060713 | 4 | O. | 22.55944 | 13.36944 | 31.74944 |
| Posterior | 23 | 9 | 0.045016 | 5 | F O | 48.90225 | 41.92225 | 55.88225 |
| Lateral | 11 | 12 | 0.265506 | 10 | % | 73.82051 | 61.30051 | 86.34051 |
| Medial | 12 | 15 | 0.300065 | 6 | L | | | |
| Total Overall Count | 62 | 45 | 0.6713 | 25 | N H | 12.415 | 0.295 | 24.535 |

| Case #9 | ID: 80-3 | Skeletal Age: 30-40 | | Lab Age: NA | Estimated Age: 44.64 (45) | | | |
|---|---|---|---|---|---|---|---|---|
| FOV | | | | | Results of Regression Equations | | | |
| | Osteon | Frag. Osteon | % of Lamellar | Nonhaversian | | Est Age | SSE- | SSE+ |
| Anterior | 17 | 5 | 0.116302 | 11 | O. | 37.414 | 28.224 | 46.604 |
| Posterior | 24 | 14 | 0.050114 | 12 | F O | 56.5858 | 49.6058 | 63.5658 |
| Lateral | 26 | 19 | 0.065061 | 14 | % | 74.47811 | 61.95811 | 86.99811 |
| Medial | 23 | 14 | 0.070158 | 10 | L | | | |
| Total Overall Count | 90 | 52 | 0.301635 | 47 | N H | 10.09092 | -2.02908 | 22.21092 |

## Plate A-13

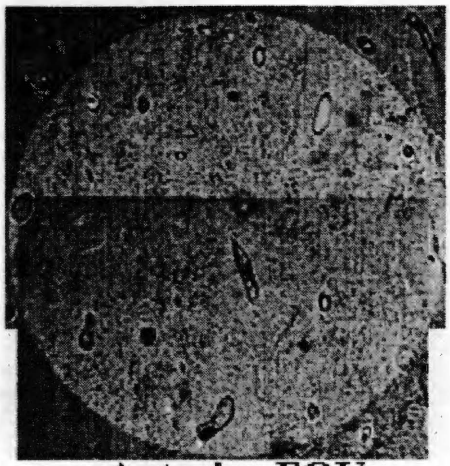

Anterior FOV

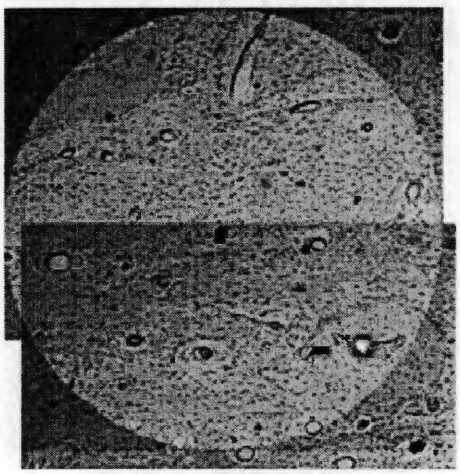

Lateral FOV

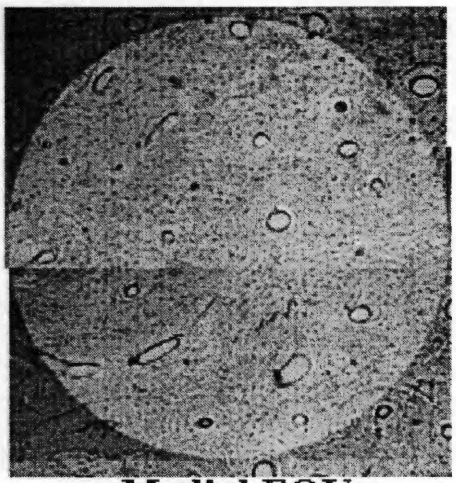

Medial FOV

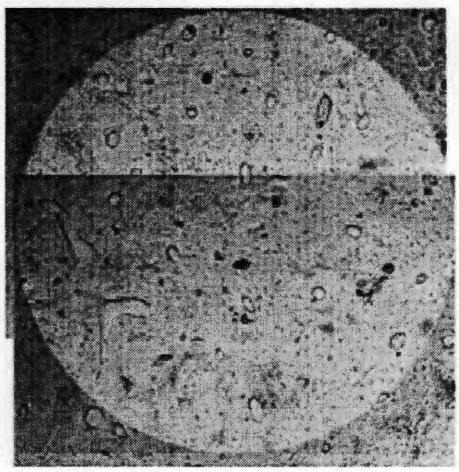

Posterior FOV
Case #7: 80-12

**Plate A-14**

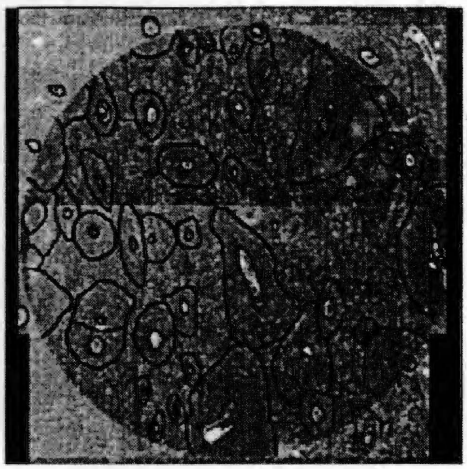

**Anterior FOV**

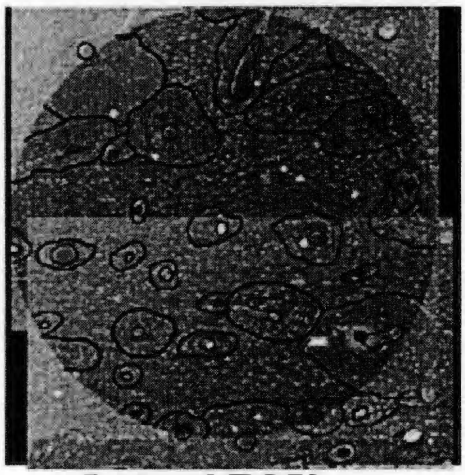

**Lateral FOV**

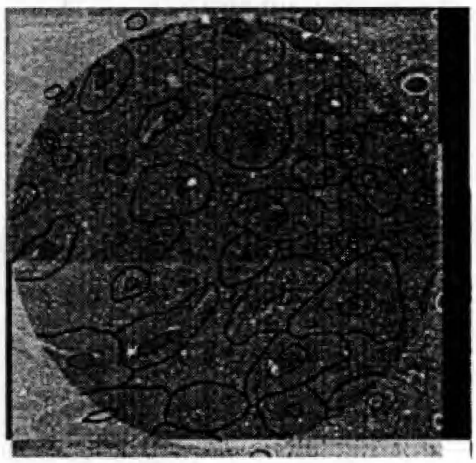

**Medial FOV**

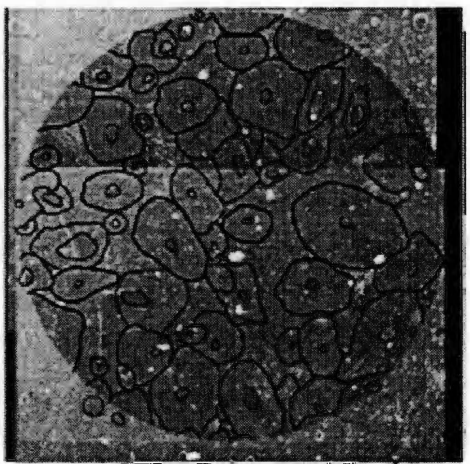

**Posterior FOV**
**Case #7: 80-12**

## Plate A-15

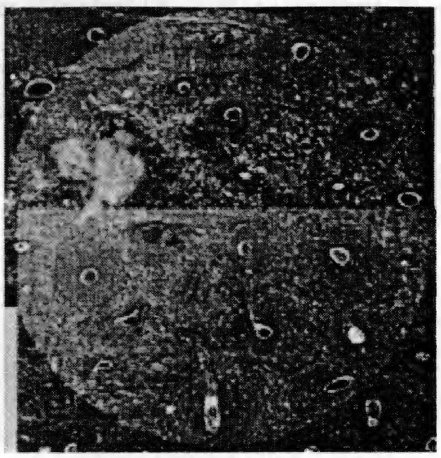

Anterior FOV

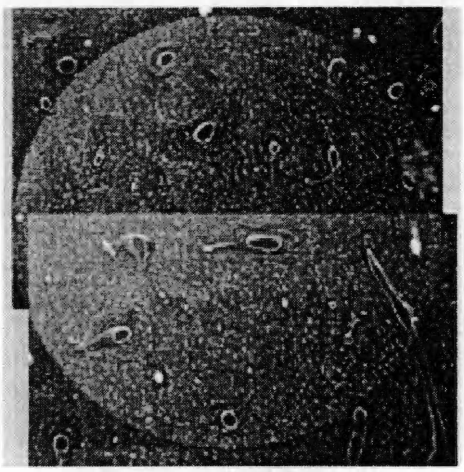

Lateral FOV

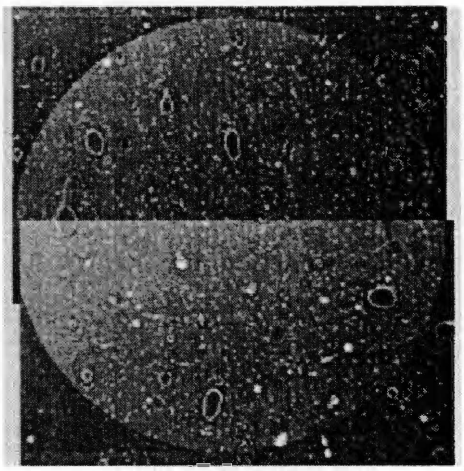

Medial FOV

Posterior FOV
Case #8: 80-15

## Plate A-16

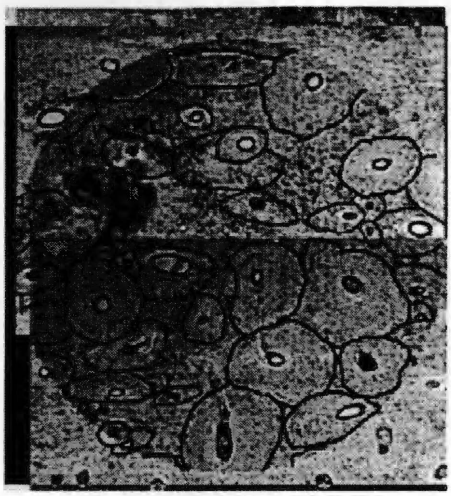

**Anterior FOV**

**Lateral FOV**

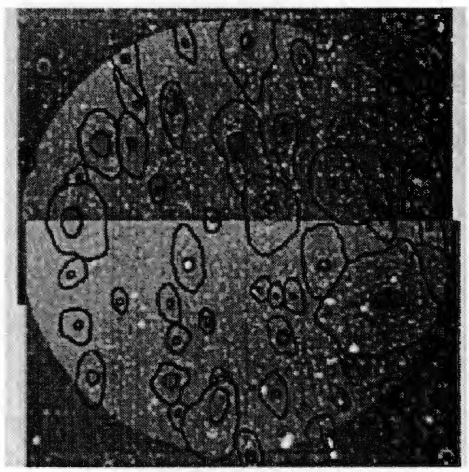

**Medial FOV**

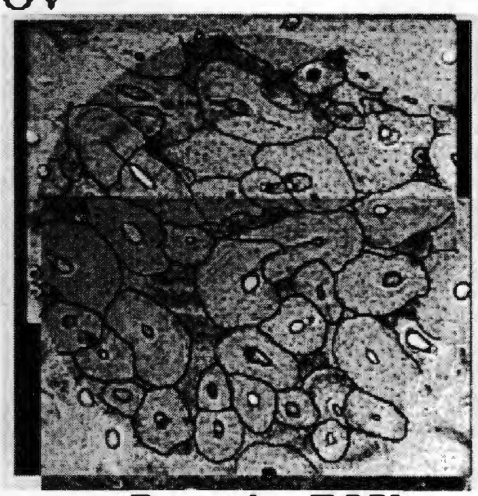

**Posterior FOV**
**Case #8: 80-15**

**Plate A-17**

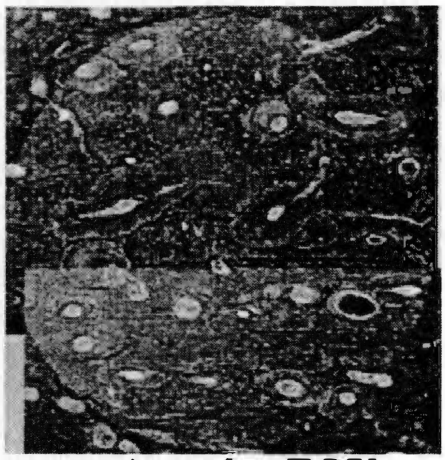

**Anterior FOV**

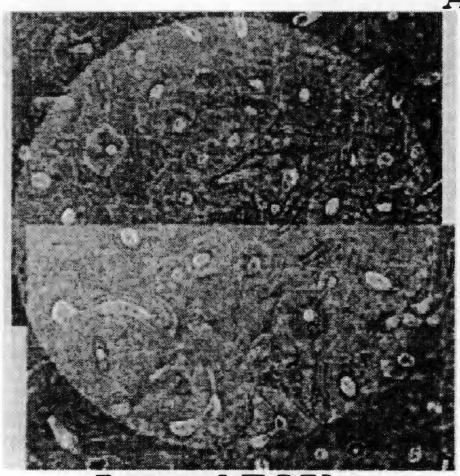

**Lateral FOV**

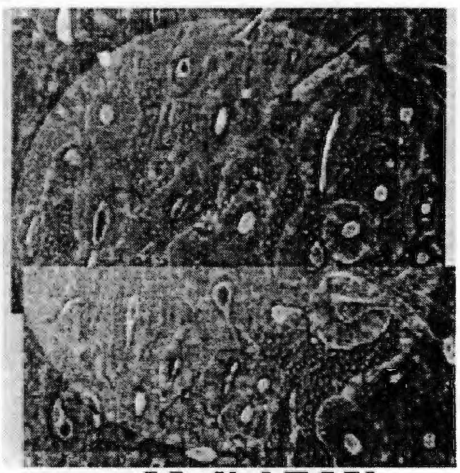

**Medial FOV**

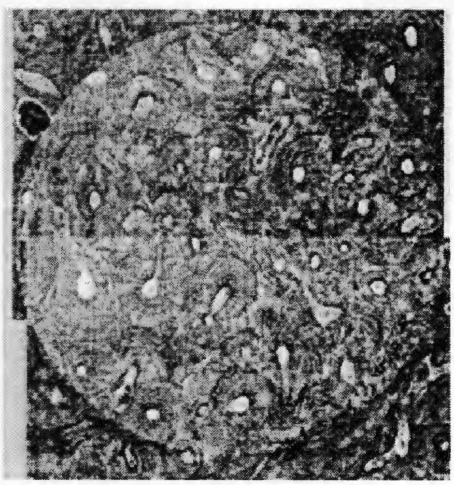

**Posterior FOV**
**Case #9: 80-3**

**Plate A-18**

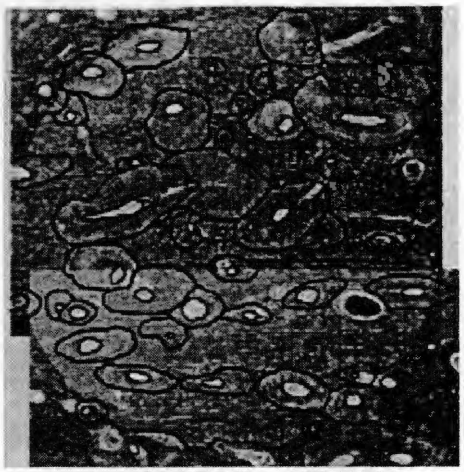

**Anterior FOV**

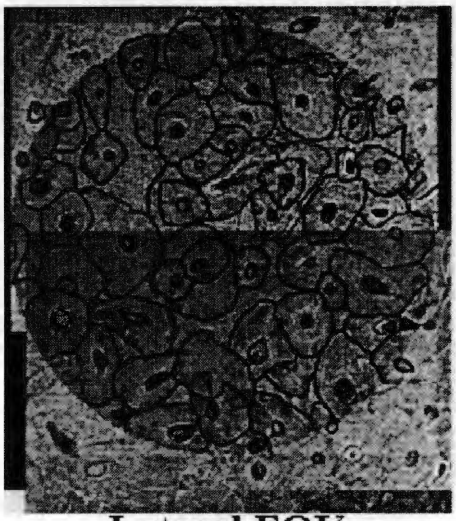

**Lateral FOV**

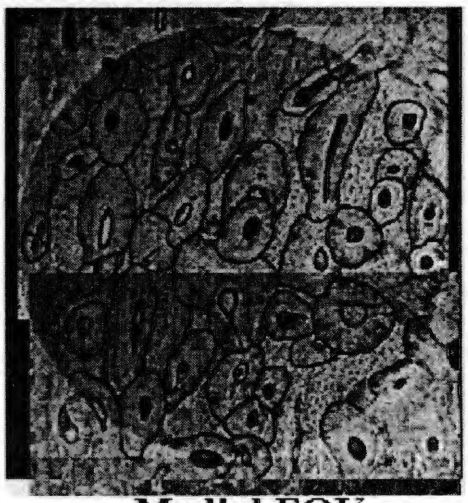

**Medial FOV**

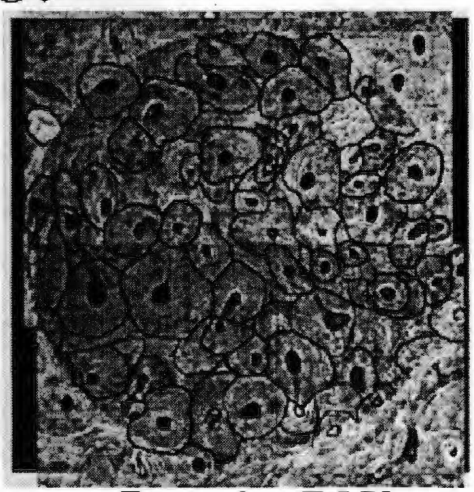

**Posterior FOV**
**Case #9: 80-3**

# Table A-3: Data Collection Sheets (continued)

| Case#10 | ID: 80-6 | Actual Age: 65 | | Lab Age: NA | Estimated Age: 63.03 (63) | | | |
|---|---|---|---|---|---|---|---|---|
| FOV | | | | | Results of Regression Equations | | | |
| | Osteon | Frag. Osteon | % of Lamellar | Nonhaversian | | Est Age | SSE- | SSE+ |
| Anterior | 34 | 16 | 0.057016 | 7 | O. | 44.21926 | 35.02926 | 53.40926 |
| Posterior | 22 | 15 | 0.068599 | 7 | F O | 70.54255 | 63.56255 | 77.52255 |
| Lateral | 24 | 19 | 0.149468 | 6 | % L | 74.3407 | 61.8207 | 86.8607 |
| Medial | 21 | 17 | 0.103654 | 5 | | | | |
| Total Overall Count | 101 | 67 | 0.378737 | 25 | N H | 12.415 | 0.295 | 24.535 |
| Case#11 | ID: 81-110 | Actual Age: NA | | Lab Age: NA | Estimated Age: 41.53 (42) | | | |
| FOV | | | | | Results of Regression Equations | | | |
| | Osteon | Frag. Osteon | % of Lamellar | Nonhaversian | | Est Age | SSE- | SSE+ |
| Anterior | 24 | 16 | 0.066926 | 5 | O. | 26.442 | 17.252 | 35.632 |
| Posterior | 12 | 13 | 0.074128 | 8 | F O | 51.14355 | 44.16355 | 58.12355 |
| Lateral | 16 | 8 | 0.068329 | 2 | % L | 74.54099 | 62.02099 | 87.06099 |
| Medial | 18 | 10 | 0.056995 | 8 | | | | |
| Total Overall Count | 70 | 47 | 0.266378 | 23 | N H | 13.99908 | 1.87908 | 26.11908 |
| Case#12 | ID: 81-13 | Actual Age: NA | | Lab Age: NA | Estimated Age: 39.24 (39) | | | |
| FOV | | | | | Results of Regression Equations | | | |
| | Osteon | Frag. Osteon | % of Lamellar | Nonhaversian | | Est Age | SSE- | SSE+ |
| Anterior | 20 | 11 | 0.058837 | 9 | O. | 25.44424 | 16.25424 | 34.63424 |
| Posterior | 29 | 15 | 0.083176 | 6 | F O | 46.63495 | 39.65495 | 53.61495 |
| Lateral | 6 | 5 | 0.205158 | 6 | % L | 74.31259 | 61.79259 | 86.83259 |
| Medial | 13 | 12 | 0.047348 | 7 | | | | |
| Total Overall Count | 68 | 43 | 0.394519 | 28 | N H | 10.57048 | -1.54952 | 22.69048 |

**Plate A-19**

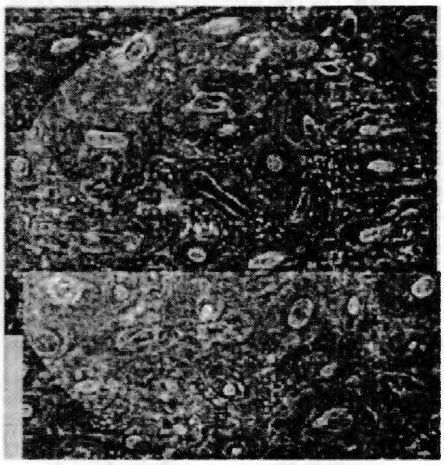

**Anterior FOV**

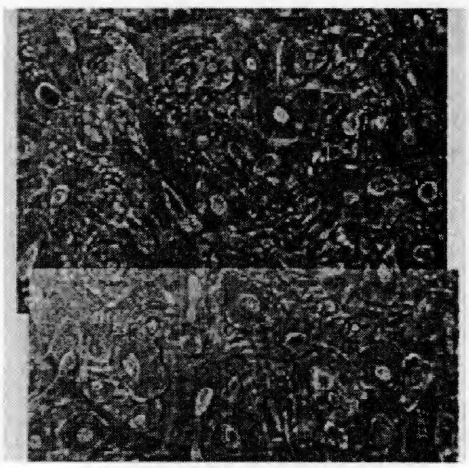

**Lateral FOV**

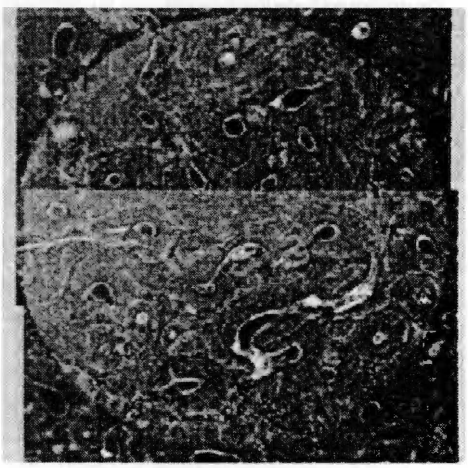

**Medial FOV**

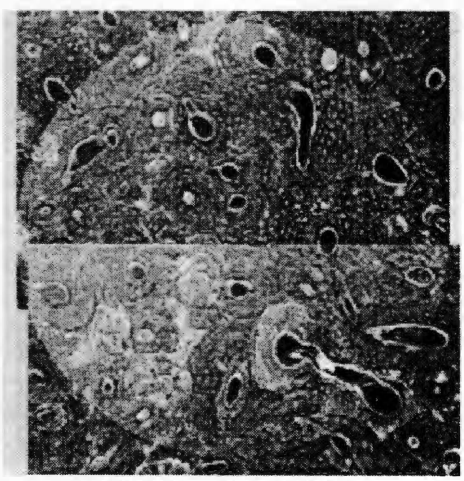

**Posterior FOV**
**Case #10: 80-6**

**Plate A-20**

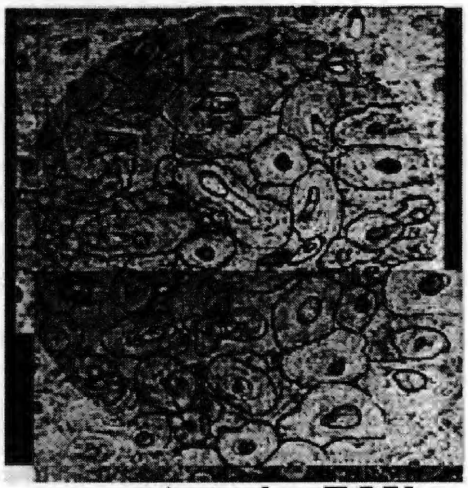

**Anterior FOV**

**Lateral FOV**

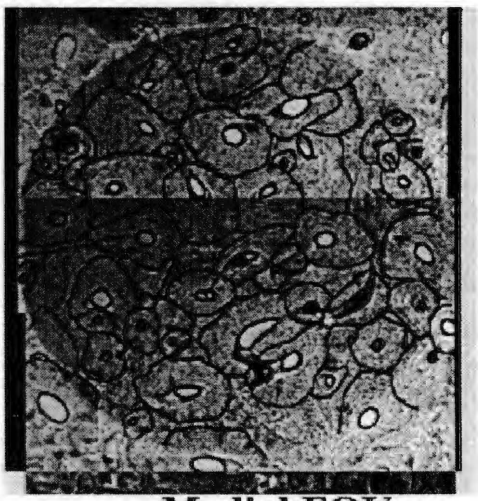

**Medial FOV**

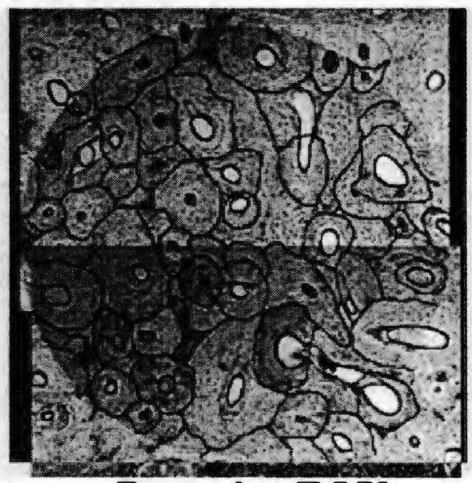

**Posterior FOV**
**Case #10: 80-6**

**Plate A-21**

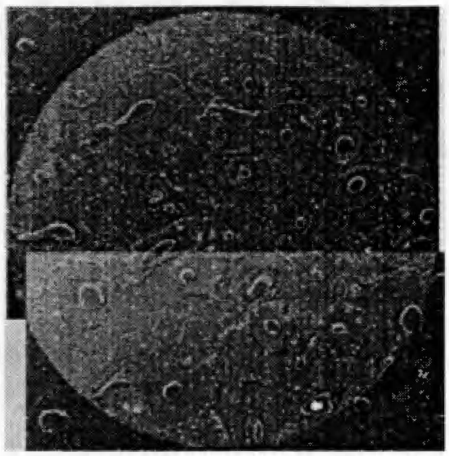

**Anterior FOV**

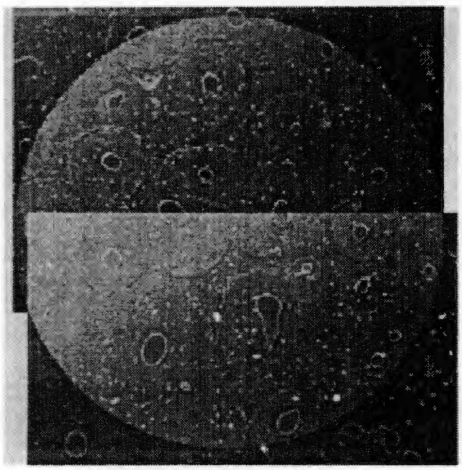

**Lateral FOV**

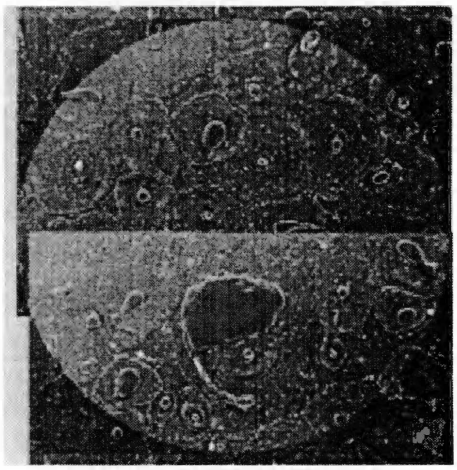

**Medial FOV**

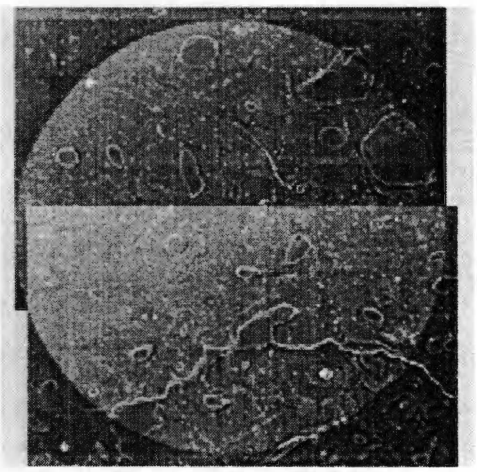

**Posterior FOV**
**Case #11: 81-110**

**Plate A-22**

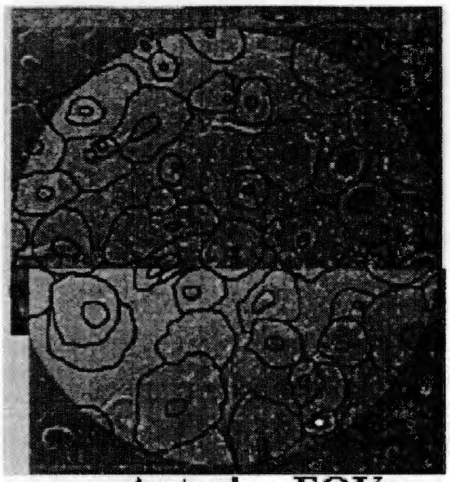

**Anterior FOV**

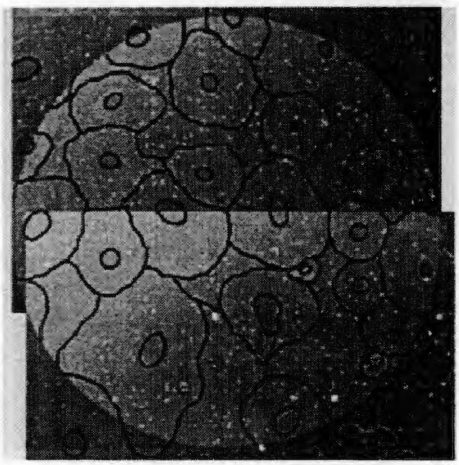

**Lateral FOV**

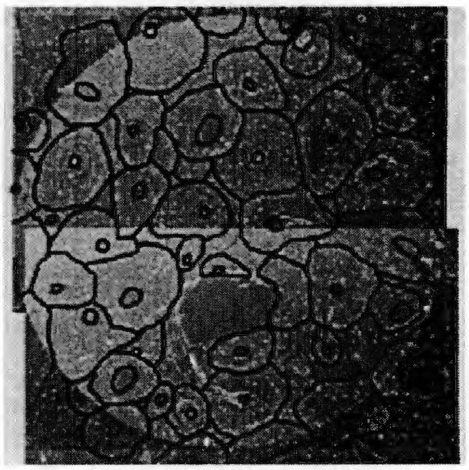

**Medial FOV**

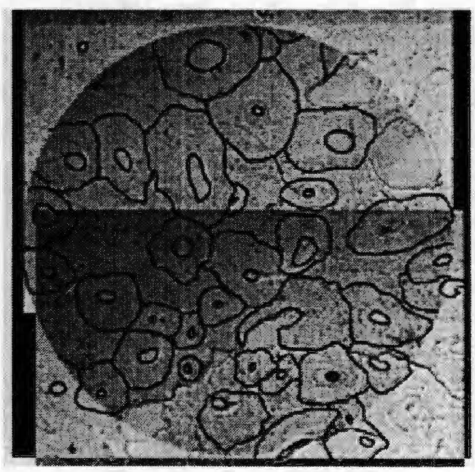

**Posterior FOV**
**Case #11: 81-110**

## Plate A-23

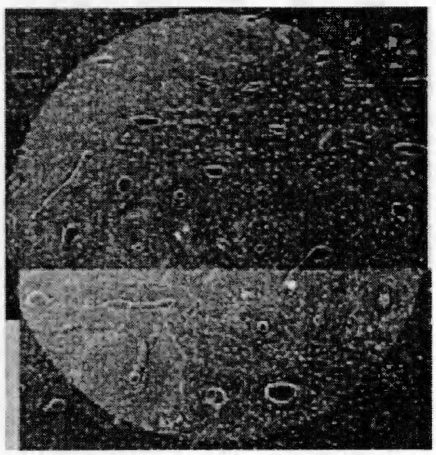

**Anterior FOV**

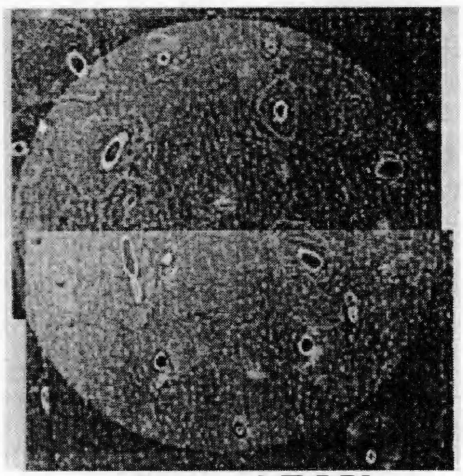

**Lateral FOV**

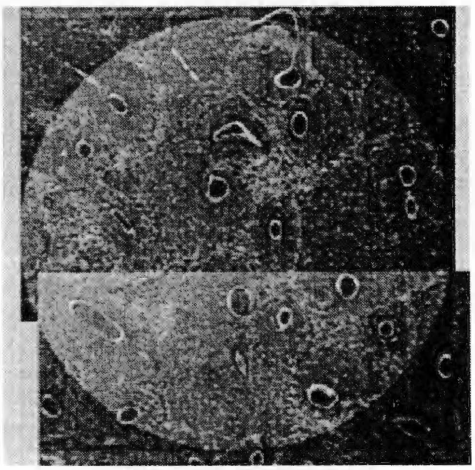

**Medial FOV**

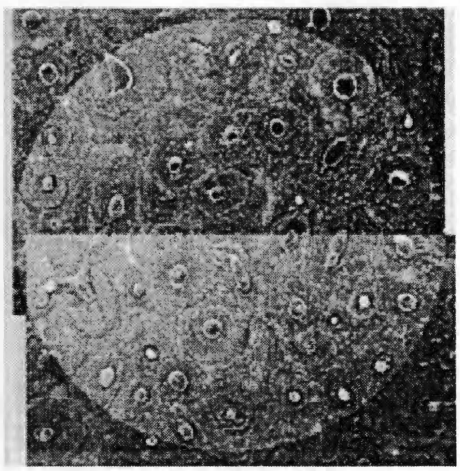

**Posterior FOV**
**Case #12: 81-13**

## Plate A-24

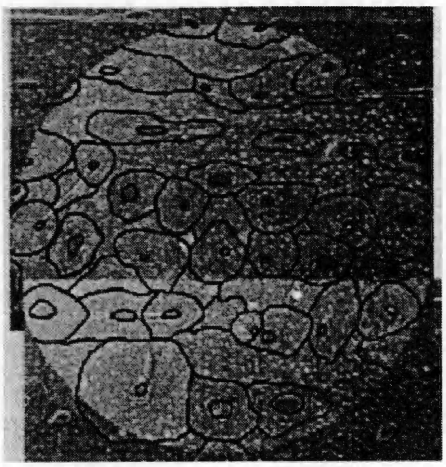

Anterior FOV

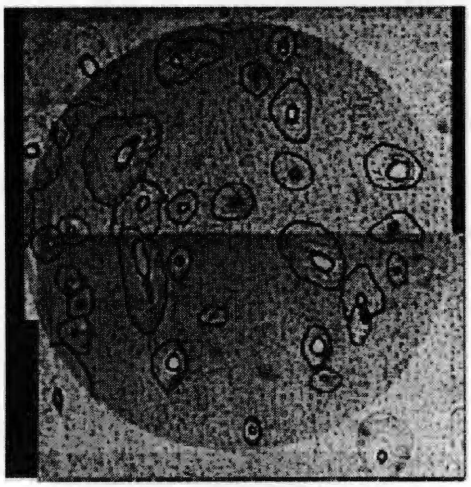

Lateral FOV

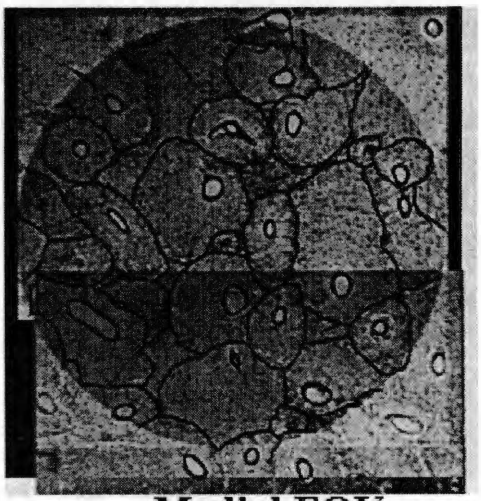

Medial FOV

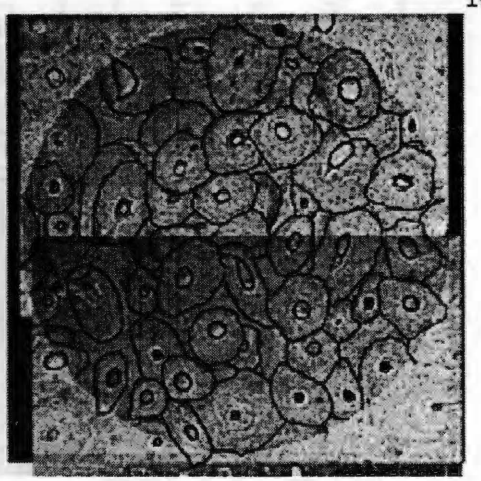

Posterior FOV
Case #12: 81-13

# Table A-3: Data Collection Sheets (continued)

| Case#13 | ID: 812005 | Actual Age: NA | Lab Age: NA | | Estimated Age: 42.82 (43) | | |
|---|---|---|---|---|---|---|---|
| FOV | | | | | Results of Regression Equations | | |
| | Osteon | Frag. Osteon | % of Lamellar | Nonhaversian | Est Age | SSE- | SSE+ |
| Anterior | 19 | 14 | 0.078317 | 6 | O. | 31.15566 | 21.96566 | 40.34566 |
| Posterior | 19 | 11 | 0.074388 | 4 | F O | 54.441 | 47.461 | 61.421 |
| Lateral | 24 | 14 | 0.061445 | 6 | % L | 74.56176 | 62.04176 | 87.08176 |
| Medial | 17 | 11 | 0.04059 | 11 | N H | 11.11732 | -1.00268 | 23.23732 |
| Total Overall Count | 79 | 50 | 0.25474 | 27 | | | | |
| Case#14 | ID: 81-9 | Actual Age: 25 | Lab Age: NA | | Estimated Age: 32.63 (33) | | |
| FOV | | | | | Results of Regression Equations | | |
| | Osteon | Frag. Osteon | % of Lamellar | Nonhaversian | Est Age | SSE- | SSE+ |
| Anterior | 13 | 10 | 0.132185 | 4 | O. | 25.44424 | 16.25424 | 34.63424 |
| Posterior | 11 | 10 | 0.044832 | 3 | F O | 48.90225 | 41.92225 | 55.88225 |
| Lateral | 19 | 10 | 0.329266 | 4 | % L | 74.0265 | 61.5065 | 86.5465 |
| Medial | 25 | 15 | 0.049032 | 4 | N H | 23.545 | 11.425 | 35.665 |
| Total Overall Count | 68 | 45 | 0.555315 | 15 | | | | |
| Case#15 | ID: 82-16 | Actual Age: NA | Lab Age: NA | | Estimated Age: 17.04 (17) | | |
| FOV | | | | | Results of Regression Equations | | |
| | Osteon | Frag. Osteon | % of Lamellar | Nonhaversian | Est Age | SSE- | SSE+ |
| Anterior | 18 | 16 | 0.167335 | 9 | O. | 23.9815 | 14.7915 | 33.1715 |
| Posterior | 12 | 7 | 0.069206 | 5 | F O | 57.63945 | 50.65945 | 64.61945 |
| Lateral | 17 | 15 | 0.023201 | 7 | % L | 74.44244 | 61.92244 | 86.96244 |
| Medial | 18 | 15 | 0.061899 | 8 | N H | 10.08876 | -2.03124 | 22.20876 |
| Total Overall Count | 65 | 53 | 0.321641 | 29 | | | | |

## Plate A-25

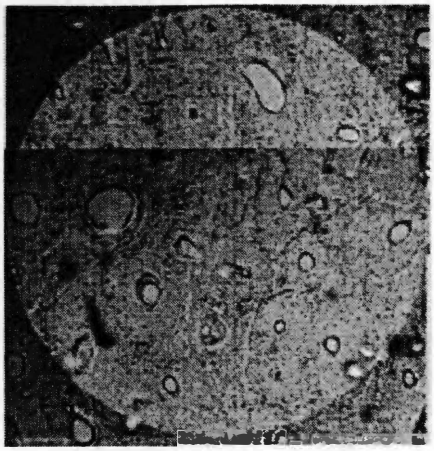

**Anterior FOV**

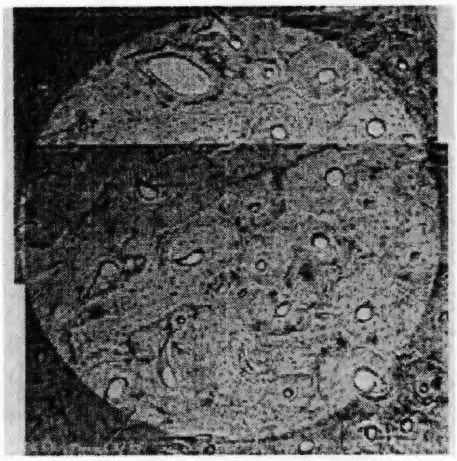

**Lateral FOV**

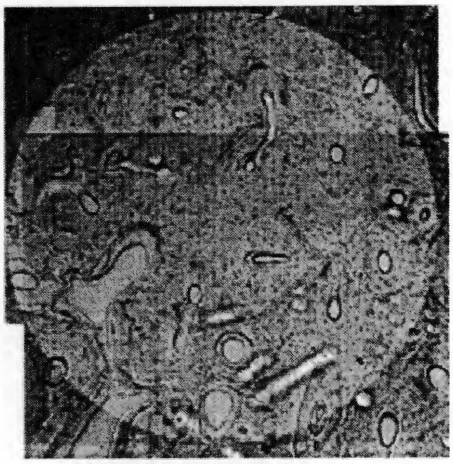

**Medial FOV**

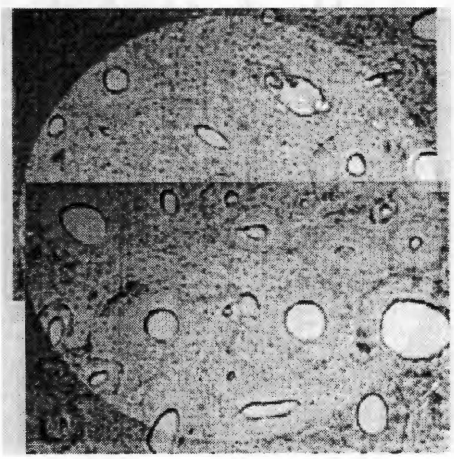

**Posterior FOV**
**Case #13: 81-2005**

**Plate A-26**

**Anterior FOV**

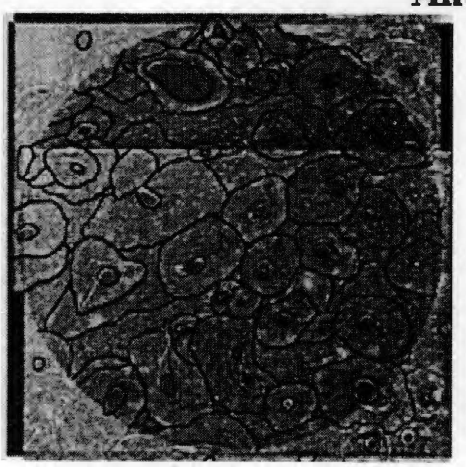

**Lateral FOV**

**Medial FOV**

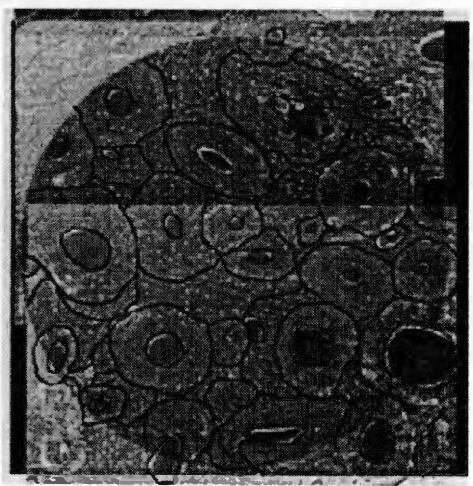

**Posterior FOV**

**Case #13: 81-2005**

**Plate A-27**

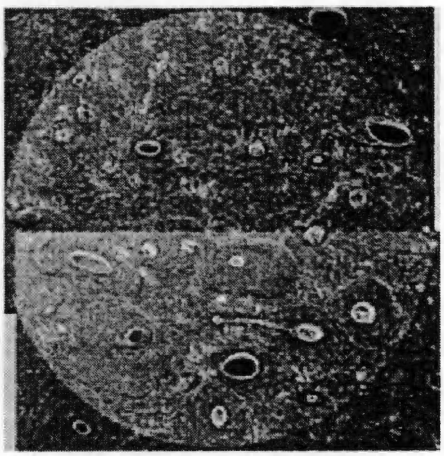

**Anterior FOV**

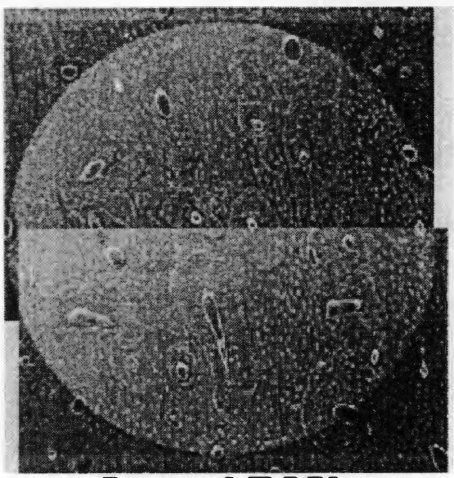

**Lateral FOV**

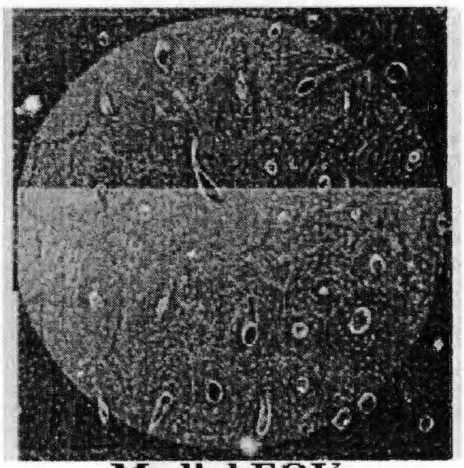

**Medial FOV**

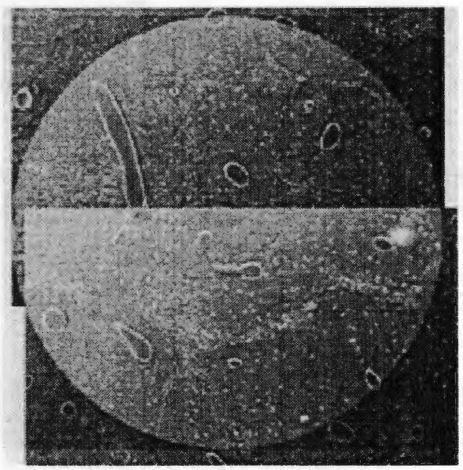

**Posterior FOV**
**Case #14: 81-9**

## Plate A-28

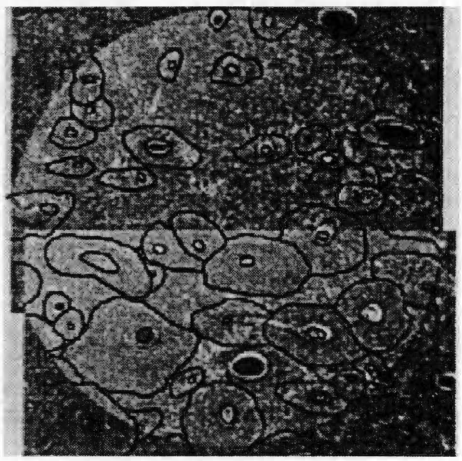

Anterior FOV

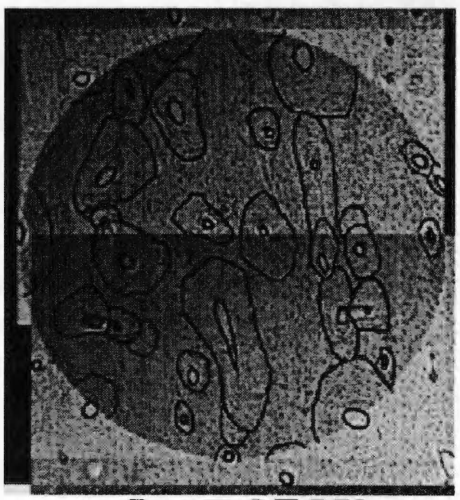

Lateral FOV

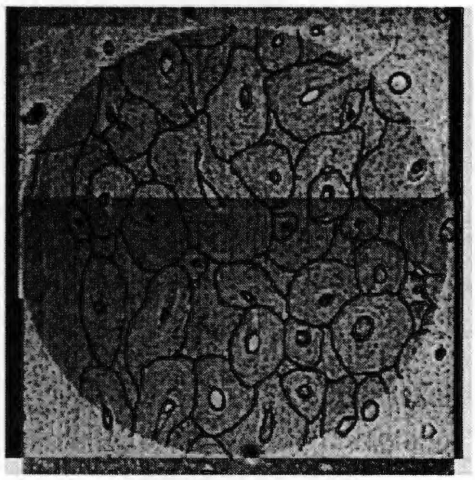

Medial FOV

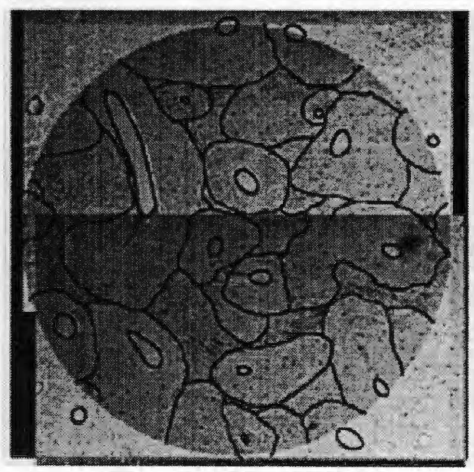

Posterior FOV
Case #14: 81-9

## Plate A-29

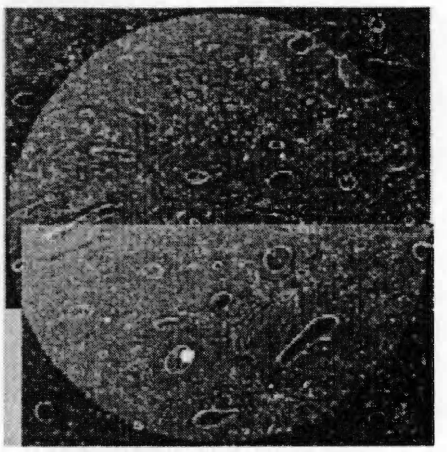

**Anterior FOV**

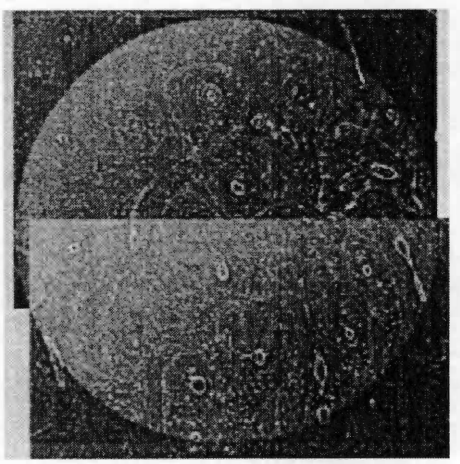

**Lateral FOV**

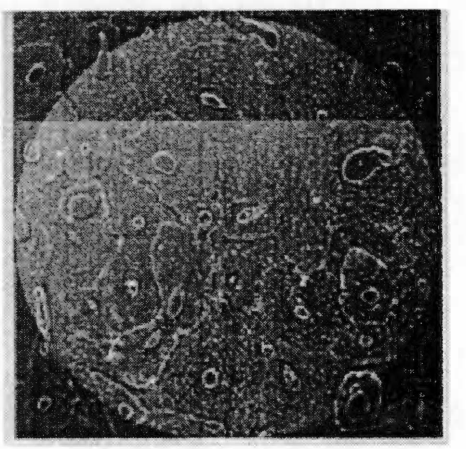

**Medial FOV**

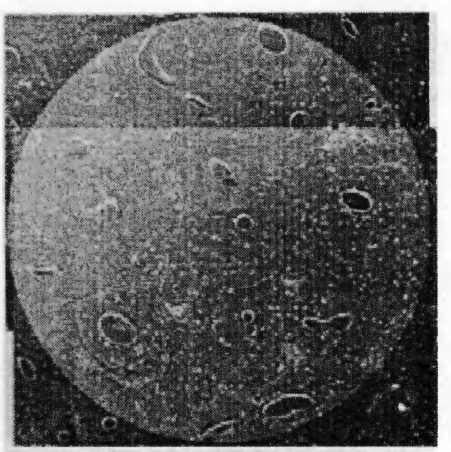

**Posterior FOV**
**Case #15: 82-16**

## Plate A-30

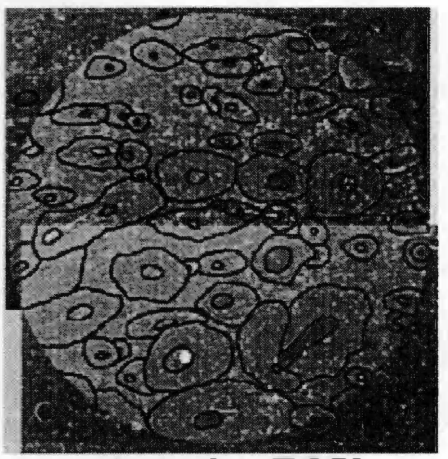

Anterior FOV

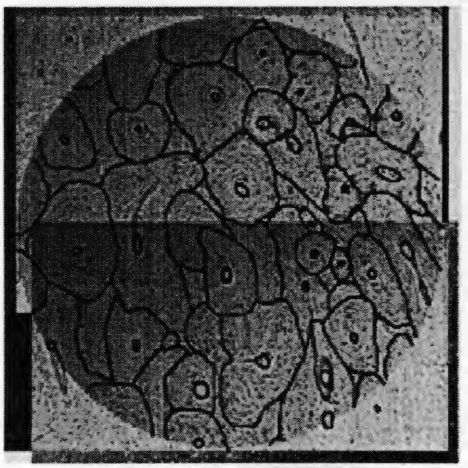

Lateral FOV

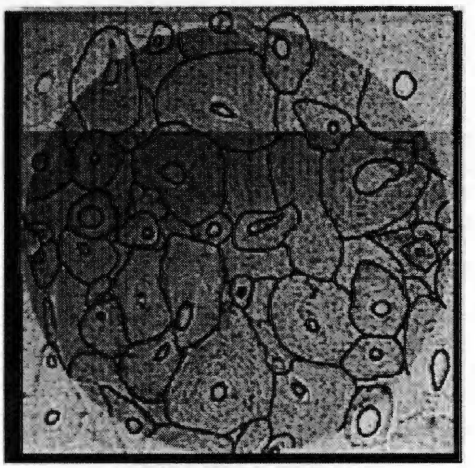

Medial FOV

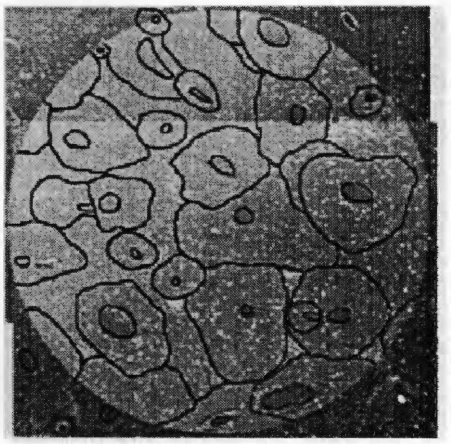

Posterior FOV

Case #15: 82-16

# Table A-3: Data Collection Sheets (continued)

| Case#16 | ID: 82-1 | Actual Age: 60 | Lab Age: 56.50 | | Estimated Age: 59.09 (59) | | |
|---|---|---|---|---|---|---|---|
| FOV | | | | | Results of Regression Equations | | |
| | Osteon | Frag. Osteon | % of Lamellar | Nonhaversian | Est Age | SSE- | SSE+ |
| Anterior | 31 | 13 | 0.0592 | 5 | O. | 48.16174 | 38.97174 | 57.35174 |
| Posterior | 22 | 13 | 0.037799 | 6 | F O | 54.441 | 47.461 | 61.421 |
| Lateral | 34 | 12 | 0.061484 | 7 | % | 74.67006 | 62.15006 | 87.19006 |
| Medial | 20 | 12 | 0.035576 | 6 | L | | | |
| Total Overall Count | 107 | 50 | 0.194059 | 24 | N H | 13.17016 | 1.05016 | 25.29016 |
| Case#17 | ID: 83-10 | Actual Age: NA | Lab Age: NA | | Estimated Age: 27.82 (28) | | |
| FOV | | | | | Results of Regression Equations | | |
| | Osteon | Frag. Osteon | % of Lamellar | Nonhaversian | Est Age | SSE- | SSE+ |
| Anterior | 15 | 8 | 0.272985 | 10 | O. | 24.46456 | 15.27456 | 33.65456 |
| Posterior | 22 | 12 | 0.056224 | 6 | F O | 48.90225 | 41.92225 | 55.88225 |
| Lateral | 16 | 14 | 0.04564 | 8 | % | 73.99163 | 61.47163 | 86.51163 |
| Medial | 13 | 11 | 0.200086 | 5 | L | | | |
| Total Overall Count | 66 | 45 | 0.574935 | 29 | N H | 10.08876 | -2.03124 | 22.20876 |
| Case#18 | ID: 83215 | Actual Age: NA | Lab Age: NA | | Estimated Age: 22.59 (23) | | |
| FOV | | | | | Results of Regression Equations | | |
| | Osteon | Frag. Osteon | % of Lamellar | Nonhaversian | Est Age | SSE- | SSE+ |
| Anterior | 15 | 8 | 0.104342 | 1 | O. | 21.634 | 12.444 | 30.824 |
| Posterior | 14 | 12 | 0.057027 | 7 | F O | 48.90225 | 41.92225 | 55.88225 |
| Lateral | 16 | 11 | 0.375942 | 3 | % | 74.01441 | 61.43441 | 86.53441 |
| Medial | 15 | 14 | 0.024808 | 4 | L | | | |
| Total Overall Count | 60 | 45 | 0.562119 | 15 | N H | 23.545 | 11.425 | 35.665 |

## Plate A-31

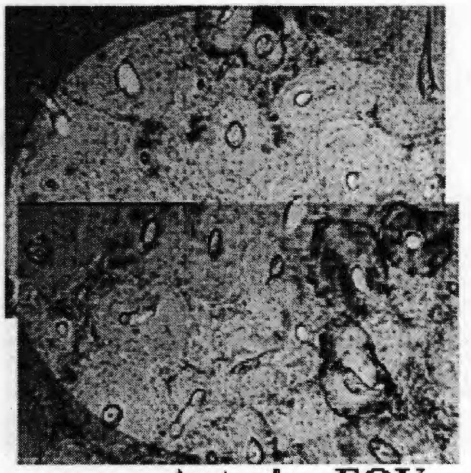

Anterior FOV

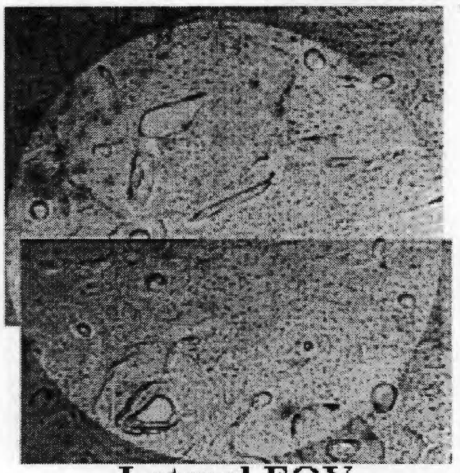

Lateral FOV

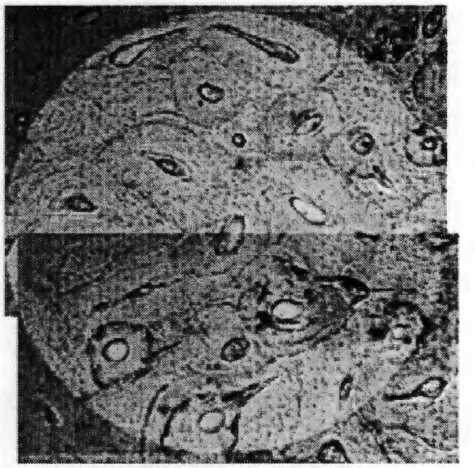

Medial FOV

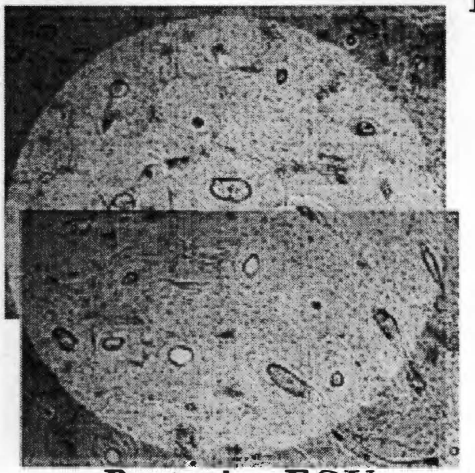

Posterior FOV

Case #16: 82-1

## Plate A-32

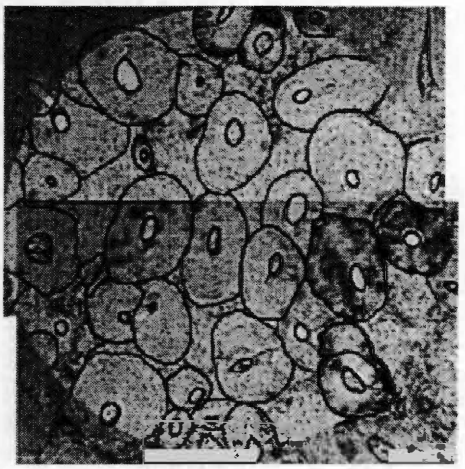

Anterior FOV

Lateral FOV

Medial FOV

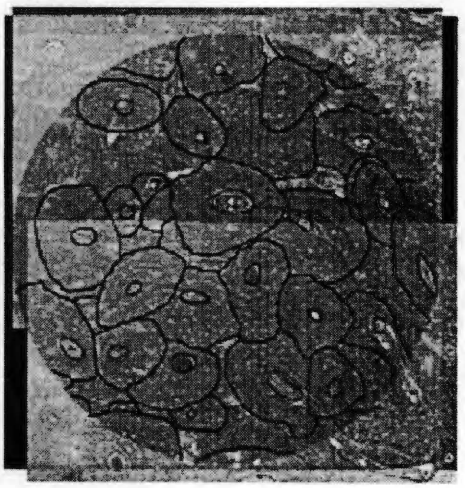

Posterior FOV
Case #16: 82-1

## Plate A-33

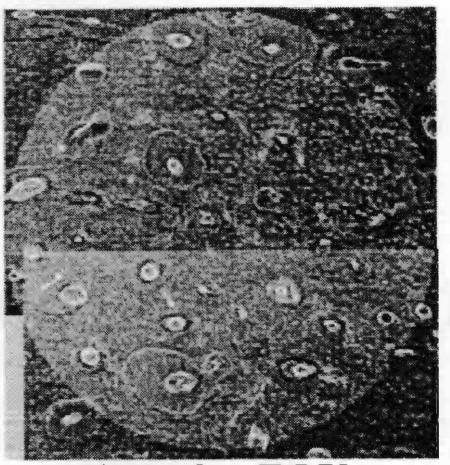

**Anterior FOV**

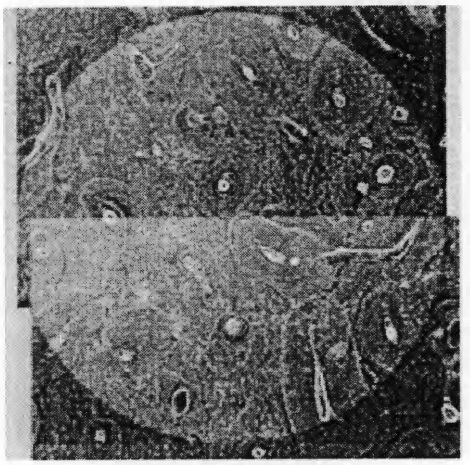

**Lateral FOV**

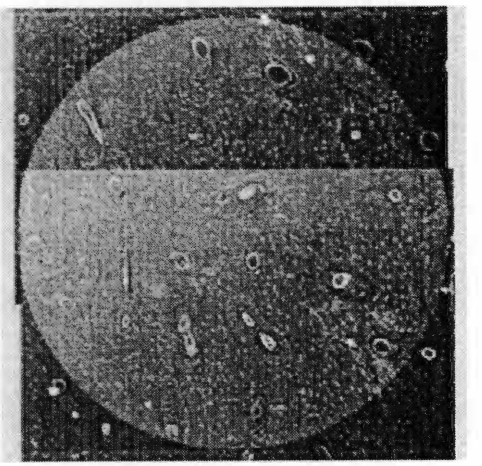

**Medial FOV**

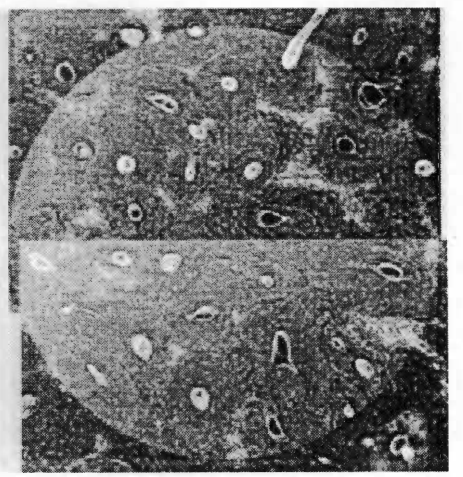

**Posterior FOV**
**Case #17: 83-10**

**Plate A-34**

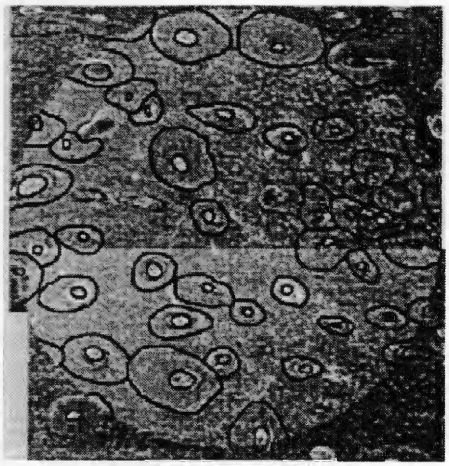

**Anterior FOV**

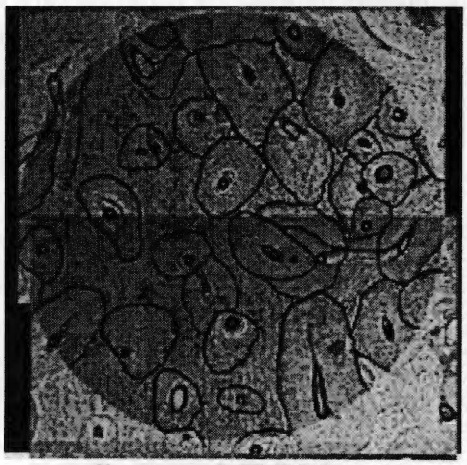

**Lateral FOV**

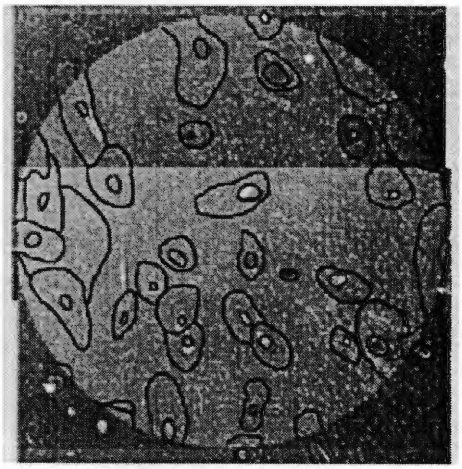

**Medial FOV**

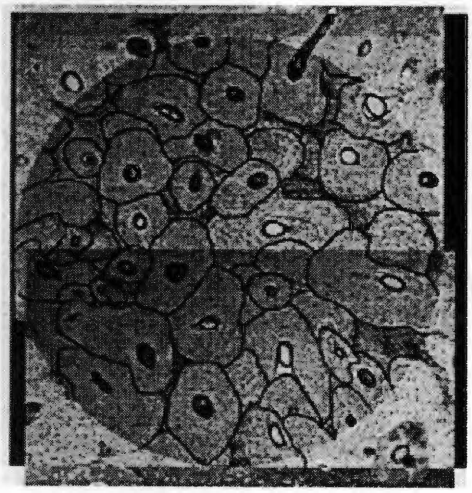

**Posterior FOV**
**Case #17: 83-10**

**Plate A-35**

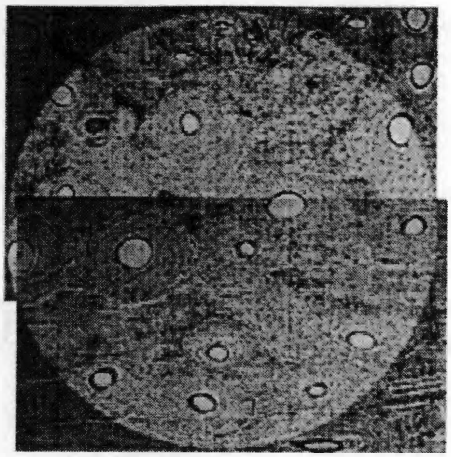

**Anterior FOV**

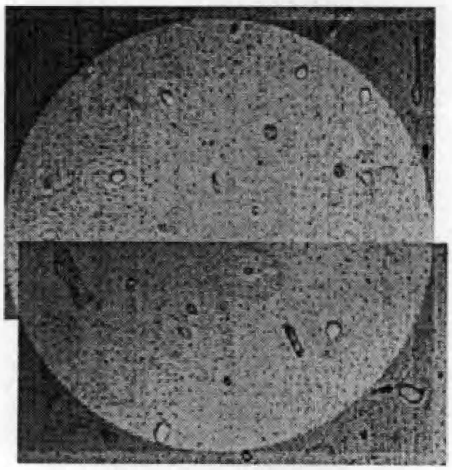

**Lateral FOV**

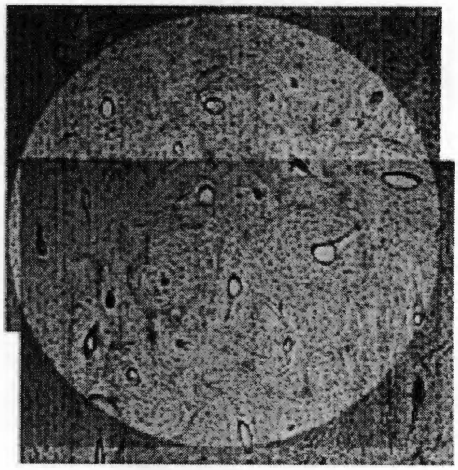

**Medial FOV**

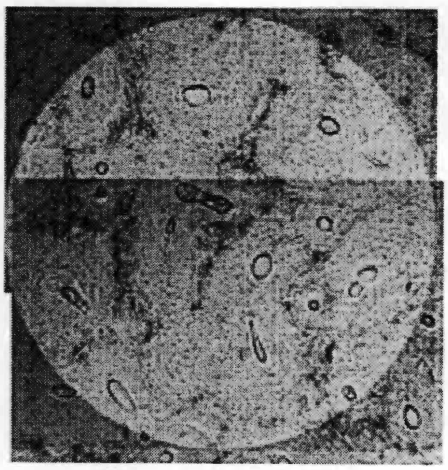

**Posterior FOV**
**Case #18: 83-215**

## Plate A-36

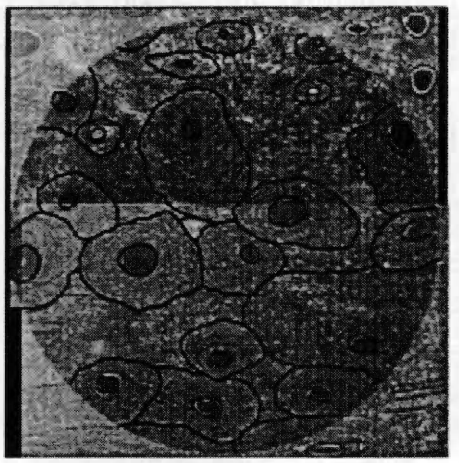

**Anterior FOV**

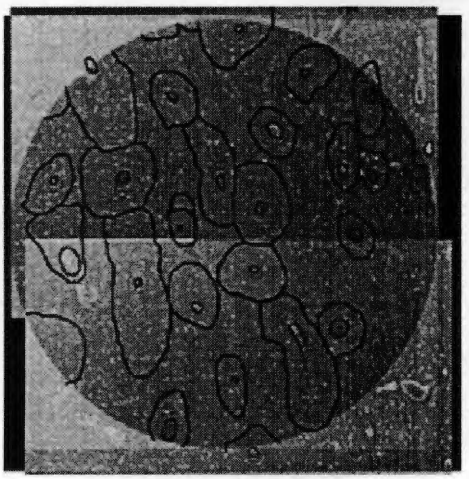

**Lateral FOV**

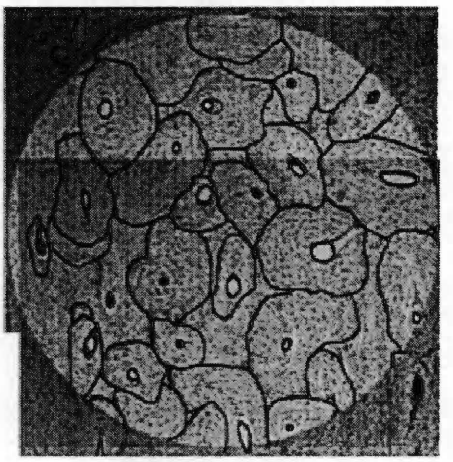

**Medial FOV**

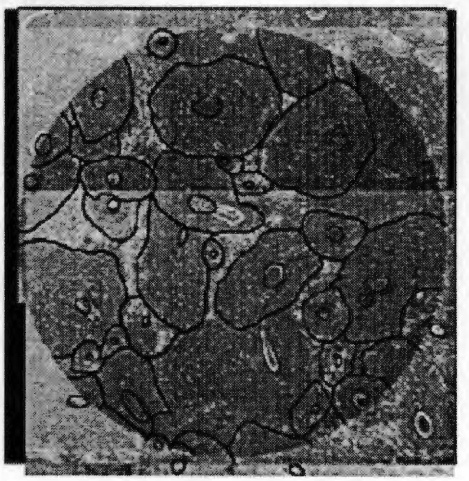

**Posterior FOV**
**Case #18: 83-215**

# Table A-3: Data Collection Sheets (continued)

| Case#19 | ID: 83-25 | Actual Age: 26 | | Lab Age: 54 | | Estimated Age: 24.71 (25) | | |
|---|---|---|---|---|---|---|---|---|
| FOV | | | | | Results of Regression Equations | | | |
| | Osteon | Frag. Osteon | % of Lamellar | Nonhaversian | | Est Age | SSE- | SSE+ |
| Anterior | 28 | 14 | 0.03884 | 6 | O. | 41.05816 | 31.86816 | 50.24816 |
| Posterior | 23 | 12 | 0.038473 | 6 | F O | 67.27395 | 60.29395 | 74.25395 |
| Lateral | 25 | 20 | 0.043544 | 8 | % L | 74.72164 | 62.20164 | 87.24164 |
| Medial | 20 | 17 | 0.044324 | 16 | | | | |
| Total Overall Count | 96 | 63 | 0.165181 | 36 | N H | 8.35864 | -3.76136 | 20.47864 |
| Case#20 | ID: 83-9 | Actual Age: 18 | | Lab Age: 18.45 | | Estimated Age: 24.75 (25) | | |
| FOV | | | | | Results of Regression Equations | | | |
| | Osteon | Frag. Osteon | % of Lamellar | Nonhaversian | | Est Age | SSE- | SSE+ |
| Anterior | 25 | 11 | 0.081524 | 7 | O. | 39.82536 | 30.63536 | 49.01536 |
| Posterior | 23 | 15 | 0.033426 | 4 | F O | 62.6842 | 55.7042 | 69.6642 |
| Lateral | 13 | 17 | 0.181877 | 14 | % L | 74.41976 | 61.89976 | 86.93976 |
| Medial | 33 | 15 | 0.037539 | 5 | | | | |
| Total Overall Count | 94 | 58 | 0.334366 | 30 | N H | 9.67 | -2.45 | 21.79 |
| Case#21 | ID: 84-14 | Actual Age: 45 | | Lab Age: 45 | | Estimated Age: 42.74 (43) | | |
| FOV | | | | | Results of Regression Equations | | | |
| | Osteon | Frag. Osteon | % of Lamellar | Nonhaversian | | Est Age | SSE- | SSE+ |
| Anterior | 15 | 9 | 0.054592 | 5 | O. | 24.95214 | 15.76214 | 34.14214 |
| Posterior | 13 | 8 | 0.116796 | 4 | F O | 53.35165 | 46.37165 | 60.33165 |
| Lateral | 24 | 15 | 0.044725 | 4 | % L | 74.55636 | 62.03636 | 87.07636 |
| Medial | 15 | 17 | 0.041652 | 6 | | | | |
| Total Overall Count | 67 | 49 | 0.257765 | 19 | N H | 18.09556 | 5.97556 | 30.21556 |

## Plate A-37

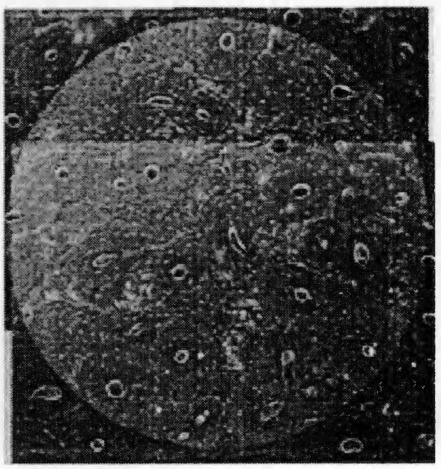

**Anterior FOV**

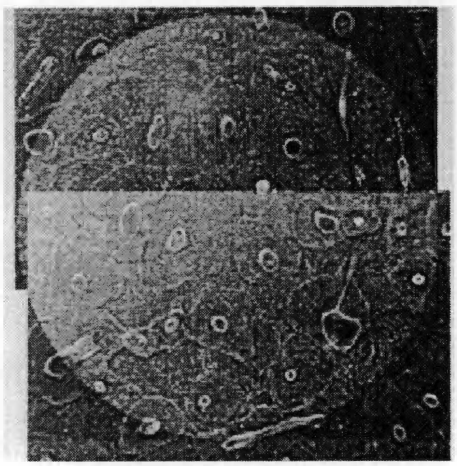

**Lateral FOV**

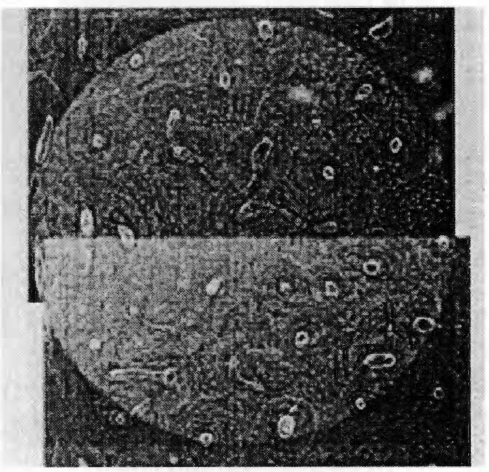

**Medial FOV**

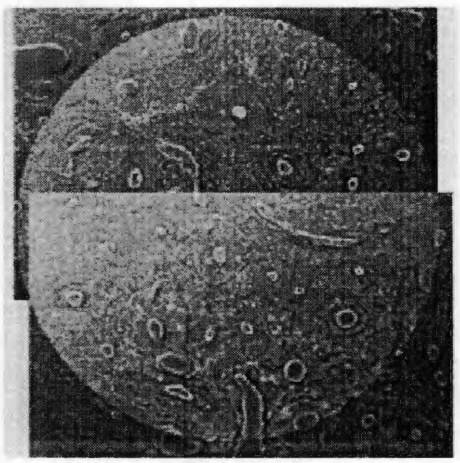

**Posterior FOV**
**Case #19: 83-25**

## Plate A-38

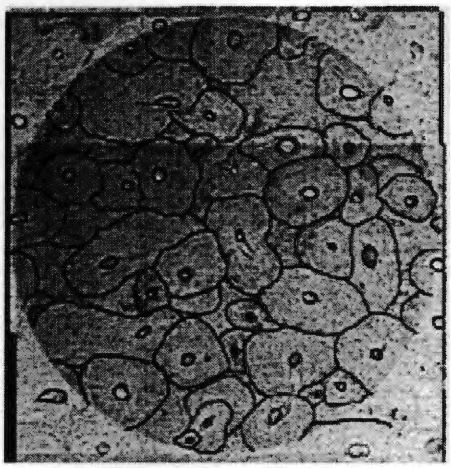

Anterior FOV

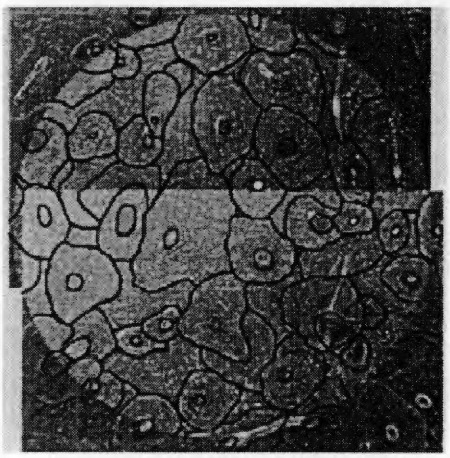

Lateral FOV

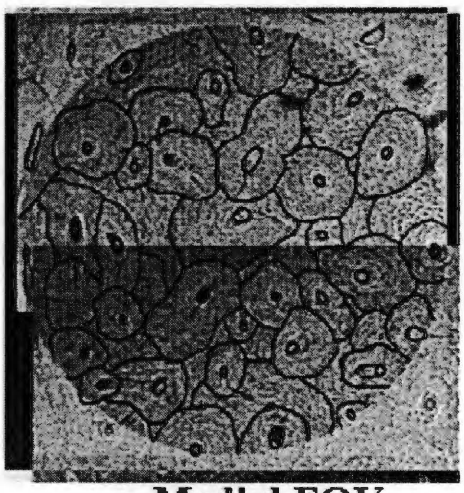

Medial FOV

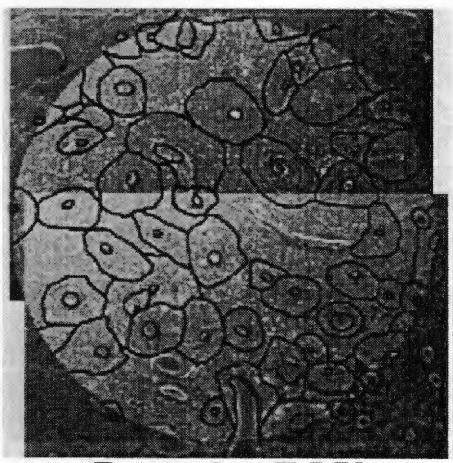

Posterior FOV
Case #19: 83-25

## Plate A-39

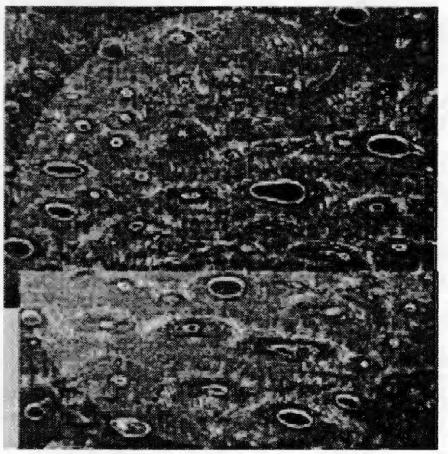

**Anterior FOV**

**Lateral FOV**

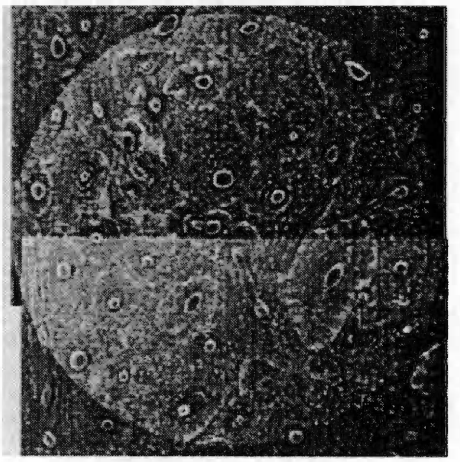

**Medial FOV**

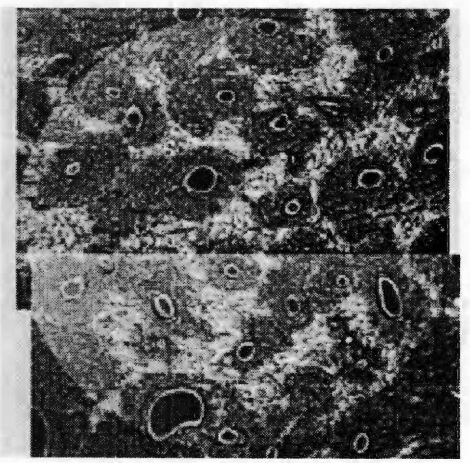

**Posterior FOV**
**Case #20: 83-9**

## Plate A-40

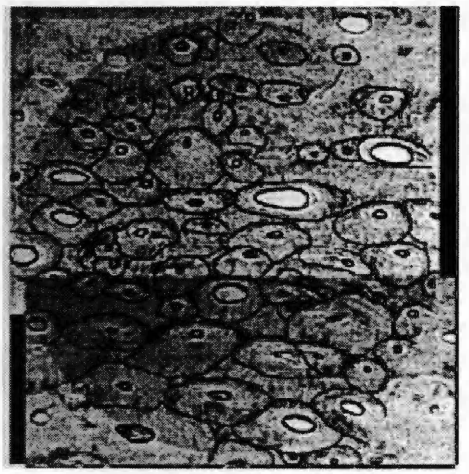

Anterior FOV

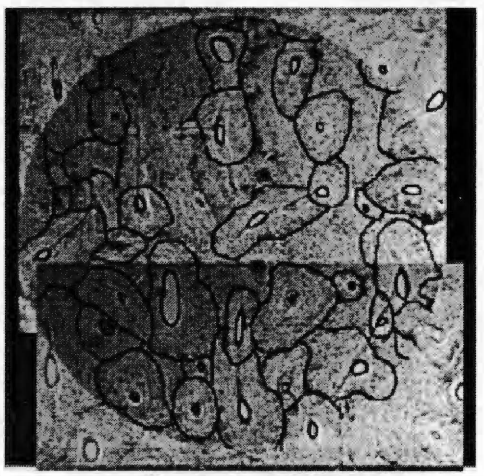

Lateral FOV

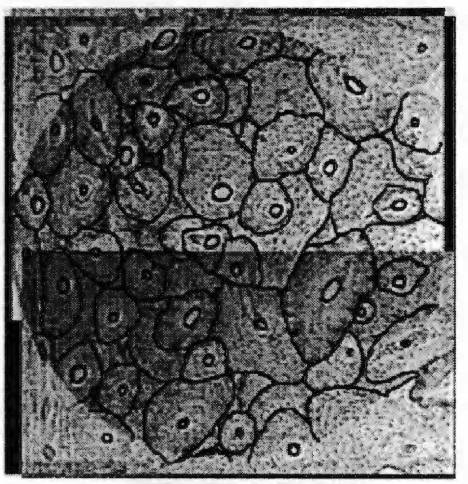

Medial FOV

Posterior FOV
Case #20: 83-9

## Plate A-41

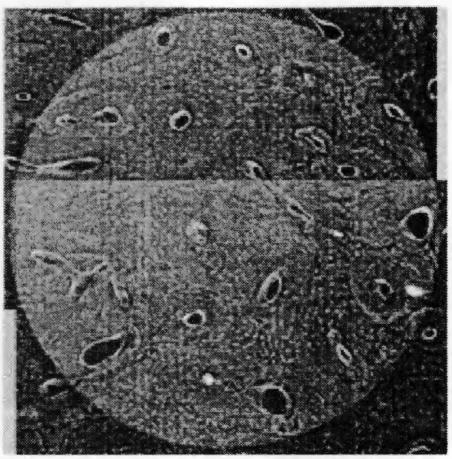

**Anterior FOV**

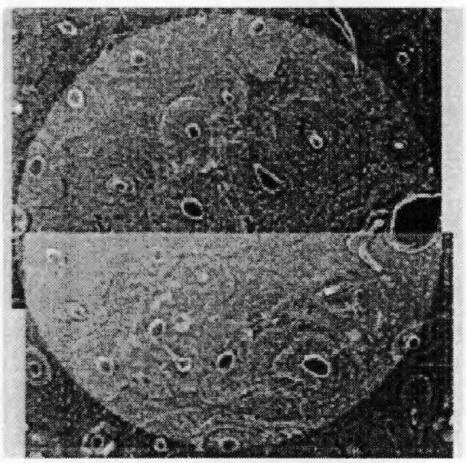

**Lateral FOV**

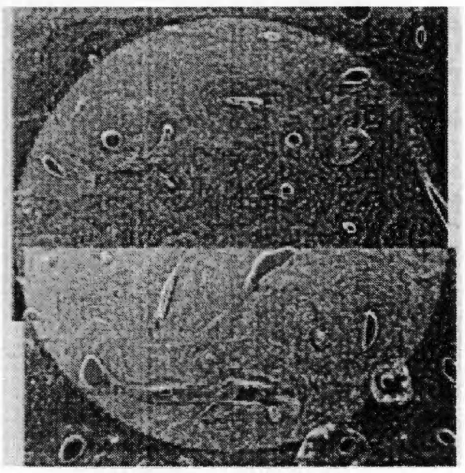

**Medial FOV**

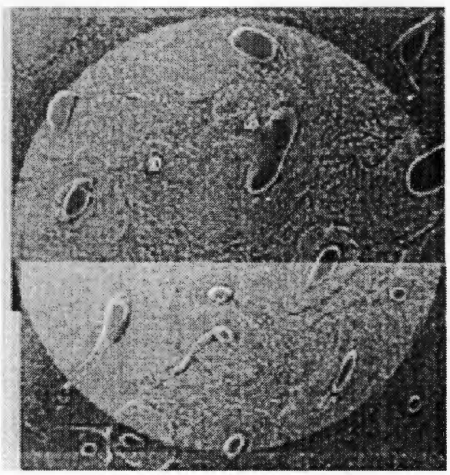

**Posterior FOV**
**Case #21: 84-14**

**Plate A-42**

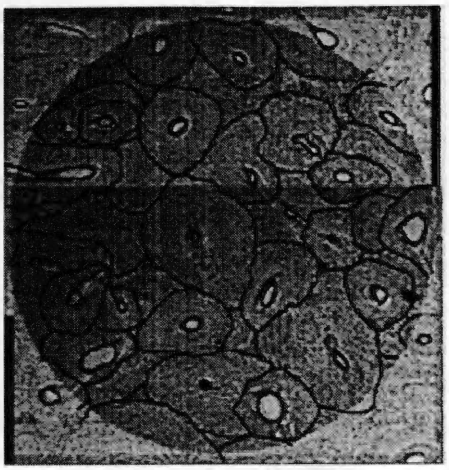

**Anterior FOV**

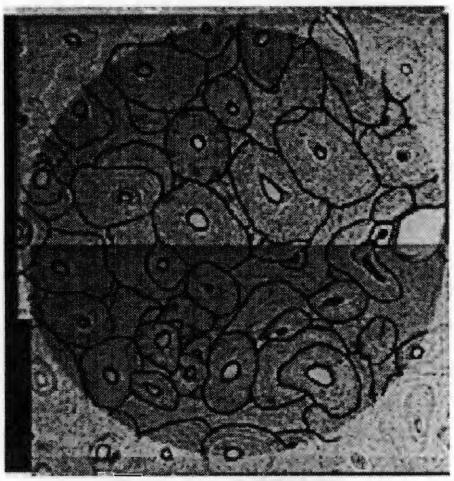

**Lateral FOV**

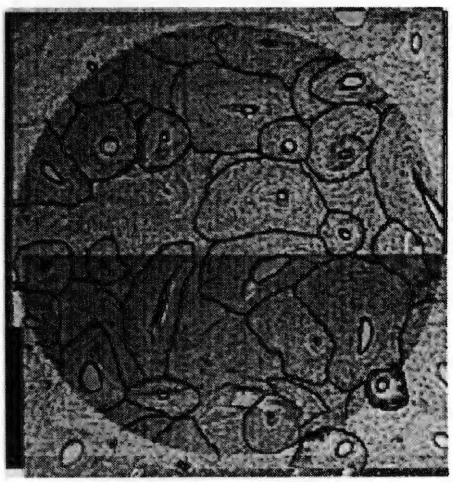

**Medial FOV**

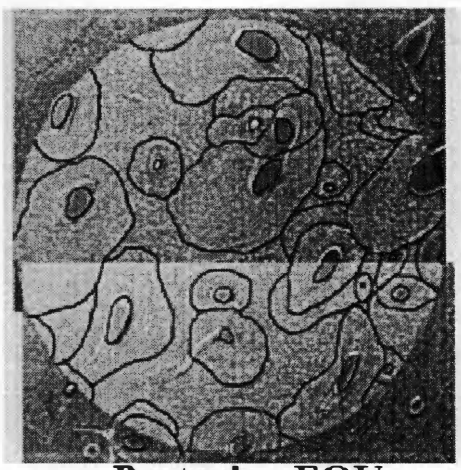

**Posterior FOV**
**Case #21: 84-14**

# Table A-3: Data Collection Sheets (continued)

| Case#22 | ID: 85-1 | Actual Age: NA | | Lab Age: NA | Estimated Age: 43.06 (43) | | | |
|---|---|---|---|---|---|---|---|---|
| FOV | | | | | Results of Regression Equations | | | |
| | Osteon | Frag. Osteon | % of Lamellar | Nonhaversian | | Est Age | SSE- | SSE+ |
| Anterior | 17 | 8 | 0.115495 | 3 | O. | 29.54376 | 20.35376 | 38.73376 |
| Posterior | 16 | 11 | 0.032934 | 7 | FO | 56.5858 | 49.6058 | 63.5658 |
| Lateral | 28 | 19 | 0.07789 | 8 | % | 74.37566 | 61.85566 | 86.89566 |
| Medial | 15 | 14 | 0.132794 | 8 | L | | | |
| Total Overall Count | 76 | 52 | 0.359113 | 26 | NH | 11.73144 | -0.38856 | 23.85144 |
| Case#23 | ID: 85-24 | Actual Age: 32.70 | | Lab Age: NA | Estimated Age: 43.54 (44) | | | |
| FOV | | | | | Results of Regression Equations | | | |
| | Osteon | Frag. Osteon | % of Lamellar | Nonhaversian | | Est Age | SSE- | SSE+ |
| Anterior | 19 | 17 | 0.176617 | 6 | O. | 25.44424 | 16.25424 | 34.63424 |
| Posterior | 17 | 11 | 0.042717 | 5 | FO | 63.64215 | 56.66215 | 70.62215 |
| Lateral | 16 | 16 | 0.044096 | 7 | % | 74.49938 | 61.97938 | 87.01938 |
| Medial | 16 | 15 | 0.026277 | 10 | L | | | |
| Total Overall Count | 68 | 59 | 0.289707 | 28 | NH | 10.57048 | -1.54952 | 22.69048 |
| Case#24 | ID: 85-7 | Skeletal Age: 30-40 | | Lab Age: NA | Estimated Age: 41.43 (41) | | | |
| FOV | | | | | Results of Regression Equations | | | |
| | Osteon | Frag. Osteon | % of Lamellar | Nonhaversian | | Est Age | SSE- | SSE+ |
| Anterior | 20 | 14 | 0.034205 | 8 | O. | 22.09446 | 12.90446 | 31.28446 |
| Posterior | 13 | 8 | 0.053975 | 5 | FO | 59.70475 | 52.72475 | 66.68475 |
| Lateral | 15 | 16 | 0.084207 | 10 | % | 74.62066 | 62.10066 | 87.14066 |
| Medial | 13 | 17 | 0.049347 | 8 | L | | | |
| Total Overall Count | 61 | 55 | 0.221734 | 31 | NH | 9.31204 | -2.80796 | 21.43204 |

**Plate A-43**

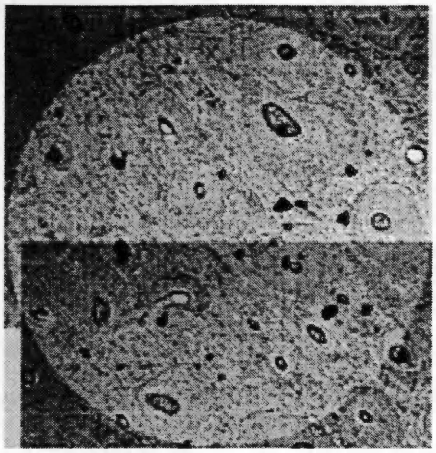

**Anterior FOV**

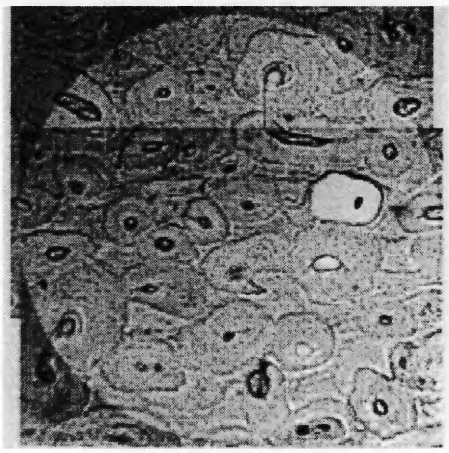

**Lateral FOV**

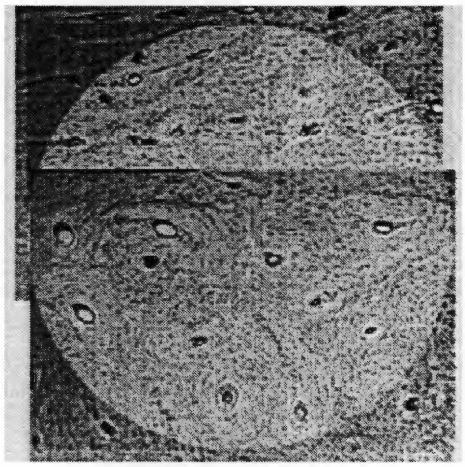

**Medial FOV**

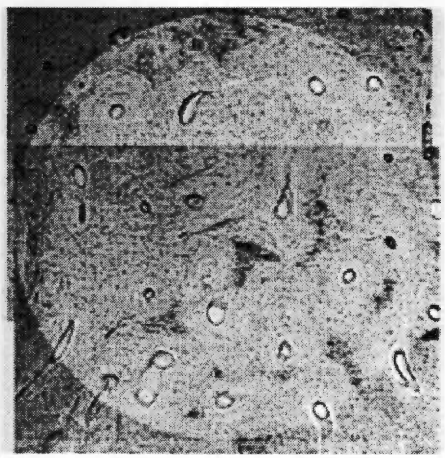

**Posterior FOV**
**Case #22: 85-1**

**Plate A-44**

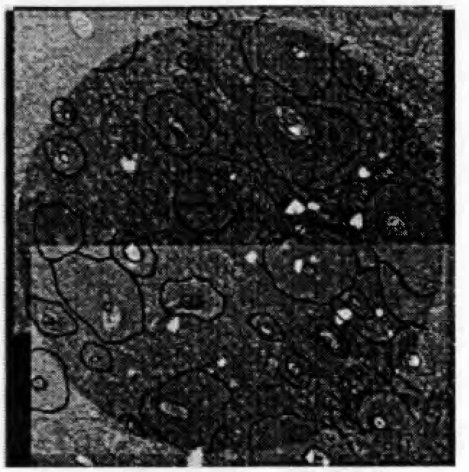

**Anterior FOV**

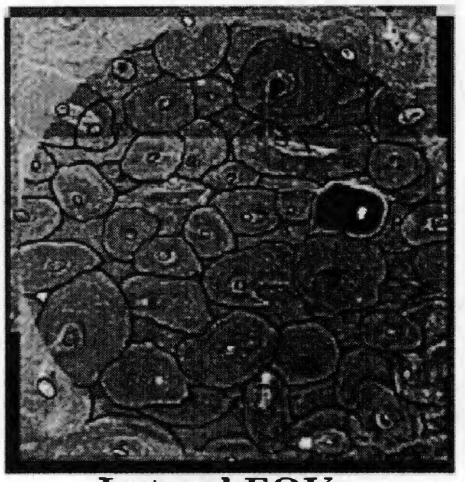

**Lateral FOV**

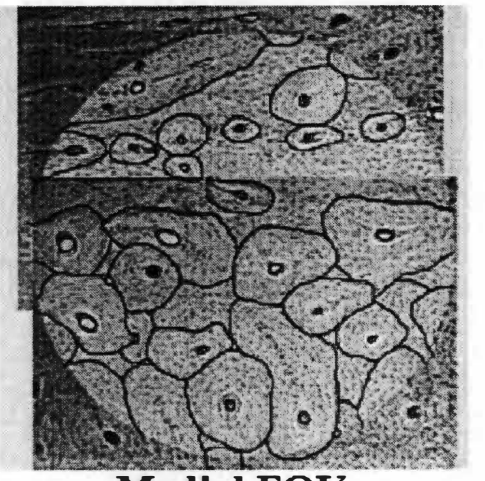

**Medial FOV**

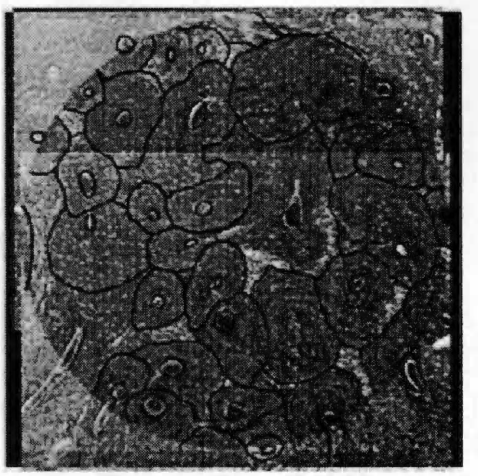

**Posterior FOV**
**Case #22: 85-1**

## Plate A-45

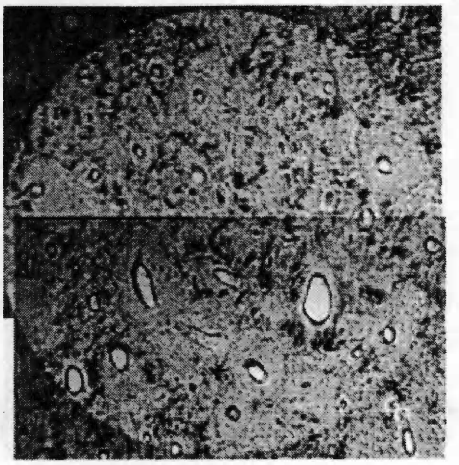

**Anterior FOV**

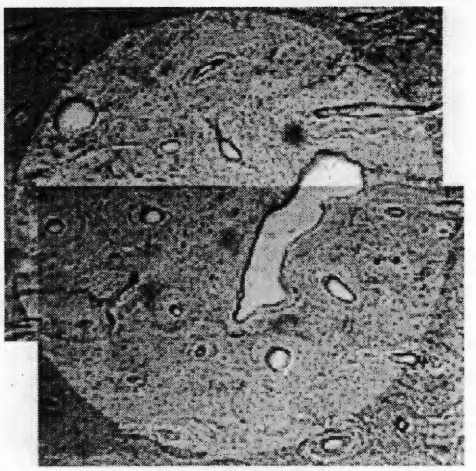

**Lateral FOV**

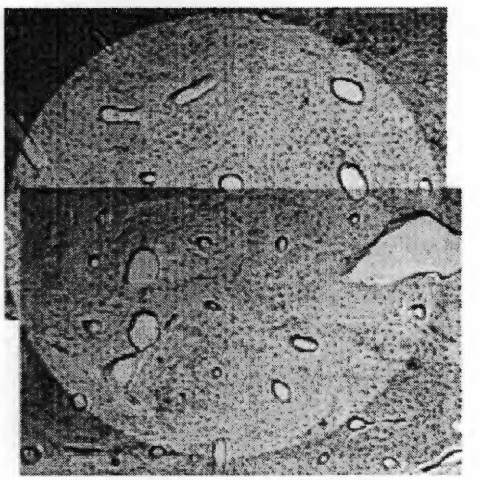

**Medial FOV**

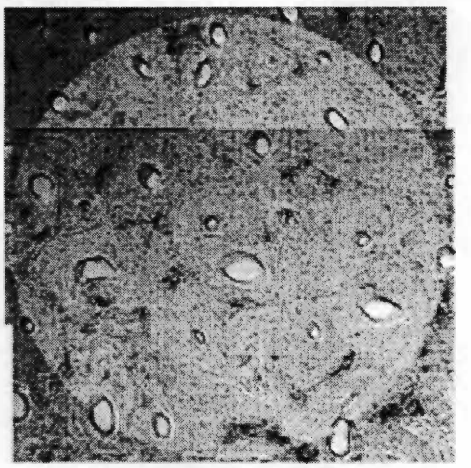

**Posterior FOV**
**Case #23: 85-24**

## Plate A-46

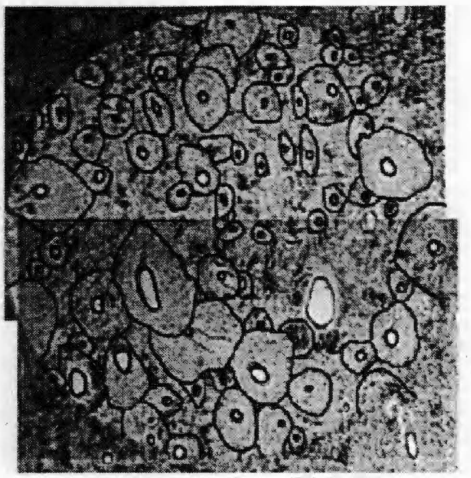

Anterior FOV

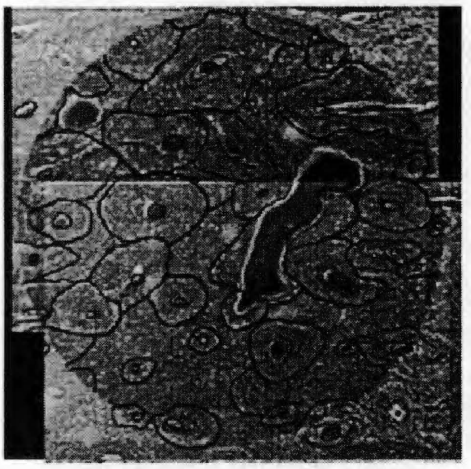

Lateral FOV

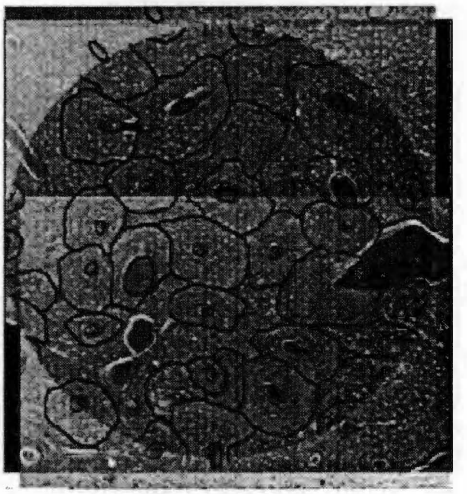

Medial FOV

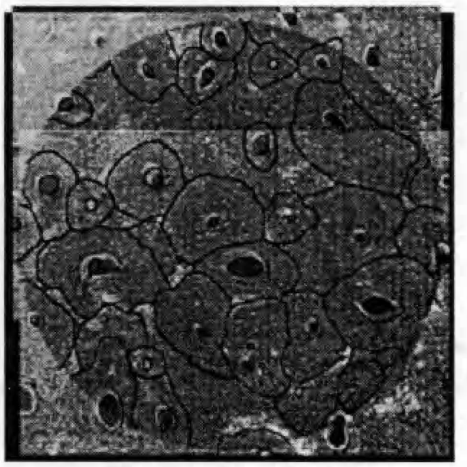

Posterior FOV
Case #23: 85-24

**Plate A-47**

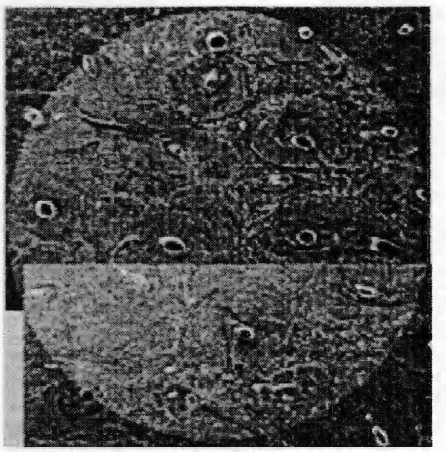

**Anterior FOV**

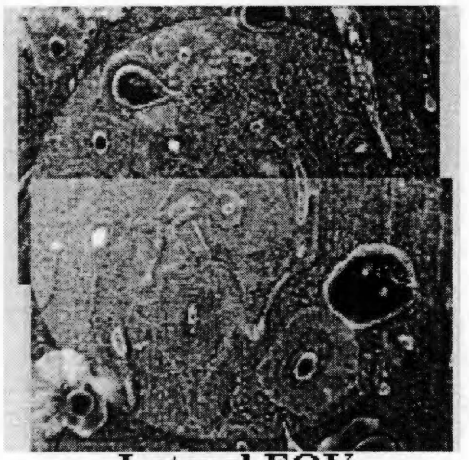

**Lateral FOV**

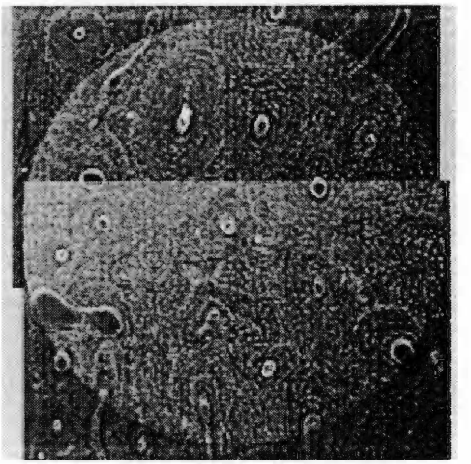

**Medial FOV**

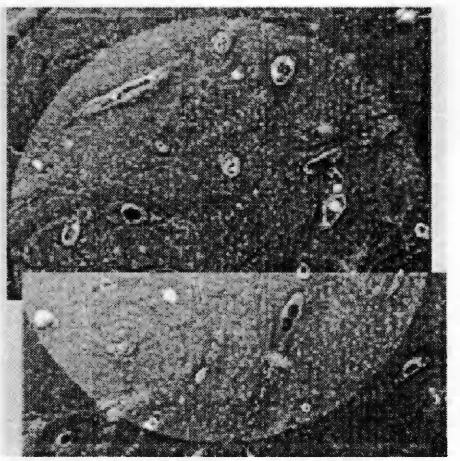

**Posterior FOV**
**Case #24: 85-7**

## Plate A-48

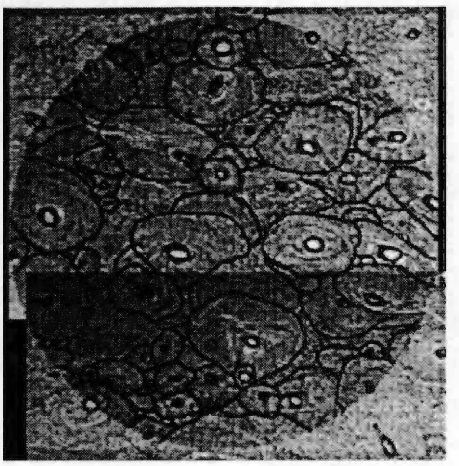

Anterior FOV

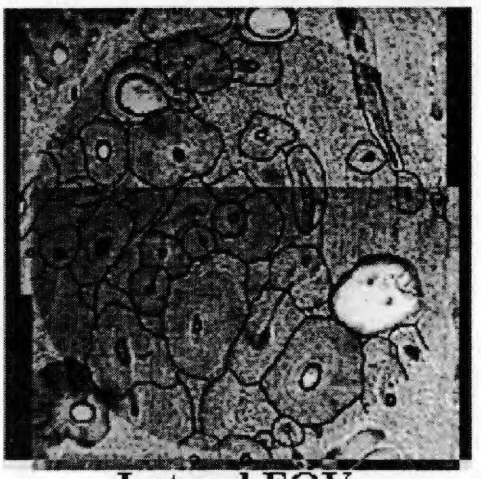

Lateral FOV

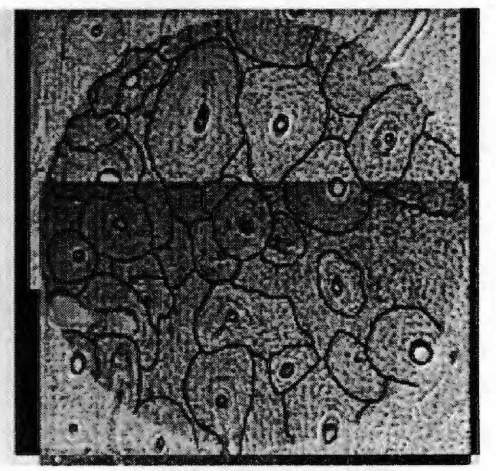

Medial FOV

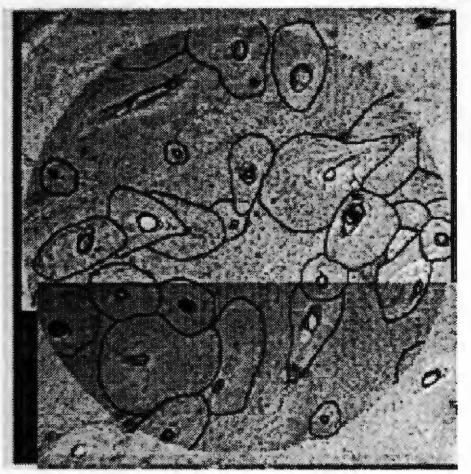

Posterior FOV
Case #24: 85-7

# Table A-3: Data Collection Sheets (continued)

| Case#25 | ID: F83215 | Actual Age: NA | | Lab Age: NA | | Estimated Age: 57.30 (57) | | |
|---|---|---|---|---|---|---|---|---|
| FOV | | | | | Results of Regression Equations | | | |
| | Osteon | Frag. Osteon | % of Lamellar | Nonhaversian | | Est Age | SSE- | SSE+ |
| Anterior | 24 | 15 | 0.059552 | 4 | O. | 28.49176 | 19.30176 | 37.68176 |
| Posterior | 18 | 11 | 0.057126 | 4 | F O | 53.35165 | 46.37165 | 60.33165 |
| Lateral | 14 | 10 | 0.37645 | 5 | % L | 73.67048 | 61.15048 | 86.19048 |
| Medial | 18 | 13 | 0.262759 | 7 | | | | |
| Total Overall Count | 74 | 49 | 0.755887 | 20 | N H | 16.95 | 4.83 | 29.07 |
| Case#26 | ID: F83539 | Actual Age: 54.40 | | Lab Age: NA | | Estimated Age: 54.52 (55) | | |
| FOV | | | | | Results of Regression Equations | | | |
| | Osteon | Frag. Osteon | % of Lamellar | Nonhaversian | | Est Age | SSE- | SSE+ |
| Anterior | 24 | 10 | 0.054874 | 6 | O. | 33.36814 | 24.17814 | 42.55814 |
| Posterior | 29 | 12 | 0.042922 | 9 | F O | 55.51935 | 48.53935 | 62.49935 |
| Lateral | 14 | 13 | 0.039982 | 5 | % L | 74.68355 | 62.16355 | 87.20355 |
| Medial | 16 | 16 | 0.048728 | 9 | | | | |
| Total Overall Count | 83 | 51 | 0.186506 | 29 | N H | 10.08876 | -2.03124 | 22.20876 |
| Case#27 | ID: FA12 | Actual Age: 48 | | Lab Age: NA | | Estimated Age: 42.82 (43) | | |
| FOV | | | | | Results of Regression Equations | | | |
| | Osteon | Frag. Osteon | % of Lamellar | Nonhaversian | | Est Age | SSE- | SSE+ |
| Anterior | 22 | 12 | 0.073362 | 5 | O. | 27.45784 | 18.26784 | 36.64784 |
| Posterior | 20 | 12 | 0.040863 | 6 | F O | 50.0266 | 43.0466 | 57.0066 |
| Lateral | 10 | 12 | 0.142373 | 3 | % L | 74.45386 | 61.93386 | 86.97386 |
| Medial | 20 | 10 | 0.05864 | 4 | | | | |
| Total Overall Count | 72 | 46 | 0.315238 | 18 | N H | 19.32568 | 7.20568 | 31.44568 |

**Plate A-49**

**Anterior FOV**

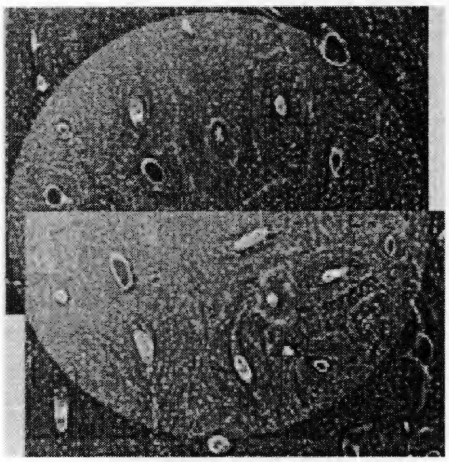

**Lateral FOV**

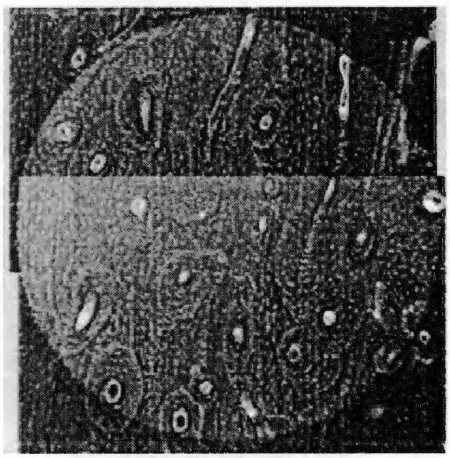

**Medial FOV**

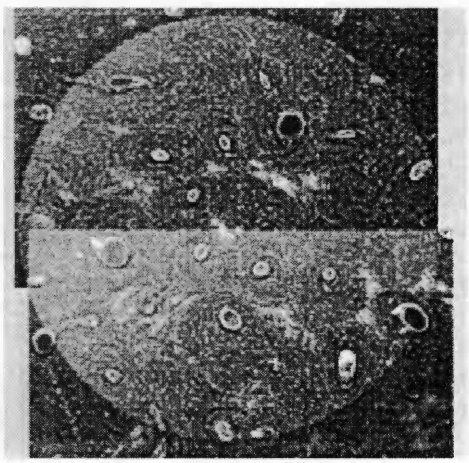

**Posterior FOV**
**Case #25: F83-215**

## Plate A-50

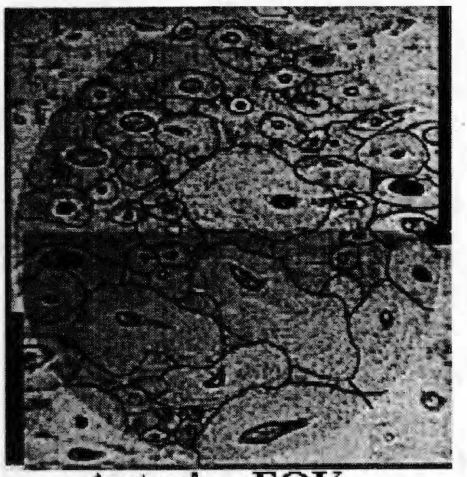

Anterior FOV

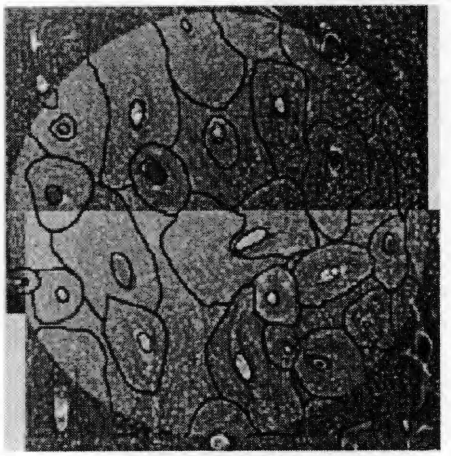

Lateral FOV

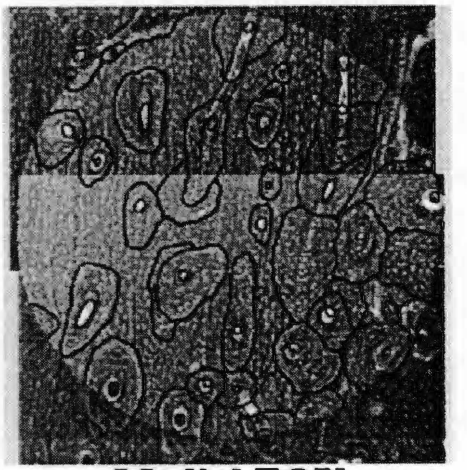

Medial FOV

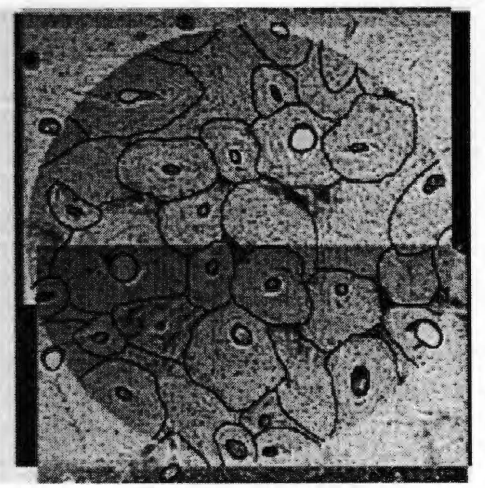

Posterior FOV
Case #25: F83-215

## Plate A-51

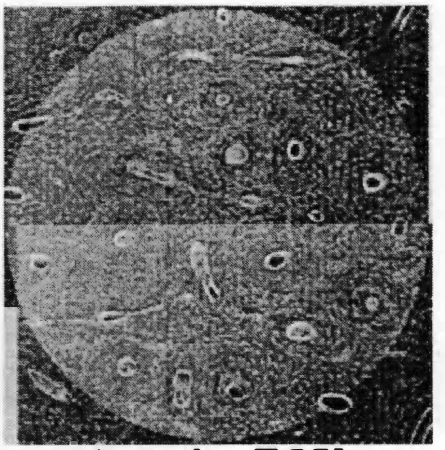

Anterior FOV

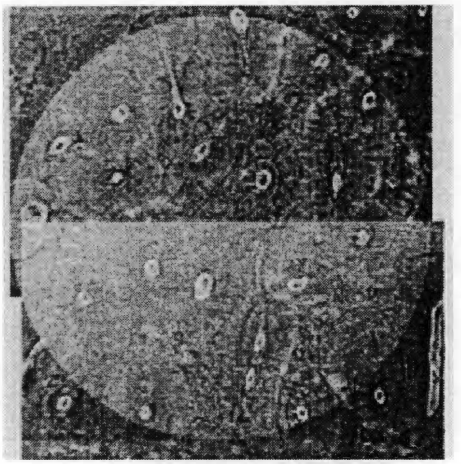

Lateral FOV

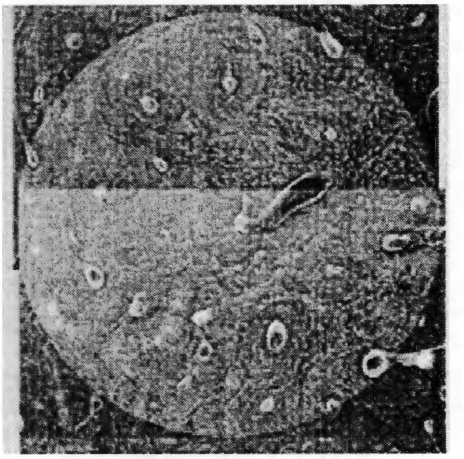

Medial FOV

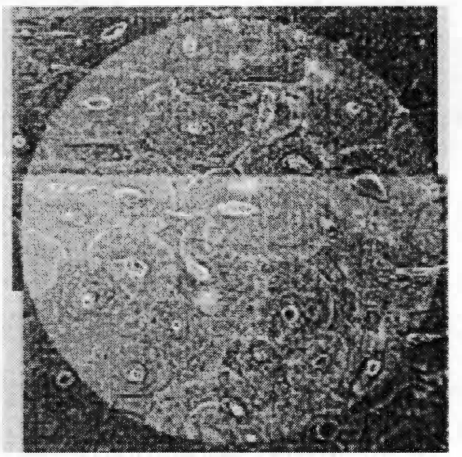

Posterior FOV
Case #26: F83-539

## Plate A-52

Anterior FOV

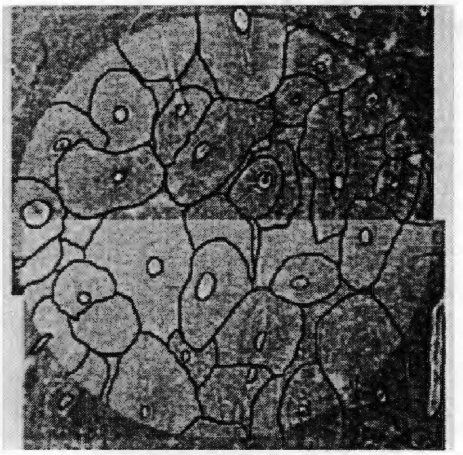

Lateral FOV

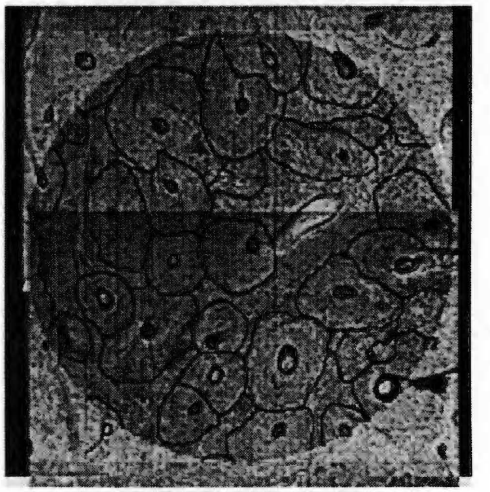

Medial FOV

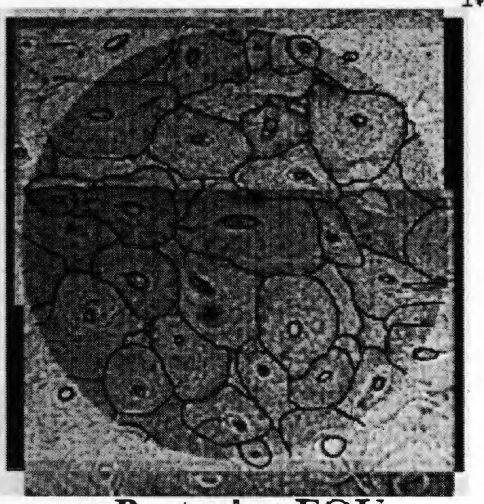

Posterior FOV
Case #26: F83-539

## Plate A-53

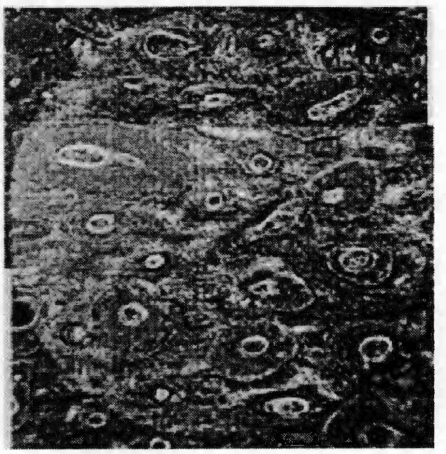

**Anterior FOV**

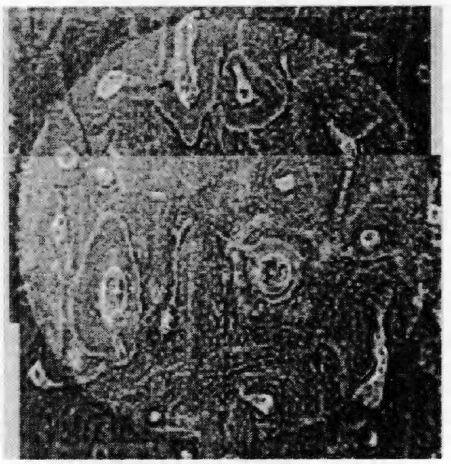

**Lateral FOV**

**Medial FOV**

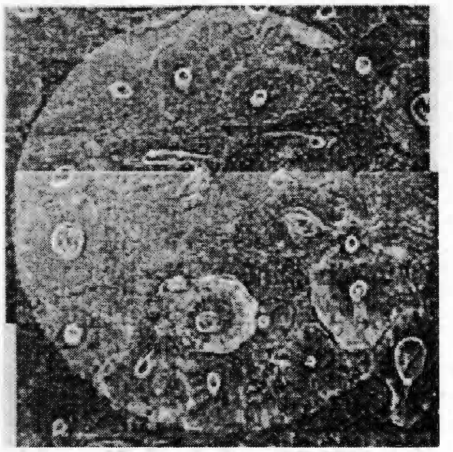

**Posterior FOV**
**Case #27: FA12**

## Plate A-54

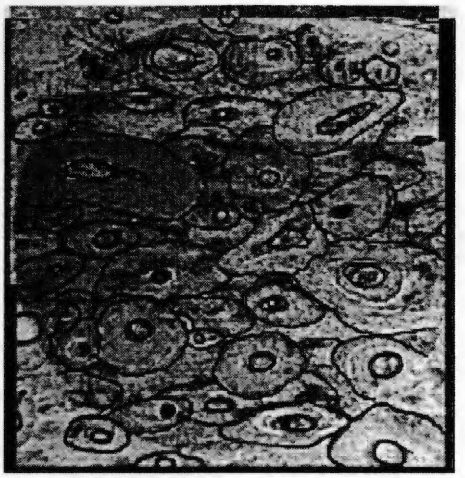

Anterior FOV

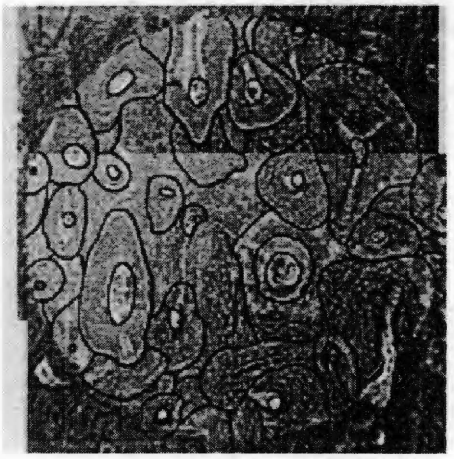

Lateral FOV

Medial FOV

Posterior FOV
Case #27: FA12

# Table A-3: Data Collection Sheets (continued)

| Case#28 | ID:O80120 | Actual Age: NA | | Lab Age: NA | | Estimated Age: 59.67 (60) | | |
|---|---|---|---|---|---|---|---|---|
| FOV | | | | | Results of Regression Equations | | | |
| | Osteon | Frag. Osteon | % of Lamellar | Nonhaversian | | Est Age | SSE- | SSE+ |
| Anterior | 26 | 11 | 0.067235 | 7 | O. | 31.15566 | 21.96566 | 40.34566 |
| Posterior | 16 | 16 | 0.093664 | 11 | F O | 73.39035 | 66.41035 | 80.37035 |
| Lateral | 15 | 23 | 0.089027 | 7 | % L | 74.46222 | 61.94222 | 86.98222 |
| Medial | 22 | 21 | 0.06062 | 8 | | | | |
| Total Overall Count | 79 | 71 | 0.310546 | 33 | N H | 8.76988 | -3.35012 | 20.88988 |
| Case#29 | ID: O81-9 | Actual Age: 25 | | Lab Age: NA | | Estimated Age: 24.31 (24) | | |
| FOV | | | | | Results of Regression Equations | | | |
| | Osteon | Frag. Osteon | % of Lamellar | Nonhaversian | | Est Age | SSE- | SSE+ |
| Anterior | 24 | 7 | 0.132299 | 7 | O. | 23.02894 | 13.83894 | 32.21894 |
| Posterior | 12 | 10 | 0.029579 | 7 | F O | 40.9002 | 33.9202 | 47.8802 |
| Lateral | 12 | 13 | 0.028308 | 9 | % L | 74.61509 | 62.09509 | 87.13509 |
| Medial | 15 | 8 | 0.034668 | 9 | | | | |
| Total Overall Count | 63 | 38 | 0.224854 | 32 | N H | 9.01272 | -3.10728 | 21.13272 |
| Case#30 | ID: O82-2 | Actual Age: 6-7 | | Lab Age: NA | | Estimated Age: 21.20 (21) | | |
| FOV | | | | | Results of Regression Equations | | | |
| | Osteon | Frag. Osteon | % of Lamellar | Nonhaversian | | Est Age | SSE- | SSE+ |
| Anterior | 20 | 7 | 0.128421 | 7 | O. | 23.9815 | 14.7915 | 33.1715 |
| Posterior | 16 | 6 | 0.070523 | 10 | F O | 29.5282 | 22.5482 | 36.5082 |
| Lateral | 13 | 9 | 0.046923 | 6 | % L | 74.47707 | 61.95707 | 86.99707 |
| Medial | 16 | 6 | 0.056349 | 6 | | | | |
| Total Overall Count | 65 | 28 | 0.302216 | 29 | N H | 10.08876 | -2.03124 | 22.20876 |

## Plate A-55

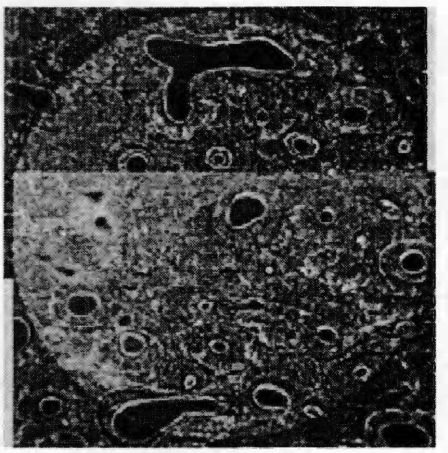

**Anterior FOV**

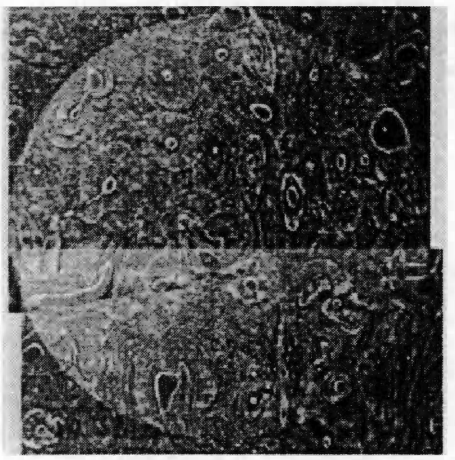

**Lateral FOV**

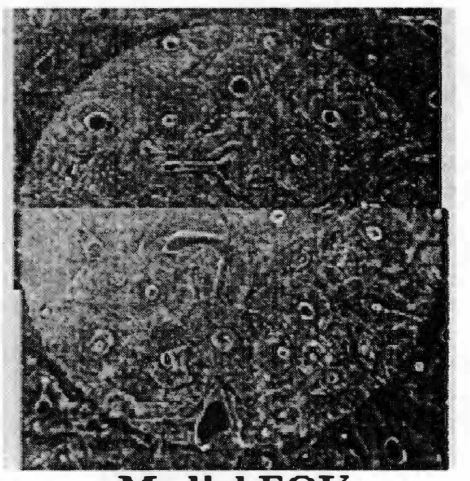

**Medial FOV**

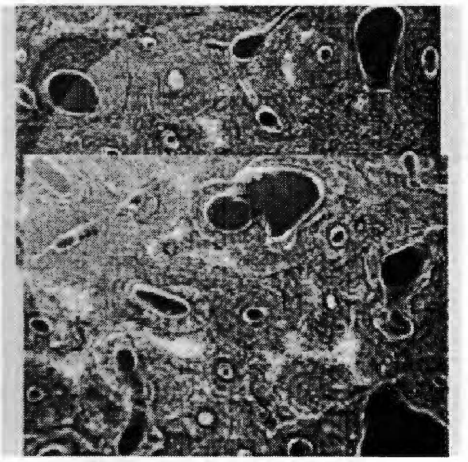

**Posterior FOV**
**Case #28: O80-120**

## Plate A-56

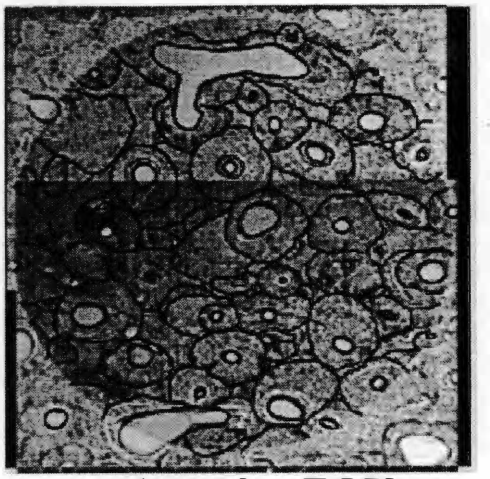

Anterior FOV

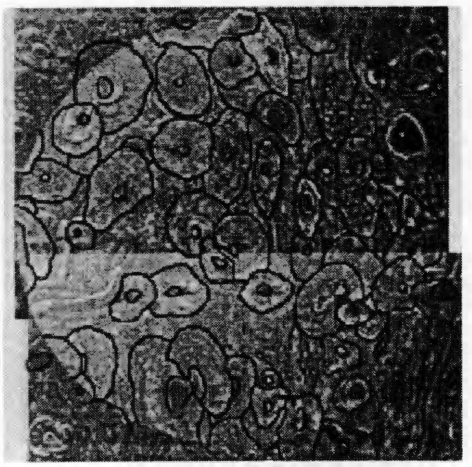

Lateral FOV

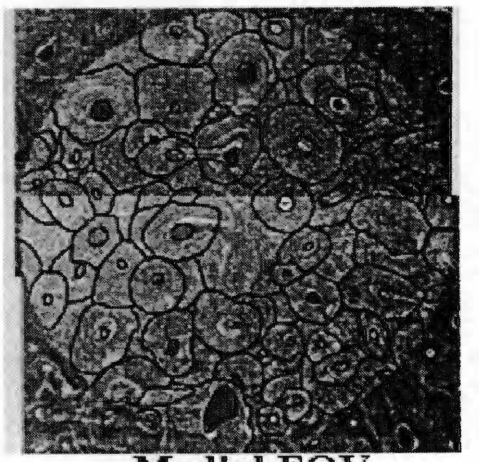

Medial FOV

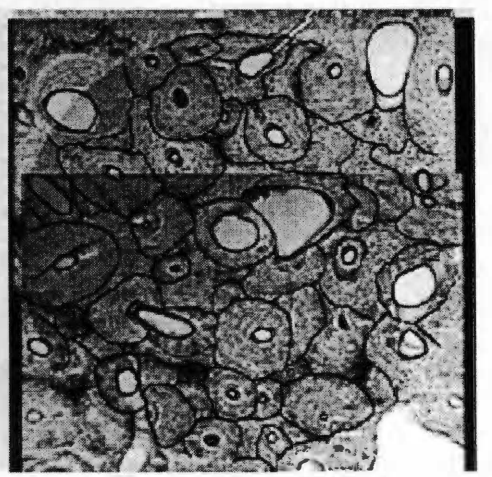

Posterior FOV
Case #28: O80-120

## Plate A-57

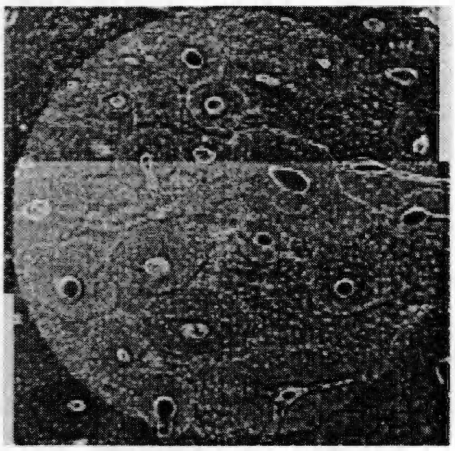

**Anterior FOV**

**Lateral FOV**

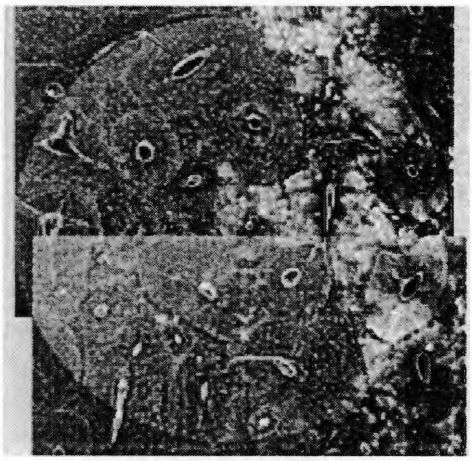

**Medial FOV**

**Posterior FOV**
**Case #29: O81-9**

## Plate A-58

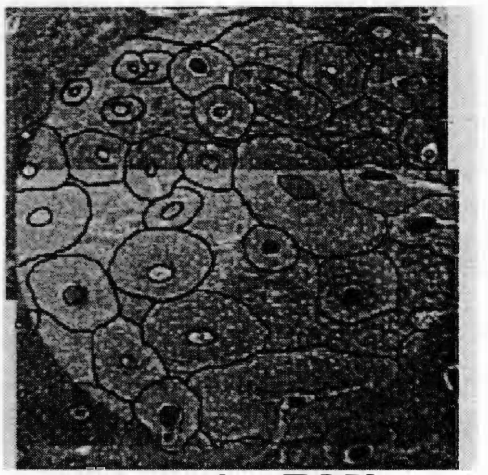

**Anterior FOV**

**Lateral FOV**

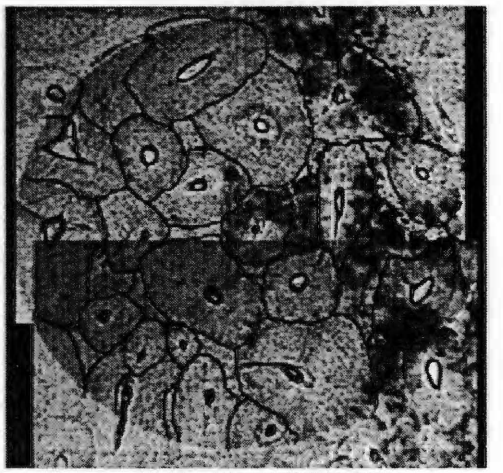

**Medial FOV**

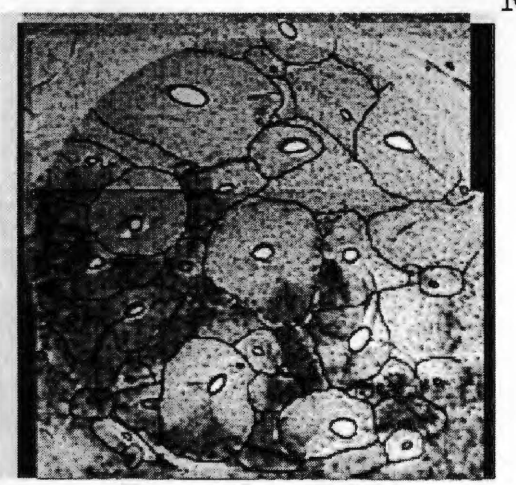

**Posterior FOV**
**Case #29: O81-9**

## Plate A-59

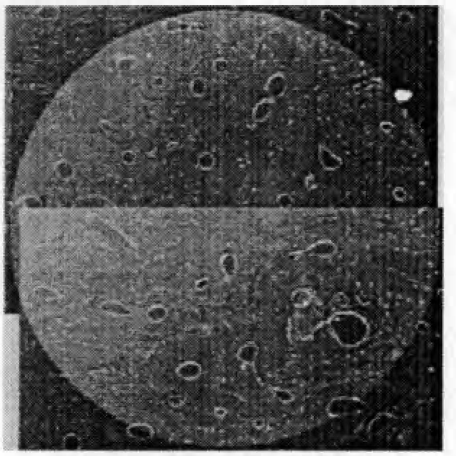

**Anterior FOV**

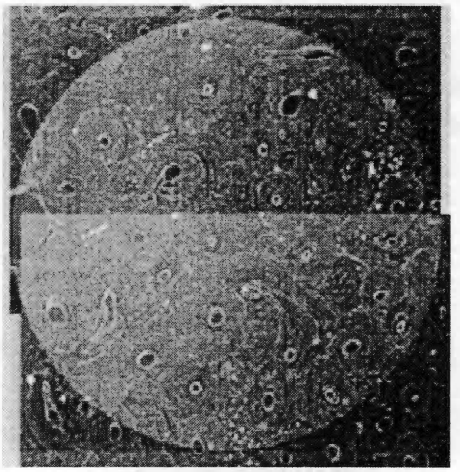

**Lateral FOV**

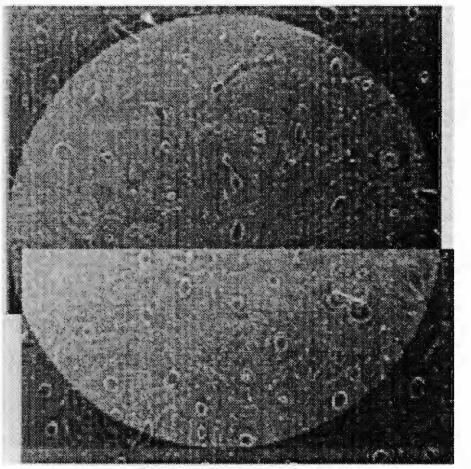

**Medial FOV**

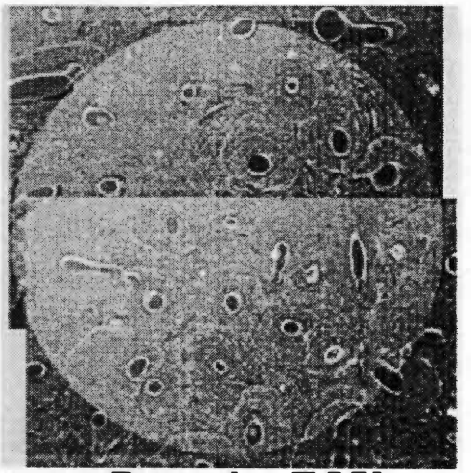

**Posterior FOV**
**Case #30: O82-2**

## Plate A-60

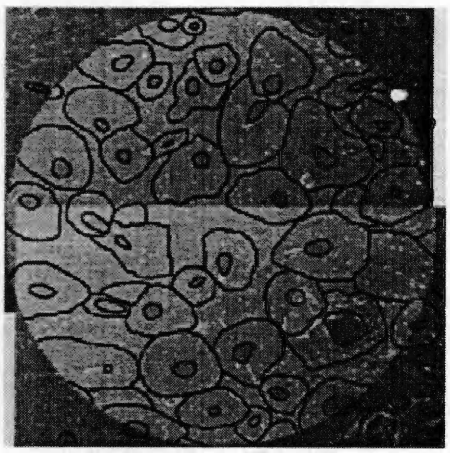

Anterior FOV

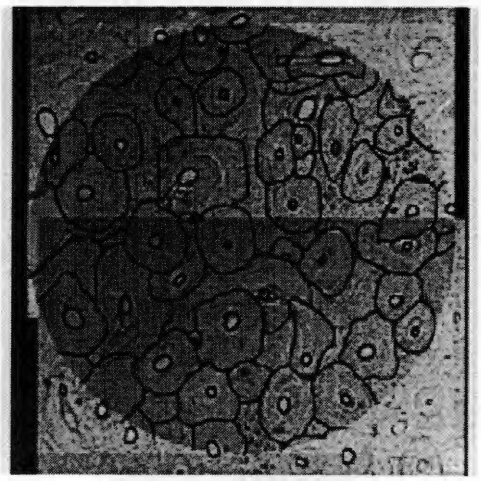

Lateral FOV

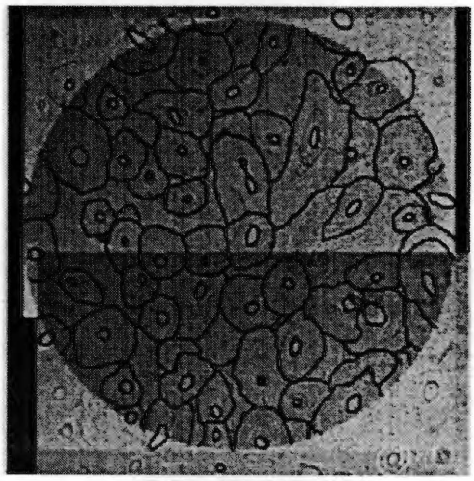

Medial FOV

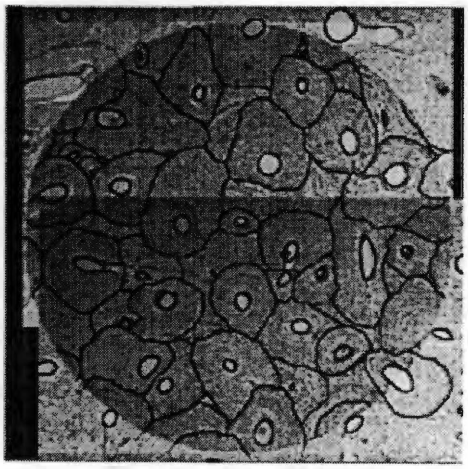

Posterior FOV
Case #30: O82-2

## Table A-4 to A-12: HISTOLOGY THIN-SECTION DEMOGRAPHIC TABLES

| Table A-4: Histological Collection Overview | | |
|---|---|---|
| *Total Number of Femur Slides (Including Complete (34) and Partial (29)* | | *63* |
| **Total Males** | **(M= Male)** | 22 |
| **Total Females** | **(F= Female)** | 15 |
| **Total White** | **(W= White)** | 26 |
| **Total Black** | **(B= Black)** | 8 |
| **Total Amerindian** | **(AI= Amerindian)** | 1 |

| Table A-5: Histological Collection Age Distribution | | | |
|---|---|---|---|
| *Age Distribution (yrs)* | *Lab Age (Frequency)* | *Known Age (Frequency)* | *Known Sex & Race (Freq.)* |
| **0-9** | 0 | 1 | F&B |
| **10-19** | 1 | 4 | F&B (2); M&W; F&W |
| **20-29** | 1 | 6 | F&W (2); F&B; M&B; M&W (2) |
| **30-39** | 1 | 6 | M&W (5); F&W; M&AI |
| **40-49** | 4 | 3 | M&B; M&W; F&B |
| **50-59** | 3 | 3 | M; F&W; M&W |
| **60-69** | 0 | 4 | M&W (4) |
| **70-79** | 0 | 1 | F&W |
| **80-89** | 0 | 1 | F&W |

| Table A-6: Histological Thin-Sections Descriptions | | | | | | | |
|---|---|---|---|---|---|---|---|
| *Designation* | *Lab Age* | *Age* | *Sex* | *Race* | *Positive Id?* | *Which Side?* | *Number of Slides* |
| **Berryman FA-12 A84-446** | 48 | | M | B | YES | | 1 |
| **Berryman OC81-110** | | | | | | | 1 |
| **Conradi FA83-539** | 54.4 | 51 | M | | | | 1 |
| **Berryman C81-2005** | | | | | | | 1 |
| **Owsley 0-82-2** | | 6-7 | F | B | Yes | Right | 1 |
| **Owsley 2-27-81** | | | | | | | 1 |
| **Owsley 2-81** | | | | | | | 1 |
| **Owsley 81-9 3/15/82** | | 25 | F | W | | | 3 |
| **Owsley 82-16** | | | M | W | | Left | 1 |
| **Berryman OC80-120** | | | M | | | | 2 |
| **Owsley 80-12** | | 27 | F | B | | Right | 3 |
| **74-5** | | | | | | | 1 |
| **80-9** | | 37 | M | W | Yes | Left | 1 |
| **81-1** | | 60 | M | W | Yes | | 1 |
| **81-6** | | | | | | | 1 |
| **81-13** | | | | | | | 1 |
| **82-1** | 56.5 | 60 | M | W? | Tentative | | 1 |

| Table A-6 (continued) | | | | | | | |
|---|---|---|---|---|---|---|---|
| ***Designation*** | ***Lab Age*** | ***Age*** | ***Sex*** | ***Race*** | ***Positive Id?*** | ***Which Side?*** | ***Number of Slides*** |
| **83-9** | 18.45 | 18 | F | B | | Right | 1 |
| **Owsley 83-10** | | | F | W | | | 1 |
| **83-12 FA83-215** | | | M? | B? | | Right | 3 |
| **83-25** | 54 | 26 | M | B | Yes | Left | 2 |
| **84-14** | 45 | 45 | M | W | Yes | | 1 |
| **Owsley 85-1** | | | F | W | | | 1 |
| **85-7** | 30-40 | | F | W | | Right | 1 |
| **85-24** | 32.7 | | M | W | | Right | 1 |
| **81-9** | | 25 | M | W | Yes | Right | 1 |

| Table A-7: Femur Sections from Histological Collection | | | | | | | |
|---|---|---|---|---|---|---|---|
| Key: A= Anterior P= Posterior L=Left Side R=Right Side | | | | | | | |
| ***Designation*** | ***Lab Age*** | ***Age*** | ***Sex*** | ***Race*** | ***Positive Id?*** | ***Which Location & Side?*** | ***Number of Slides*** |
| **72-3** | | 34 | M | W | Yes | AL (3)<br>PL (4) | 7 |
| **73-1** | | 18-21 | F | B | | AL (2)<br>PL (2) | 4 |
| **74-2** | | 28 | F | B | Yes | AL (2)<br>PL (2) | 4 |
| **74-5** | | 43 | F | B | Yes | AL (2)<br>PL (2) | 4 |
| **75-3** | | | | | | | 1 |
| **79-13** | 26-28 | 36 | M | W | | AL (1)<br>PL (1) | 2 |
| **80-3** | | 30-40 | M | AI | | AL (1)<br>PL (1) | 2 |
| **80-6** | | 65 | M | W | Yes | AR (2)<br>PR (1) | 3 |

| Table A-8: Fibula Sections from Histological Collection | | | | | | | |
|---|---|---|---|---|---|---|---|
| ***Designation*** | ***Lab Age*** | ***Age*** | ***Sex*** | ***Race*** | ***Positive Id?*** | ***Which Side?*** | ***Number of Slides*** |
| **W.G.A.75-5** | | | | | | | 1 |
| **82-1** | 30-26 | 25-29 | M | W? | | Left | 1 |
| **83-26** | 46+ | 27 | F | W | Yes | Right | 2 |
| **84-5** | 40 | 36 | M | W | Yes | Right | 1 |
| **FA 80-81** | | | | | | | 4 |

| Table A-9: Tibia Sections from Histological Collection | | | |
|---|---|---|---|
| *Designation* | *Positive Id?* | *Which Side?* | *Number of Slides* |
| **Amputee 128693 ds** | Yes | Right | 1 |
| **Amputee 128693 ro** | | | 1 |
| **Amputee 128693 W.R.C.** | | | 1 |

| Table A-10: Burn Cases Sections from Histological Collection | | | | | | |
|---|---|---|---|---|---|---|
| Burn Cases (Thin-Sections) Total =13 | | | | | | |
| *Designation* | *Age* | *Sex* | *Race* | *Positive Id?* | *Which Side?* | *Number of Slides* |
| **85-27** | 32 | M | W | Yes | Right | 1 |
| **77-8** | 27 | F | W | | | 1 |
| **77-6** | 82 | F | W | Yes | | 1 |
| **78-2** | | | | | | 1 |
| **77-10** | | | | | | 1 |
| **77-9** | | | | | | 1 |
| **76-1** | 70 | F | W | | | 1 |
| **79-11** | 60+ | M | W | Yes | | 1 |
| **9-8** | | | | | | 1 |
| **79-7** | | F | W | Yes | | 1 |
| **79-3** | | | | | | 1 |
| **78-17** | | | | | | 1 |
| **78-4** | 38 | M | W | Yes | | 1 |

| Table A-11: Records of Sections from Histological Collection without Slides | | | | | | | |
|---|---|---|---|---|---|---|---|
| *Designation* | *Lab Age* | *Age* | *Sex* | *Race* | *Positive Id?* | *Which Side?* | *Number of Slides* |
| **82-18** | 55 | 57 | F | W | Yes | Right Femur | 2 |
| **85-16** | | | M | W | | Right Femur | 1 |
| **82-20** | 57 | 52-62 | M | W | | Left Fibula | 2 |
| **81-23** | | 14-17 | F | W | | Left Femur | 1 |

| Table A-12: Sections without Records Found from the Histological Collection |
|---|
| **82-2** |
| **88-14** |

# VITA

John Edward Mailen was born in Oak Ridge, Tennessee on July 19, 1966. He attended both private, religious and later Oak Ridge High School, where he graduated in 1984. After attending University of Florida Gainesville, he earned a Real Estate License in the State of Tennessee. In the Summer of 1987, he returned to school and entered the University of Tennessee Knoxville where in May 1990, he received a Bachelor of Arts in Psychology with Honors. In the Fall of 1990, he entered the Master's program in Psychology at Georgia State University in Atlanta. In the Fall of 1991, he reentered the University of Tennessee Knoxville program, where he finally decided to enter the graduate program of Anthropology. In December of 1992, he received a Bachelor of Arts in Anthropology and entered the Master's program in Anthropology in January 1993 at the University of Tennessee Knoxville. He also has a certificate from a seminar on *the Field and Laboratory Methods in the Location, Recovery, and Analysis of Human Remains in a Rural Setting* from May 1993. The seminar was taught at Mercyhurst College in Erie, Pennsylvania. In addition, he maintains and operates a retail store, which has allowed him to gain five years of administrative and management level experience. The Master's degree was received May 1999.

He is now in the process to enter the Dissertation program in Anthropology at the University of Tennessee Knoxville for Fall 2000 and seeking opportunities to gain experience in the field of Anthropology, possibly with a part of the Mass Disaster Response Team based in East Tennessee. The author has used and built computers since 1979, as a major interest and hobby. He is knowledgeable in Fortran, BASIC, MSDOS, and Visual Basic. Since 1987 the author has been very interested in scanned images and image files. He has designed commercial and personal website pages and received several awards for design and content. In addition, he has built and maintained the computer systems used in his Master's research. Further, he is an active member in the Better Business Bureau of the Greater Knoxville Area since 1995 and a member of the Oak Ridge Chamber of Commerce since 1998.